國立臺灣大學生命科學院分子與細胞生物學研究所

博士論文

Graduate Institute of Molecular and Cellular Biology

College of Life Science

National Taiwan University

Doctoral Dissertation

MicroRNA-148a 與其標靶基因 14-3-3β 在胃癌轉移機制

之探討

The Metastatic Mechanism of MicroRNA-148a and Its

Target Gene 14-3-3β in Gastric Cancer

曾建偉

Chien-Wei Tseng

指導教授：阮雪芬 博士

Advisor: Hsueh-Fen Juan, Ph.D.

中華民國 100 年 7 月

July, 2011

國立臺灣大學博士學位論文
口試委員會審定書

MicroRNA-148a 與其標靶基因 14-3-3β 在胃癌轉移機制之探討

The Metastatic Mechanism of MicroRNA-148a and Its Target Gene 14-3-3β in Gastric Cancer

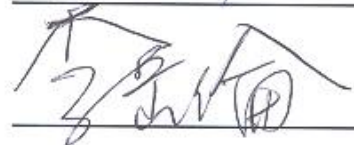　　本論文係曾建偉君（F93B43013）在國立臺灣大學分子與細胞生物學研究所完成之博士學位論文，於民國 100 年 7 月 4 日承下列考試委員審查通過及口試及格，特此證明

口試委員：

_____（指導教授）

陳炯年　　　　　　　　

_____

所長　_____

Acknowledgments

參透為何，才能迎接任何。我，歷經了一趟博士旅程。偶而遇有顛簸，也曾經歷風浪，卻也體驗到許多事物，也享受了這趟驚奇之旅。獲得更進階的知識、探索未曾接觸過的領域、認識許多師長、同學及朋友們。原來，博士不只是追求探索知識，培養獨立思考以及解決問題的能力更為重要。一位著名的劇作家-George Bernard Shaw 曾說 "A man learns to skate by staggering about making a fool of himself; indeed, he progresses in all things by making a fool of himself." 學習之中失敗了不用害怕丟臉，當從這些一次又一次的學習中，發現自己會不斷的成長。現在，我順利取得博士學位，為這趟旅程記錄下美好的文字與回憶，以飲水思源的心情感謝一路上所有幫助過我的人們。日後，我秉持這份勇敢的態度再度去迎接新的人生、新的挑戰。

首先要感謝指導教授阮雪芬老師，感謝她在學術研究與生活上的指導及給予經驗分享。阮老師在研究上給了我相當大的學習空間，使我在研究學習過程中逐漸培養了獨立思考與解決問題的能力。她也鼓勵我們多參與一些與自身研究主題相關的研討會，參與研討會的過程，多與其他老師及同學們做學術上的交流討論與相互學習。感謝黃宣誠老師在研究上的協助指導。黃老師在課程上總會給予我們不同角度的思維；也因為黃老師，使得我的論文研究上有更多元的研究方向。以系統生物學為研究基礎，結合生物與生物資訊的分析，不只讓我的研究方向更為擴展，也讓我的研究內容深度更為精進。感謝陳炳年醫師在臨床研究上的大力協助。陳醫師總是熱心的提供大量檢體給予我研究上的幫助，也參與臨床研究上的討論並給予許多很好的方向思考。因為陳醫師的幫忙，以結合基礎研究與臨床分析使得我的論文研究在轉譯醫學研究方向上更為紮實。感謝陳玉如老師在 iTRAQ 實驗上的支持，在我學習 iTRAQ 過程中，讓我充份了解 iTRAQ 技術、知識與應用。謝謝陳水田老師一開始在我研究之初提供了實驗空間與資源。

在我的論文研究過程中，要感謝許多學長姐與同學們的幫忙。謝謝振慶在研究上的合作。在合作過程中，不時與他討論資料分析，逐漸讓我對生物資訊有更多的了解外，也使得我的研究內容更為充實。謝謝陳玉如老師的博士班學生芷薇與韓嘉莉博士在 iTRAQ 的技術指導與討論上的協助。謝謝家怡在檢體與病理資料上
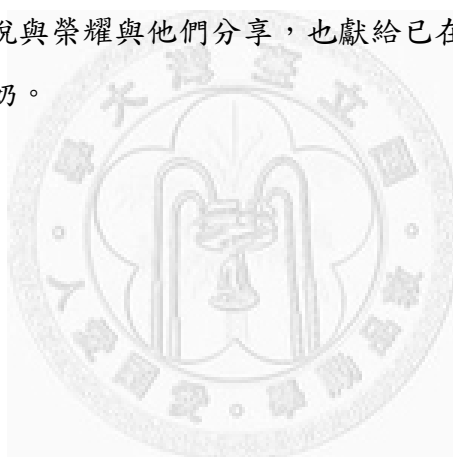
中文摘要

　　胃癌在全世界中為癌症致死率的第二名（世界衛生組織 2009 年報導）。被診斷晚末期的胃癌病人五年存活率不到 35%。較差的預後能力主要與腫瘤轉移有關。此外，有些微型核醣核酸被報導與腫瘤相關，其功能可能是致癌基因或腫瘤抑制基因，並且涉及了腫瘤形成及癌症發展。在本研究中，我們研究胃癌轉移的機制並鑑定出一個抗轉移的微型核醣核酸-148a，它在腫瘤組織中的表現較低。Kaplan–Meier 存活方法顯示，相較於含有較低微型核醣核酸-148a 含量的病人 (32.1%)，其含有較高微型核醣核酸-148a 含量的病人具有較高的五年整體存活率 (71.4%) (*P* = 0.03)。臨床資料指出微型核醣核酸-148a 表現量增加與腫瘤遠處轉移 (*P* = 0.043)、器官侵犯 (*P* = 0.013) 及腹膜侵犯 (*P* = 0.04) 有高度相關性。大量表現微型核醣核酸-148a 減少腫瘤細胞侵犯、轉移及附著能力。此外，大量表現微型核醣核酸-148a 抑制細胞生長並誘導細胞凋亡。我們利用了同位素標記相對和絕對定量方法分析微型核醣核酸-148a 所調控的蛋白質體表現。微型核醣核酸-148a 所調控的蛋白質體與腫瘤發展有高度相關性，其包括了細胞移動、生長與增生以及細胞凋亡。這些結果與我們之前的結果一致，微型核醣核酸-148a 抑制胃癌細胞轉移相關的功能。另一方面，進一步的利用了冷光酶分析方法，我們確認了微型核醣核酸-148a 可以直接調控 14-3-3β 表現。14-3-3β 在腫瘤組織中的表現增加 (*N = 40, P* < 0.01)，而且血液 14-3-3β 在胃癌病人的含量也顯著的比正常人高(*N = 63*) (*P* < 0.0001)。具有較高血液 14-3-3β 含量的病人有較差的整體存活率(*P* = 0.038)。大量表現 14-3-3β 增加了腫瘤細胞生長、侵犯與移動能力。綜合上述結果，14-3-3β 涉及了胃癌的轉移。微型核醣核酸-148a 也許功能上是個腫瘤抑制基因，並且透過調控一個有潛力作為胃癌偵測與預後的 14-3-3β 生物標記表現以抑制了腫瘤細胞的轉移。

關鍵字：微型核醣核酸-148a; 14-3-3β; 胃癌; 轉移; 生物標記

ABSTRACT

Gastric cancer is the second leading cause of cancer deaths worldwide (WHO 2009 report). Patients diagnosed with advanced stages have a survival rate of less than 35% beyond 5 years. The poor prognosis is mainly related to tumor metastasis. In addition, some microRNAs (miRNAs) are reported as oncomirs which function as either oncogenes or tumor suppressors and involved in tumorigenesis and cancer progression. Here, we studied the mechanisms of gastric cancer metastasis and identified an antimetastatic miRNA, miR-148a, that was down-regulated in tumor tissues. Kaplan–Meier survival method revealed that patients with higher miR-148a expression levels had higher 5-year overall survival rates (71.4%) compared with patients with low miR-148a levels (32.1%, $P = 0.03$). Clinical data indicated that elevated miR-148a levels highly correlated with distant metastasis ($P = 0.043$), organ ($P = 0.013$) and peritoneal invasion ($P = 0.04$). Over-expression of miR-148a could decrease invasiveness, migration and adhesion of tumor cells. Moreover, Over-expression of miR-148a could repress cell growth and induce cell apoptosis. We further used isobaric tag for relative and absolute quantitation (iTRAQ) method to analyze miR-148a-regulated proteome. The results showed that miR-148a-regulated proteome was closely related with tumor progression, including cell movement, growth and proliferation as well as cell death. These results are consistent with our previous data that miR-148a suppresses metastasis-related functions of gastric cancer cells. On the other hand, we verified that miR-148a could directly regulate 14-3-3β expression using luciferase assay. 14-3-3β levels were elevated in tumor tissues ($N = 40$, $P < 0.01$), and serum 14-3-3β levels in cancer patients ($N = 145$) were also significantly higher than healthy controls ($N = 63$) ($P < 0.0001$). Patients with higher serum 14-3-3β levels had

worse overall survival ($P = 0.038$). Over-expression of 14-3-3β enhanced the growth, invasiveness and migration of tumor cells. In conclusion, 14-3-3β is involved in metastasis of gastric cancer. miR-148a may function as a tumor suppressor in gastric cancer, suppressing cell metastasis through targeting 14-3-3β, a potential detective and prognostic marker in gastric cancer.

Key Words: miR-148a; 14-3-3β; gastric cancer; metastasis; biomarker

CONTENTS

LIST OF FINGURES

LIST OF TABLES

Chapter 1 Introduction

1.1 Biogenesis of miRNAs and Their Roles in Cancers

miRNAs are small non-coding, single stranded RNA of ~22 nucleotides in length that are abundantly found in eukaryotic cells [1]. The complementarity is between seed regions of mature miRNA and their target messengers, enabling miRNA-mRNA interactions to occur. These interactions are crucial for post-transcriptional regulation of target gene expression by obstructing the mRNA translation or stability in the cytoplasm, and depend on both the expression levels of miRNAs and target mRNAs [2, 3]. Some miRNAs are reported as oncomirs which could function as either oncogenes or tumor suppressors [4]. For example, miR-21 decreased tumor suppressor Pdcd4 expression and promoted invasion, intravasation and metastasis in colorectal cancer [5]. MiR-21 also regulated PTEN-dependent pathway and affected cell growth, migration and invasion of hepatocellular cancer [6]. On the other hand, let-7 decreased cell proliferation and migration of glioblastoma and reduced tumor size in xenograft model [7]. let-7 prevented early cancer progression through suppressing embryonic gene high mobility group, A2 (HMGA2) expression [8]. Metastatic gastric cancer cells secreted let-7 via exosomes into the extracellular environment to maintain their oncogenesis [9].

1.2 Analysis of Correlation Between miRNAs and Target Genes

Recently, many reports showed that they successfully identified miRNA targets using miRNA expression profiles [10, 11]. Huang *et al*. used RNA expression data to identify 1597 high-confidence target predictions for 104 human miRNAs and further

verified let-7b was down-regulated in retinoblastoma and CDC25A and BCL7A were targets of let-7b using qRT-PCR and microarray profile. Li *et al*. combined sequence complementarity, miRNA expression level, and protein abundance to identify miRNA targets for elevating their predictions. They also found that translational repression of targets by miRNAs was dominant mechanism in miRNA regulation. Moreover, sequence-based computational methods have been broadly used to predict putative miRNA targets [12], and can reach pretty good prediction rate, including cancer-related miRNAs [13, 14]. Previous report has also indicated that computational prediction should take into account the expression profiles of both miRNA and mRNA [3]. Therefore, the development of an integrative approach that incorporated expression data to facilitate the identification of condition-specific targets of miRNAs becomes increasingly important.

1.3 miRNA-regulated Network and Biological Functions

miRNA can obstruct the translation of mRNA, thereby directly affecting protein abundance [13, 14] and protein interaction networks (PINs) [15, 16]. For example, Yu *et al.* analyzed correlations between transcription factors (TFs) and miRNAs and further discovered that different regulatory networks formed by miRNA and TFs were involved in different biological functions [15]. Additionally, Liang *et al.* found global correlation between miRNA repression and protein-protein interactions and elucidated the related biological processes of miRNA-regulated PINs [16]. PINs are sets of interactions formed by two physically interacting proteins, which are fundamental to most biological processes [17]. With the accumulation of protein-protein interaction (PPI) data, it is becoming increasingly possible to understand the architecture and function of the

cellular network by computational approaches [18, 19]. Recently, we characterized the global properties of miRNA regulation in human PIN and proposed possible mechanisms of how these miRNAs regulate PINs [20]. Additionally, previous studies have demonstrated that miRNAs can affect specific biological functions which are involved in tumorigenesis and cancer progression through the regulation of a small number of genes within biological networks, such as PINs [21, 22]. Thus, assessing how miRNAs affect PINs could facilitate the discovery of potential miRNA-related networks and allow the characterization of associated biological functions.

1.4 miRNA-regulated Proteome and Associated Biological Functions

Recently a new amine labeling method at the peptide level using isobaric tag for relative and absolute quantitation (iTRAQ) was developed for multiplexed protein quantitation [23, 24]. It used the relative intensity of signature reporter ions of *m/z* 114, 115, 116 and 117 in an MS/MS spectrum to quantify protein levels. This method has become popular based on the following advantages. First, the multiplexing reagents are conjugated with the N terminus and the lysine amino acid of peptides; thus, each peptide fragment can be labeled with better efficiency compared with protein-level labeling [24]. Second, the intensity of both the precursor ion and the MS/MS fragments is greatly increased by summing of four isobarically iTRAQ-labeled sample sets, increasing the number of peptides identified and quantified and thus elevating the quantification accuracy [24]. The iTRAQ strategy has been widely applied for identification of potential targets of miRNAs and correlation between their expression and cancer progression. For example, iTRAQ method was used to identified potential

targets of miR-21 in human breast cancer cells [25]. Additionally, Sulfatase 1 was identified as a target of miR-516a-3p by using iTRAQ analysis and miR-516a-3p could inhibit metastatic dissemination of gastric cancer [26]. We have known that miRNA can obstruct the translation of mRNA, thereby directly affecting protein abundance [13, 14] and PINs [15, 16]. In this study, iTRAQ approach was used to detect potential targets of miR-148a and further analyzed associated biological functions of miR-148a-regulated protein-protein interaction network, providing deeply insight into the regulatory role of miR-148a in gastric cancer progression.

1.5 14-3-3β

In this study, we identified one miRNA, miR-148a, was expressed lower in tumor tissues than normal tissues and miR-148a-regulated PIN was involved in metastasis-related biological processes, including integrin-mediated signaling, cell-matrix adhesion and wound healing.

On the other hand, we found 14-3-3β was a predicted target gene of miR-148a based on TargetScanHuman 5.1 [27] and Pictar [28] databases. 14-3-3β was reported as a potential oncogene in cancers and associated with metastasis of cancer cells [29, 30]. Thus, a key question is whether miR-148a affects metastasis of gastric cancer cells through targeting 14-3-3β expression.

1.5.1 Role of 14-3-3β in Cancers

14-3-3 protein plays crucial roles in tumorigenesis, including the maintenance of cell cycle and DNA repair, the prevention of apoptosis. It contains at least seven isoforms: β, ε, ζ, η, θ, γ and σ [31]. Reports indicate that 14-3-3β is abundant in human

lung cancer relative to normal tissues [32] and mutated chronic lymphocytic leukemia (M-CLL) relative to unmutated chronic lymphocytic leukemia (UM-CLL) [33]. Over-expression of 14-3-3β in NIH 3T3 cells (mouse embryonic fibroblast cell line) stimulated cell growth and supported anchorage-independent growth in soft agar medium and tumor formation in nude mice [34], while reducing 14-3-3β expression led to an inhibition of tumor progression due to decreased vascular endothelial growth factor (VEGF) production, inhibition of angiogenesis and increased apoptosis. In addition, it has been shown that 14-3-3β promotes cell migration by interacting with integrin β1 [35] and activating the MAPK pathway, causing tumor cell metastasis [29, 30]. Thus, these studies support the idea that 14-3-3β could function as an oncogene. Chan *et al.* reported that 14-3-3β showed stronger expression in gastric cancer cells than in paired normal cells by using immunohistochemical staining analysis [30]; however, the roles of 14-3-3β in human gastric cancer are still poorly understood.

1.5.2 Biomarkers for Gastric Cancer

Gastric cancer is the second leading cause of cancer deaths worldwide (WHO 2009 report) [36], with more than 80% of patients being diagnosed at an advanced stage of tumor progression or experiencing tumor recurrence after surgical resection [37]. Gastric cancer patients diagnosed with advanced stages have a survival rate of less than 35% beyond 5 years [38]. The poor prognosis is mainly due to the fact that most patients are diagnosed with advanced stages or tumor recurrence after curative surgery. Thus, identification of serum markers for early detection and prognosis in gastric cancer is critical for prolonged patient survival.

Serological tumor markers are routinely used for the detection and screening of

early stage cancers in asymptomatic patients. Several gastric cancer markers have been discovered, including carcinoembryonic antigen (CEA), carbohydrate antigen 19-9 (CA19-9) and carbohydrate antigen 72-4 (CA72-4) [39, 40]; however, these are not sensitive nor specific enough for disease detection [41, 42]. Therefore, the identification of novel gastric cancer biomarkers that are sensitive and specific enough to facilitate early detection is required.

1.6 Motivation

In this study, we proposed an integrative analysis which suggested that miRNA-regulated PINs could be identified based on the combination of down-regulated miRNAs and up-regulated mRNAs. We subsequently elucidated associated biological processes of these miRNA-regulated networks. Among these was the miR-148a-regulated PIN, which was involved in metastasis-related biological processes that were associated with tumor suppression. We also verified the roles of miR-148a in gastric cancer based on *in vitro* cell experiments. Furthermore, we analyzed miR-148a-regulated proteome in gastric cancer using iTRAQ method. On the other hand, 14-3-3β, a predicted target gene of miR-148a, was reported to be associated with cancer metastasis. Thus, we analyzed the correlation between miR-148a and 14-3-3β and elucidate the metastatic mechanism of them in gastric cancer.

Chapter 2 Materials and Methods

2.1 Expression Profiles of miRNAs and mRNA

The mRNA expression profiles of gastric cancer were retrieved from Gene Expression Omnibus (GEO), accession number GSE13911 [43]. The miRNA expression profiles were obtained from 22 paired tumor and non-tumor specimens of gastric cancer patients who underwent curative gastrectomy at National Taiwan University Hospital (Taipei, Taiwan) between 2001 and 2006. All the human tissue samples have been approved and human subject confidentiality has been protected by the Institute Review Board (IRB, 9261700703). 100 ng of total RNA were dephosphorylated with 11.2 units of calf intestine alkaline phosphatase (GE Healthcare Life Sciences, Sweden) for 30 min at 37℃. The reaction was terminated after dephosphorylation at 100℃ for 5 min and then immediately frozen. 5μL of DMSO was added and samples were heated to 100℃ for 5 min and immediately frozen again. Ligase buffer and BSA were added and ligation was performed with 50μM pCp-Cy3 and 28μL T4 RNA ligase (GE Healthcare Life Sciences, Sweden) at 16℃ for 2h. The labeled miRNAs were desalted with MicroBioSpin6 columns (BioRad, USA). 2X hybridization buffer (Agilent Technologies, USA) was added to the labeled mixture to a final volume of 45μl. The mixture was heated for 5 min at 100℃ and immediately frozen. Each 45μl sample was hybridized onto Agilent human miRNA Microarray (Agilent Technologies, USA) at 55℃ for 20h. After hybridization, slides were washed at room temperature in Gene Expression Wash Buffer 1, then in Gene Expression Wash Buffer 2 (Agilent Technologies) for 5 min, respectively. Slides were scanned using an Agilent microarray scanner (Agilent Technologies, model G2565A) at 100% and 5% sensitivity settings. Feature Extraction (Agilent Technologies) software version 9.5.3 was used for image

analysis. We have submitted the miRNA microarray data to the GEO database and the series record is GSE28700.

2.2 Tissue Specimens

RNA from paired normal and tumor specimens from gastric cancer patients were extracted for miRNA microarray hybridization. The paired tissue specimens were dissected within 30 minutes of gastrectomy and frozen in liquid nitrogen tank. Healthy mucosa samples were taken from areas of grossly normal mucosa located at least 3 cm from the tumor border. Gastric cancer and normal tissues from these patients were collected at the National Taiwan University Hospital after receiving patient consent. The protocol was approved by the local ethics committees, National Taiwan University Hospital.

The criteria for curative resection included the complete removal of primary gastric tumor, D2 dissection of regional lymph nodes and absence of macroscopic tumor remaining after surgery. No other previous or concomitant primary cancer was present. No patient had received chemotherapy and radiotherapy before surgery. Clinicopathologic factors including age, sex, gross types of tumors (Borrmann classification), histologic types of tumors (Lauren classification), depth of tumor invasion, lymph node status, direct invasion of organs such as duodenum, esophagus, liver, pancreas, and mesocolon, and distant metastasis documented histologically were reviewed and stored in a patients' database. The patients were followed up for 2 to 140 months after surgery. The follow-up intervals were calculated as survival intervals after surgery.

2.3 MiRNA-regulated PIN Identification and Analysis

The procedure for miRNA-regulated PIN identification and analysis is illustrated in Figure 1. For identifying the miRNA-regulated PINs, significantly differentially expressed miRNAs and genes were determined by Significance Analysis of Microarrays (SAM) [44] (delta of 5 and fold change of 2), implemented in MultiExperiment Viewer (MeV) v4.5.1 [45]. As we applied this cutoff, we could control the false discovery rate was less than 0.00001% (evaluated by SAM). Finally, only 23 significantly down-regulated miRNAs and no significantly up-regulated miRNAs were found. The regulated network of each miRNA consists of its significantly up/down-regulated target genes and their interacting partners in the human PIN. The putative target genes of miRNAs were obtained from TargetScan 5.1 [46], and the human PIN was from Human Protein Reference Database (HPRD) [47]. The enrichment of co-expressed PPIs (CePPIs) involved in the network was used to evaluate the activation state of miRNA-regulated PINs in tumor and normal tissues. MicroRNA-regulated biological functions were predicted by functional enrichment analyses of their regulated PINs. To investigate the functional roles of miRNAs, the predicted target genes of miRNAs was integrated into and analyzed within PIN. We defined L0 genes as the predicted target genes of miRNAs and L0 proteins were encoded by L0 genes, while L1 proteins are interacting partners of L0 proteins in the human PIN. The functional roles that miRNAs play within the PIN constructed by L0 and L1 proteins were predicted as significantly over-represented Gene Ontology (GO) terms [48]. BiNGO [49] , a Cytoscape [50] plug-in, was used to determine which GO terms were significantly over-represented (Hypergeometric test $P \leq 0.001$) in miRNA-regulated PINs. A Hypergeometric test was performed to determine whether the GO terms were significantly over-represented.

2.4 qRT-PCR for miRNA

Total RNA from 62 paired tumor and normal tissues was obtained using Trizol (Invitrogen) and the mirVana miRNA isolation kit (Applied Biosystems, California, U.S.A.) for miRNA detection. Samples were analyzed by SDS-PAGE to confirm that there was no RNA degradation. The concentration of total RNA was quantified using a ND-1000 spectrophotometer (NanoDrop Technologies) and diluted to 5ng/μL for further analysis. RNA samples were mixed with miRNA-specific primers and a PCR reaction was performed for 30 minutes at 16℃, 30 minutes at 42℃, and 5 minutes at 85℃. cDNA products were mixed with miRNA-specific assay probes and incubated for 10 minutes at 95℃, 15 seconds at 95℃ and 1 minute at 60℃ for a total of 40 cycles using a 7300 real-time PCR system (Applied Biosystems). U6 small nuclear RNA was measured using the same method and was used for normalization.

2.5 Cell Culture and Authentication of Cell Lines

Human gastric cancer AGS, SC-M1, MKN-45, TSGH and N87 cells were obtained from the cell line databank in National Taiwan University Hospital in 2008 and have been tested and authenticated in our laboratory on a monthly basis. These cells were last tested by morphology check using microscope and mycoplasma detection using Hoechst 33258 in March 2010. These cells were maintained in RPMI-1640 medium supplemented with 10% fetal bovine serum (FBS; Invitrogen, Carlsbad, California, U.S.A) and cultured at 37 ℃ in an atmosphere of 5% CO_2.

2.6 Cell Invasion and Migration Assays Using Boyden

Chambers

For miR-148a analysis, cells were transfected with a miR-148a precursor and a miR-148a inhibitor (50 pmol). For 14-3-3β analysis, cells were transfected with 14-3-3β and pcDNA3 control vector (8 μg). They were mixed with lipofectamine 2000 and transfected into the tumor cells according to manufacturer's instructions (Invitrogen Inc.). After 24hr, migration assays were performed with modified Boyden chambers with filter inserts (pore size, 8 μm) and invasion assays were also studied by coating the chambers with Matrigel (35 μg, BD Biosciences, California, USA) based on previously described methods [51]. AGS (2.5×10^4 cells), TSGH (2.5×10^4 cells), N87 (2.5×10^4 cells), SC-M1 (1×10^5 cells) and MKN-45 cells (2×10^5 cells) in 100μl medium were added to the upper chamber and cells were fixed, stained, viewed and counted by a light microscope (Olympus) after 48hr in culture. Each experiment was performed in triplicate.

2.7 Wound Healing Assay

Cell monolayers were wounded after transfection for 48hr by scratching with a 200 μl pipette tip. Debris was removed by washing and the scratched cells were incubated for 24hr. Distances between wound edges were measured at five different locations under x20 magnification by a microscope and analyzed using Metamorph version 7.0 software.

2.8 Cell Adhesion Assay

Adhesion assays were performed using Matrigel coated 96-well plates that were incubated at 37°C for 1hr. 5×10^3 cells per 100μl were seeded in each well and

incubated at 37℃ for 15 minutes. After incubation, non-adhesive cells were washed with PBS and the cells were fixed with 4% formaldehyde at room temperature for 20 minutes. Cells were washed and stained with 0.05% crystal violet. Cells were viewed and counted using a microscope (Olympus). Each experiment was repeated three times.

2. 9 Cell Proliferation Assay

Cell growth was measured in real-time using the xCELLigence system (Roche Applied Science and ACEA Biosciences). 7.5 x 10^3 cells were seeded in each well of an E-plate 16 (Roche Applied Science and ACEA Biosciences) and incubated at 37℃ for 48hr. After incubation, cells were transfected with a miR-148a precursor and inhibitor and the growth of living cells were monitored in real-time.

2.10 Luciferase Reporter Assay

A luciferase assay was used to analyze the relationship between miR-148a and plasminogen activator inhibitor 1 (PAI-1), guanine nucleotide exchange factor VAV2 (VAV2), integrin alpha-5 (ITGA5), integrin beta-8 (ITGB8) and 14-3-3β. Luciferase reporters containing the target sites in 3'-UTRs of these genes were constructed using the following oligonucleotides: for PAI-1: (sense) 5'-AATGCGAGCTCTTTTGATTTTGCACTGGACGGTGACGTGCTCAGCAAGCTT AATGC-3' and (antisense) 5'-GCATTAAGCTTGCTGAGCACGTCACCGT CCAGTGCAAAATCAAAAGAGCTCGCATT-3'; for VAV2: (sense) 5'-AATGCGAGCTCTGGTTTTTGCACTGCAGCTCAGCAAGCTTAATGC-3' and (antisense) 5'-GCATTAAGCTTGCTGAGCTGCAGTGCAAAAACCAGAGCT CGCATT-3'; for ITGA5: (sense) 5'-AATGCGAGCTCCCTGCCAGCTGCACTGAT

12

GCTGGCTCAGCAAGCTTAATGC-3' and (antisense) 5'-GCATTAAGCTTGC TGAGCCAGCATCAGTGCAGCTGGCAGGGAGCTCGCATT-3'; for ITGB8: (sense) 5'-AATGCGAGCTCGCACTGAGCTCAGCAAGCTTAATGC-3' and (antisense) 5'-GCATTAAGCTTGCTGAGCTCAGTGCGAGCTCGCATT-3' and for 14-3-3β: (sense) 5'-AATGCGAGCTCTGCACTGAGCTCAGAAGCTTAATGC-3' and (antisense) 5'-GCATTAAGCTTCTGAGCTCAGTGCAGAGCTCGCATT-3'. The oligonucleotides were annealed and the product was digested with HindIII and SacI (New England Biolabs Ltd., Ipswich, MA, USA) and cloned into the pMIR-REPORT luciferase expression vector (Ambion, Austin, TX). Positive clones were digested with BlpI restriction enzyme for screening (New England Biolabs Ltd., Ipswich, MA, USA) and the selected clones were verified by sequencing (Mission Biotech Co. Ltd). AGS cells cultured in a 24-well plate (8×10^4 cells per well) were transfected with 200ng each of luciferase and β-galactosidase luciferase reporter vectors and co-transfected with 50μM miR-148a precursor or miR-148a inhibitor. After transfection for 48hr, firefly luciferase and β-galactosidase were measured sequentially with a Spectramax M5 ELISA reader (Molecular Devices Corporation) using the Dual-Light system (Applied Biosystems) according to the manufacturer's protocol. β-galactosidase activity was used for normalization of transfection efficiency.

2.11 Protein Extraction

Cell samples were lysed in lysis buffer containing 7M urea (Boehringer, Mannheim, Germany), 2M thiourea, 4% CHAPS (J.T. Baker, Phillipsburg, NJ) and 0.002% bromophenol blue (Amersco, OH), sonicated and clarified by centrifugation before the protein concentration of each sample was determined using a protein assay kit (Bio-Rad,

Hercules, CA, USA). Tissues were stored in liquid nitrogen until use. All tissue samples were air-dried at -50°C and homogenized by grinding in liquid nitrogen. Protein lysates were extracted, sonicated and centrifuged and the protein concentration was then measured.

2.12 Immunoblotting

Proteins were transferred onto PVDF membranes (Immobilon-P membrane; Millipore Corp, Bedford, MA), incubated with antibodies against PAI-1 (Santa Cruz Biotechnology, Santa Cruz, CA), VAV2 (Epitomics Biotechnology, Burlingame, CA), ITGA5 (Santa Cruz Biotechnology, Santa Cruz, CA) and ITGB8 (Santa Cruz Biotechnology, Santa Cruz, CA). Primary mouse monoclonal antibodies against 14-3-3β (Abcam, Cambridge, UK) were used at a 1:1000 dilution ratio and the candidate proteins were visualized with the enhanced chemiluminescence (ECL) detection kit (Pierce, Boston Technology, Woburn, MA) and exposed to X-ray film.

2.13 Isobaric Tag for Relative and Absolute Quantitation (iTRAQ)

Isobaric tags for relative and absolute quantitation (iTRAQ) was purchased from Applied Biosystems (Foster City, CA). Tris (2-carboxyethyl) phosphine hydrochloride (TCEP), triethylammonium bicarbonate (TEABC), methyl methanethiosulfonate (MMTS), trifluoroacetic acid (TFA), and HPLC grade acetonitrile (ACN), and 4-(2-hydroxyethyl)-1-piperazineethanesulfonic acid (HEPES), rabbit anti-actin polyclonal antibody were from Sigma-Aldrich (St. Louis, MO). Monomeric acrylamide/bisacrylamide solution (40%, 29:1), ammonium persulfate and protein assay

dye were from Bio-Rad (Hercules, CA). Iodoacetamide, N,N,N′,N′-Tetramethylethylethylenediamine (TEMED) and sodium dodecyl sulfate (SDS) were from Amersham Biosciencs/GE Healthcare (Pittsburgh, PA). Trypsin (modified, sequencing grade) was from Promega (Madison, WI). Water was obtained from a Milli-Q_ Ultrapure Water Purification System (Millipore, Billerica, MA).

2.13.1 Gel-Assisted Digestion of Cell Lysate

Cells were lysed in lysis buffer (0.25 M Tris-HCl, pH 6.8, 1% SDS). The protein samples from cell lysate were subjected to gel-assisted digestion [24]. Briefly, the samples were reduced with 5 mM TCEP, alkylated with 2 mM MMTS, and incorporated directly into polyacrylamide gel in the eppendorf tube. For 100 μL of lysate solution, 37 μL of acrylamide/bisacrylamide solution (40%, v/v, 29:1), 3.7 μL of 10% (w/v) APS, and 1 μL of 100% TEMED were applied for gel formation. The gel was then cut into small pieces, which were washed several times with TEABC containing 50% (v/v) ACN and further dehydrated with 100% ACN before being completely dried using a SpeedVac. Proteolytic digestion with trypsin was then carried out (protein/trypsin = 10:1, g/g) in 25 mM TEABC overnight at 37 ℃. The tryptic peptides were extracted from the gel by sequential extraction with 25 mM TEABC, 0.1% (v/v) TFA in water, 0.1% (v/v) TFA in ACN, and finally 100% ACN. The solutions were then combined and concentrated using a SpeedVac. The resultant peptides were resuspended in 0.5 M TEABC for iTRAQ labeling.

2.13.2 iTRAQ Labeling and Fractionation by Strong Cation Exchange (SCX) Chromatograph

To label peptides with iTRAQ reagent, 1 unit of iTRAQ reagent, which is sufficient to label 100 μg of protein, was thawed and reconstituted in ethanol (70 μL) by vortexing for 1 min. The peptide solutions obtained from cells with miR-148a precursor, precursor negative control, anti-miR-148a inhibitor and inhibitor negative control were labeled with $iTRAQ_{114}$, $iTRAQ_{115}$, $iTRAQ_{116}$ and $iTRAQ_{117}$, respectively, and then incubated at room temperature for 1 h. The labeled peptides were pooled, acidified by mixing with buffer A (5 mM KH2PO4 and 25% (v/v) ACN, pH 3.0) to a total volume of 1 mL, and fractionated by SCX chromatography. For peptide fractionation, iTRAQ-labeled peptides were loaded onto a 2.1 x 200-mm polysulfoethyl A column containing 5- m particles with 200- m pore size (PolyLC, Columbia, MD). The peptides were eluted at a flow rate of 200 l/min with a gradient of 0–25% buffer B (5 mM KH2PO4, 350 mM KCl, and 25% (v/v) ACN, pH 3.0) for 30 min followed by a gradient of 25–100% buffer B for 20 min. The elution was monitored by absorbance at 214 nm, and fractions were collected every 1 min. Each fraction was vacuum-dried and then resuspended in 0.1% (v/v) TFA for further desalting and concentration using ZipTips^{TM} (Millipore, Bedford, CA).

2.13.3 LC-MS/MS Analysis

iTRAQ-labeled samples were reconstituted in 6 μL of eluent buffer A (0.1% (v/v) FA in H2O) and analyzed by LC-MS/MS using a Waters Q-TOF Premier (Waters Corp., Milford, MA). Samples were injected into a 2 cm× 180 μ m capillary trap column and separated on a 25 cm × 75 μm Waters ACQUITY 1.7 μm BEH C18 column using a nanoACQUITY Ultra Performance LC system (Waters Corp., Milford, MA). The column was maintained at 35 °C and bound peptides were eluted for 120 min using a

linear gradient of 0-80% eluent buffer B (0.1% FA in ACN). Mass spectrometry was operated in ESI positive V mode with a resolving power of 10 000. A NanoLockSpray source was used for accurate mass measurement, and the lock mass channel was sampled every 30 s. The mass spectrometer was calibrated with a synthetic human [Glu^1]-Fibrinopeptide B solution (1 pmol/μL, from Sigma Aldrich) delivered through the NanoLockSpray source. Data acquisition was operated in the data directed analysis. This method included a full MS scan (m/z 400-1600, 0.6 s) and 3 MS/MS scans (m/z 100-1990, 1.2 s each scan) run sequentially on the three most intense ions present in the full scan mass spectrum.

2.13.4 Data Processing and Analysis

For protein identification, data files from the LC-MS/MS were processed using Proteinlynx GlobalServer 2.2.5 (Waters Corp., Milford, MA). The peak list in the MS/MS spectra generated under the processing parameters were as follows: background subtraction, adaptative; background threshold, 35%; background polynomial, 5; smoothing type, Savitzky-Golay; smoothing iteration, 2; smoothing window, 3 channels; deisotoping type, medium; and deisotoping threshold, 3%. The resultant MS/MS data set was exported to *mgf and searched against the International Protein Index (IPI) human database (v. 3.64, 84032 sequences) from the European Bioinformatics Institute using the Mascot algorithm (v2.2, Matrix Science, London, United Kingdom). Search parameters for peptide MS and MS/MS mass tolerance were ±0.1 and ±0.1 Da, respectively, with allowance for two missed cleavages made from the trypsin digest, and variable modifications of deamidation (NQ), oxidation (M), iTRAQ (N terminal), iTRAQ (K) and MMTS (C). For confident protein identification, we used peptides with scores ≥ 43 ($P < 0.05$, FDR = 1.05%). To evaluate the protein identification false

discovery rate (FDR), we performed the searches using identical search parameters and validation criteria against a randomized decoy database created by Mascot. For protein quantitation, the iTRAQ ratios were determined for all peptides and proteins using Multi-Q software that we previously developed.41 The raw data files from the Q-TOF Premier were converted into files in the mzXML format using Masswolf (MassLynx converter, Waters Corp., Milford, MA), and the search results in Mascot were exported in the commaseparated value (csv) data format. After the data conversions, Multi-Q selected unique, iTRAQ-labeled peptides with confident MS/MS identification (Mascot score $\geqq 43$), detected signature ions (m/z =114, 115, 116, and 117) and performed automated quantitation of the peptides' abundance. For the detector dynamic range filter, signature peaks with ion counts lower than 30 counts were filtered out by Multi-Q. To calculate average protein ratios, the ratios of quantified and unique iTRAQ peptides were weighted according to their peak intensities to minimize the standard deviation. The final results of the protein quantitation were exported to an output file in the csv data format.

2.14 Ingenuity Pathway Analysis (IPA)

IPA software is often used to analyze PPI, construct PINs and elucidate associated biological processes of PINs. Recently, many studies report that miRNA affects tumor progression through regulating network activity based on IPA analysis. For example, IPA results showed that miR-21 affects tumor growth of glioblastoma cell through regulating a key tumor-suppressive network [52]. To study the regulatory roles of miR-148a-regulated PPI network, we analyzed iTRAQ data, identified significantly differentially expressed proteins and used these identified proteins to discover

associated biological functions of its regulated network by using IPA 9.0 software (Ingenuity System).

2.15 Gastric Cancer Patients and Clinical Data

The use of human tissue samples and serum were approved and the confidentiality of human subjects was protected by the Institute Review Board (IRB, No. 200612109R). A total of 145 gastric cancer patients who had undergone curative intent radical gastrectomy at the National Taiwan University Hospital from July 2001 to March 2006 were included in this study. They were staged according to the World Health Organization, Lauren's classification and International Union against Cancer (UICC) TNM system (Table 1) [53, 54]. Patients who had undergone curative intent resection were classified according to the following criteria: complete removal of a primary gastric tumor, D2 dissection of regional lymph nodes, absence of any macroscopic tumors remaining at the site of resection and absence of metastases in the liver, lungs or distant organs at the time of surgery. In addition, the patient should have been clear of any concomitant primary cancers and had not received chemotherapy or radiotherapy prior to surgery. Clinicopathologic factors including age, sex, Borrmann and Lauren classifications, depth of tumor invasion, status and number of lymph node metastases, vascular invasion and tumor size (length × width of tumor) were also considered and stored in the patients' database. Organ invasion was defined as direct tumor invasion into at least one adjacent structure such as the duodenum, esophagus, liver, mesocolon or diaphragm. Patient follow-up occurred from 3 to 46 months after surgery and the follow-up intervals were calculated as survival intervals after surgery. Furthermore, association between serum 14-3-3β levels and the above-mentioned clinical outcomes

were evaluated.

2.16 Blood and Tissue Sample Collection

31 post-operative serum samples were also collected from the 145 gastric cancer patients. Three different control groups were included: 19 endoscopically diagnosed with gastric ulcer, 19 with non-ulcer dyspepsia and 25 healthy controls. Venous blood samples were collected in plain tubes, allowed to clot and then centrifuged at 2,000 rpm (Kubota, Bunkyo-Ku, Japan) at room temperature for 10 min. Aliquots of the separated sera were individually stored below -80°C until serum 14-3-3β concentrations were assayed. 40 pairs of tumor and tumor-adjacent normal tissue specimens were also obtained from these 145 gastric cancer patients. The paired tissue samples were dissected within 30 minutes of gastrectomy and frozen in liquid nitrogen.

2.17 ELISA for 14-3-3β

To detect the serum levels of 14-3-3β, ELISA was performed according to previously published methods [55-57]. Monoclonal anti-14-3-3β antibody (4 μg/ml, Abcam, Cambridge, U.K.) was incubated on streptavidin-coated 96-well microwell plate overnight at 4°C. After blocking, the 14-3-3β standard antigen and all diluted serum samples (1:400) were incubated on the plate for 3hr. Subsequently the plate was washed and incubated with polyclonal anti-14-3-3β antibody (0.08 μg/ml, Upstate Biotechnology, Inc., Lake Placid, NY) for 2hr. 100μl of polyclonal goat anti-rabbit horseradish peroxidase-conjugated IgG antibody (0.04 μg/ml) was added and incubated for 1h. The plate was washed and added with tetramethylbenzidine substrate solution

(TMB, Bionova Biotechnology, Dartmouth, NS, Canada) for 30 min. The reaction was stopped by adding 2 M sulfuric acid. Protein concentration of 14-3-3β and unknown samples was determined by measuring the absorbance at 450 and 570 nm using an ELISA reader.

2.18 Construction of the 14-3-3β Over-expressing Plasmid

Reverse transcription-polymerase chain reaction was used to synthesize cDNA from the total RNA extracted from TSGH cells, and amplify the 14-3-3β product using specific forward (5'-GGTACGTAAGCTTGCCACCATGACAATGGATAAAAGT-3') and reverse (5'-AGTCGAGAATTCTTAGTTCTCTCCCTCCCC-3') primers. The product was cloned into a pcDNA3 vector (Invitrogen Inc.) and verified by sequencing (Mission Biotech Co. Ltd).

2.19   3-(4,5-Dimethylthiazol-2-yl)-2,5-Diphenyltetrazolium Bromide (MTT) Assay for Cell Growth

AGS cells were cultured in a 24-well plate at 5 x 10^4 /well for 24 hours and then transfected with 3 μg each of 14-3-3β and control vectors for 24 and 48 hours. 100 μL of MTT reagent was added to each 1 mL of culture medium and measured at 570 nm using an ELISA reader. Each experiment was performed in quadruplicate.

2.20 Two Dimensional Electrophoresis and Image Analysis

The protein profiles of 14-3-3β-over-expressing and control gastric cancer AGS cells were analyzed using 2-DE. 500 μg of total protein was separated by 2-DE [58].

For separation in the first dimension, isoelectric focusing (IEF) was performed using an 18cm strip (pH 4-7) in an IPGphor isoelectric focusing system (Amersham Pharmacia Biotech, Uppsala, Sweden) at 8000V for a total of 91.2 KVhr at 20°C. The strips were then transferred onto a 12.5% non-gradient SDS-PAGE gel for second dimensional separation. The 2-D images were analyzed using ImageMaster software version 6.0 (Amersham Pharmacia Biotech) to detect and quantify protein spots. The expression profiles were performed in triplicate.

2.21 In-gel Digestion and Mass Spectrometry

The differentially expressed proteins were excised from 2D-gels, digested with trypsin and the tryptic peptides were extracted from the gel. These protein spots were analyzed according to our previously published method [58]. Samples were resuspended in 0.1% trifluoroacetic acid (TFA) and matrix (5mg/mL CHCA dissolved in 50% acetonitrile (ACN), 0.1% v/v TFA and 2% w/v ammonium citrate). The peptide mixture was then loaded onto a MALDI plate (PerSeptive Biosystems, CA, USA) and samples were analyzed by a MALDI-Q-TOF Ultima MALDI Mass Spectrometer (Micromass, Manchester, UK) that was fully automated with a predefined probe motion pattern and peak intensity threshold for switching over from MS survey scan to MS/MS, and from one MS/MS to another. The peak lists were acquired by the MassLynx^{TM} version 4.0 software and the raw data were processed to enable a database search using ProteinLynx Global Server 2.2 (PLGS 2.2). From the MS spectrum, the highest 5 precursors that had a signal-to-noise ratio of more than 50 were selected for subsequent MS/MS analysis. Starting from the peak of greatest intensity, parent ions that met the predefined criteria (any peak within the m/z 800 - 3000 range with an intensity of above a count of 10 ±

include/exclude list) were selected for collision induced dissociation (CID) MS/MS using argon as a collision gas and a mass dependent ± 5V rolling collision energy until the end of probe pattern was reached. The LM and HM resolution of the quadrupole were both set at 10 to give a precursor selection window of approximately 4 Da. The instrument was calibrated to less than 5 ppm accuracy over the mass range of m/z 800 - 3000 using a sodium iodide and PEG 200, 600, 1000 and 2000 mixture and was further adjusted with Glu-Fibrinopeptide B as the near-point lock mass calibrant during data processing. At a laser firing rate of 10Hz, individual spectra from a 5 second integration period that was acquired for each of the MS surveys and MS/MS performed were combined, smoothed, deisotoped (fast option) and centroided using the Micromass PKGS 2.2 data processing software. The following MS default parameters were used: background subtract type, normal; background threshold, 35%; background polynomial, 5; perform smoothing, yes; smoothing type, savitzky-golay; smoothing iteration, 1; smoothing window, 2 channels; combine options, all; but low mass threshold, 1500Da; intensity range, 2 to 100 were not used. The following MS/MS default parameters were used: background subtract type, normal; background threshold, 35%; background polynomial, 5; peptide filter; but perform smoothing, no; smoothing type, savitzky-golay; smoothing iteration, 2; smoothing window, 3 channels were not used [59]. The combined peptide mass fingerprinting (PMF) and MS/MS ion meta data were searched in concert against the specified protein database within the PLGS 2.2 workflow [59]. Alternatively or additionally, the PMF and individual MS/MS ion data can be displayed as Mascot-searchable .txt file and .pkl files for independent searches using MASCOT (version 2.3) against the SWISS-PROT (version 57.11) database (512994 sequences; 180531504 residues) of *Homo sapiens*. The search parameters were as follows: enzyme, trypsin; fixed modifications, carbamidomethylation of cysteines;

23

variable modifications, oxidation of methionine; one missed tryptic peptide cleavage; peptide tolerance, ±50ppm; fragment MS/MS tolerance, ±0.25Da; mass values, monoisotopic; peptide charge, +1. The cut-off score of MS/MS was approximately 21 and the score values were calculated by MASCOT based on the Mowse algorithm. Peptide matches were analyzed using mass values (MS/MS fragment ion masses) and scores were reported as $-10*LOG_{10}(P)$, where P is the absolute probability which is used to measure the significance of a result when a match is random and the size of the searched sequence database is known. The accepted threshold was defined as an event expected to occur at random with a frequency of less than 5%. Identified proteins with statistically significant protein scores higher than ion scores ($p < 0.05$, based on MS/MS spectra) were selected at 95% confidence level for matched peptides.

2.22 Statistical Analysis

To analyze the correlations between miRNAs, 14-3-3β and their corresponding clinical outcomes, patients were divided into different groups based on clinical and pathologic parameters. Student's *t*-test was used to compare the differences between two clinicopathological groups. Comparisons between multiple groups were done using one-way ANOVA (SAS 9.1 software). *P* values were two sided and the alpha level of significance was defined as $P < 0.05$. Correlations between numeric variables were analyzed using MedCalc 9.0, where the data are shown as a correlation coefficient with a *P*-value. Receiver operating characteristics (ROC) curves were used to assess miR-148a or serum 14-3-3β concentrations as a diagnostic for gastric cancer by plotting sensitivity versus 1-specificity, and the area under the curve was subsequently calculated. The area under the curve (AUC) was then used as indicators of the capacity

of miR-148a or 14-3-3β to act as a diagnostic marker, with higher AUC values reflecting higher diagnostic capacities. Recurrence-free survival and overall survival curves were generated according to the Kaplan-Meier method to study the relationship between miR-148a or serum 14-3-3β expression and patient survival, where the analytic method used was log-rank test. Cox proportional hazards regression models determined their prognostic independence of clinical factors. In addition, the difference in D values between high and low groups for the 23 down-regulated miRNAs (median was used as a cut-off value) was calculated by paired Wilcoxon rank sum test. A paired Student's t test was used to compare the changes in 14-3-3β plasma levels between pre-operative and post-operative patients. The alpha level of significance was defined as $P < 0.05$.

Chapter 3   Results

3.1 MicroRNA-regulated PINs in Gastric Cancer

Although microRNAs are known to reduce the levels of their target mRNAs [60], expression of a miRNA target may not always co-vary, in the reverse direction, with its miRNA regulator, due to the presence of primary TF regulation. A reverse correlation in expression profiles between a miRNA and corresponding predicted targets increases the confidence of the conditional miRNA-target interaction. Based on these observations, we combined differentially expressed miRNAs and target genes, down-regulated (up-regulated) miRNAs versus up-regulated (down-regulated) targets, to identify the miRNA-regulated PINs in gastric cancer. The miRNA-regulated PINs were established according to the proteins encoded by differentially expressed target genes and their interacting partners in the human PIN. However, only 23 significantly down-regulated miRNAs and no significantly up-regulated miRNAs were found (see Methods). Consequently, we identified 23 PINs that were modulated by 23 down-regulated miRNAs in gastric cancer. Furthermore, the activities of miRNA-regulated PINs in normal and tumor tissues, activated or inactivated, were investigated on the basis of the enrichment of co-expressed PPIs (CePPIs) in the network (Table 2, 3). Among the 23 down-regulated miRNA-regulated PINs, 70% (16/23) of them were activated in tumors (Fisher's exact test, $P < 0.001$). On the other hand, 51% (20/39) of the remaining 39 unchanged miRNA-regulated PINs were inactivated in both tumor and normal tissue (Fisher's exact test, $P = 0.003$). Thus, we conclude that 16/23 networks are activated in gastric cancer and that these networks are modulated as a result of down-regulated miRNAs expression. Therefore, we suggest that the 16 down-regulated miRNAs act as oncomirs and function as tumor suppressors.

Additionally, we assessed the discrimination power of miRNA expression levels to classify normal and tumor samples by calculating the receiver operating characteristic (ROC) curves and the area under the curve (AUC). Among the 23 down-regulated miRNAs, the one that provided the best discrimination was miR-29c (AUC = 0.831, $P <$ 0.001), which gave an overall correct classification of 77%. Moreover, of the 16 oncomirs, miR-29c, miR-768-3p, miR-26a, miR-143 and miR-148a were found to give an AUC of more than 0.7 ($P < 0.05$) individually. When all the 16 oncomirs were combined, the overall correct classification was elevated to 93% (AUC = 0.981, $P <$ 0.0001). Among the remaining 7 down-regulated miRNAs, only miR-16 and miR-145 were found to have an AUC of more than 0.7. When these 7 miRNAs combined, the overall correct classification was 82% (AUC = 0.888, $P < 0.0001$) (Table 4). Taken together, the 16 oncomirs showed greater discrimination between tumor and normal tissues than the remaining 7 down-regulated miRNAs.

We also investigated the relationship between the expression levels of the 23 down-regulated miRNAs and survival rates. The median was used as a cut-off value and as a result, the expression levels for each miRNA were divided into two groups; high and low expressed. The maximum of the difference in survival rates (D_{max}) between high and low groups was further calculated (Figure 2A). Our findings indicated that the D_{max} among the 16 oncomirs was more significant ($P < 0.0001$, Figure 2B) than that in the remaining 7 down-regulated miRNAs (paired Wilcoxon rank sum test, $P = 0.016$, Figure 2C). These results suggest that the 16 oncomirs may act as better prognostic markers for gastric cancer in comparison to the remaining 7 down-regulated miRNAs. Therefore, we conclude that the 16 oncomirs have the potential to suppress tumor biogenesis.

3.2 The Potential Functions of Oncomir-regulated PINs

A key question is whether the 16 oncomirs regulate tumor progression-related biological processes in gastric cancer. To address this, we developed a PIN-based approach to reveal the possible functional roles of miRNAs (see 2.3 section MiRNA-regulated PIN Identification and Analysis and Figure 1). Applying this PIN-based approach to 16 oncomirs, the enriched biological processes of their regulated PINs can be discovered (Table 5). It was observed that most of the enriched biological processes were related to tumor progression. For instance, miR-142-3p- and miR-768-3p-regulated PINs were related to apoptosis and cell cycling, respectively. Interestingly, the miR-148a-regulated PIN was the only network that was associated with cancer metastasis-related functions, such as integrin-mediated signaling, cell-matrix adhesion and wound healing. Therefore, miR-148a was chosen for the further studies.

3.3 MiR-148a-regulated PIN and Its Potential Functions in Gastric Cancer

To further confirm the abundance of miR-148a in tumor tissues, we performed qRT-PCR in 62 paired tumor and normal tissues and found its expression levels in tumor tissues were significantly lower than those in normal tissues ($P < 0.0001$, paired t-test) (Figure 3A), which was consistent with our miRNA microarray data. Additionally, the impact of miR-148a expression levels on the prognosis of gastric cancer patients by Kaplan-Meier survival analyses was studied in the 62 paired tissues. Patients with high miR-148a expression levels showed significantly higher 5-year overall survival rates (71.4%, log-rank test, $P = 0.03$; Figure 3B) compared with patients with low miR-148a

levels (32.1%, log-rank test, $P = 0.03$). Univariate analysis showed that miR-148a and early stages correlated with better survival, whereas peritoneal and vascular invasion predicted very poor outcomes. On multivariate analysis, miR-148a retained an independent prognostic power on overall survival (HR = 1.69; $P = 0.002$) (Table 6). A ROC curve was also used to evaluate miR-148a as a diagnostic marker for gastric cancer. The AUC was then used as an indicator of the capacity of miR-148a to act as a diagnostic marker, with higher AUC values reflecting a higher diagnostic potential. ROC curve analysis of miR-148a showed that it had an AUC of 0.84 (ROC curves analysis, $P = 0.0001$, Figure 3C). These results indicate that miR-148a could discriminate between normal and tumor tissues and serve as an effective prognostic marker for gastric cancer. Based on these results, we conclude that miR-148a is highly associated with gastric cancer. The miR-148a-regulated PIN was visualized in Figure 3D and the enriched biological processes of this network are shown in Figure 3E. The significantly over-represented GO functional terms were separated into three functional groups, including cell-matrix adhesion (hypergeometric test: $P = 9.5619E-6$), wound healing ($P = 5.8018E-5$) and cell surface receptor linked signal transduction ($P = 5.3054E-5$). These three enriched GO functions suggest that miR-148a is related to cancer metastasis and is likely to regulate these three functions through its regulated PIN.

3.4 PAI-1, ITGB8, VAV2 and ITGA5 Are Oncogenes and Direct Targets of MiR-148a

Four target genes of miR-148a were identified to be up-regulated within its regulated PIN, including PAI-1 (a coagulation factor), ITGB8 (an adhesion factor),

VAV2 and ITGA5 (involved in the integrin-mediated signaling pathway). To further explore whether miR-148a affected cancer metastasis through its regulated PIN, a luciferase reporter assay was performed to analyze the relationship between miR-148a and these target genes. miR-148a over-expression significantly reduced the expression levels of these target genes, while their expression levels were significantly elevated in anti-miR-148a inhibitor-transfected tumor cells (t-test, $P < 0.05$, Figure 4A). We carried out luciferase assay for site mutant to further ensure the correlations between miR-148a and these four genes (Figure 4B-4F). We constructed each putative miR-148a target sites or its site mutation in sequences corresponded to seed sequence of miR-148a into a pMIR-REPORT luciferase expression vector (Figure 4B) and analyzed reporter assays (Figure 4C-4F). Our results showed that the repressions by miR-148a in these four genes were completely abolished. These results suggest that these four genes are direct targets of miR-148a. These observations suggest that miR-148a plays a significant role in affecting the biological functions of gastric cancer cells by regulating the expression of target genes within its regulated PIN.

In addition to being markers for the detection and prognosis of many types of cancers [61-70], these four genes have previously been reported to be implicated in the promotion of cell invasion, migration, adhesion, growth and angiogenesis, which suggests a possible role for these genes in the regulation of tumor oncogenesis and progression. To determine whether these genes played a role in the oncogenesis of gastric cancer, their expression levels in tumor tissues were measured by immunoblotting. All four genes showed higher expression levels in tumor tissues compared with normal tissues (Figure 5), indicating that they might have potential oncogenic functions and were likely to be key downstream effectors of miR-148a in this network.

3.5 The Correlation Between miR-148a and Clinicopathological Factors

To evaluate the clinical significance of miR-148a in gastric cancer, the relationship between miR-148a expression levels in tumor tissues and the degree of metastasis was analyzed. Clinical analyses revealed that high expression levels of miR-148a significantly correlated with a reduction in distant metastasis (t-test, $P = 0.043$), organ invasion (t-test, $P = 0.013$) and peritoneal invasion (t-test, $P = 0.04$) (Table 7). These results suggest that miR-148a reduces the aggressiveness of gastric cancer. Interestingly, our findings revealed that several functions, including migration (integrin-mediated signaling pathway) and adhesion, were identified within the miR-148a-regulated PIN and were also associated with an aggressive tumor phenotype. This indicates that miR-148a likely plays an important role in regulating the malignant progression of tumor cells.

3.6 MiR-148a Inhibits Cell Invasion, Migration, Adhesion and Growth

In vitro invasion assays were performed to examine whether miR-148a suppressed more aggressive forms of tumors. Human gastric cancer AGS, SC-M1 and MKN-45 cell lines were transfected with a miR-148a precursor or an anti-miR-148a inhibitor. The results showed that over-expression of miR-148a in these cell lines significantly reduced tumor cell invasion, while anti-miR-148a-treated tumor cells showed elevated tumor cell invasion (Figure 6A). To determine whether miR-148a over-expression also affected tumor progression, migration, adhesion and proliferation assays were

performed on miR-148a-transfected tumor cells. Our findings indicated that over-expressed miR-148a significantly reduced tumor cell migration and adhesion, while anti-miR-148a-treated tumor cells showed significantly elevated migratory and adhesive abilities (Figure 6B and 6C). Additionally, tumor cell growth was observed to be reduced in response to miR-148a over-expression (Figure 7A and 7C), but elevated in response to anti-miR-148a inhibitor treatment (Figure 7B and 7D). Taken together, these observations indicate that miR-148a can inhibit cell invasion, migration, adhesion and growth, thereby acting as a potent regulator of tumor suppression.

3.7 miR-148a Induces Apoptosis of Gastric Cancer Cells

We have demonstrated that miR-148a could suppress growth of gastric cancer cells (Figure 8). To determine whether miR-148a over-expression also induces cell apoptosis, we observe apoptosis-related protein expression in miR-148a over-expressing AGS cells. The results indicated that over-expressed miR-148a significantly reduced Apaf-1, cytochrome c, caspase-9 and cleaved Poly (ADP-ribose) polymerase (PARP) activation, while anti-miR-148a-treated tumor cells showed significantly lower Apaf-1, cytochrome c, caspase-9 and cleaved PARP expression (Figure 8). Our findings suggest that miR-148a suppresses cell growth and induces cell apoptosis.

3.8 miR-148a-regulated Proteome and Associated Biological Functions

miRNAs have known to be involved in the regulation of tumorigenesis and cancer progression through obstructing protein translation of targets or causing their mRNA degradation [4]. To deeply understand the regulatory roles of miR-148a in gastric cancer

progression, in this study, we used iTRAQ method to discover miR-148a-regulated proteome. We first analyzed iTRAQ data and then compared as well as identified significantly differentially expressed proteins between miR-148a precursor and its negative control-treated AGS cells. The cut-off values were determined based on that the expression levels of all indentified significantly expressed proteins in the mixture of 1:1 proportion of miR-148a precursor negative control-treated tumor cells in two different biological duplicate. We determined the maximum (mean + 2SD) and minimum (mean - 2SD) cut-off values were 1.32 and 0.8, respectively, suggesting that these proteins were defined as significantly up-regulated proteins while the expression ratio of these proteins in miR-148a precursor-treated tumor cells was more than 1.32 when compared with its negative control. Additionally, as the expression ratio of other proteins in miR-148a precursor-treated tumor cells was less than 0.8 when compared with its negative control, they were defined as significantly down-regulated proteins. As shown in Table 8, we finally identified 16 significant up-regulated and 41 down-regulated proteins in miR-148a precursor-treated AGS cells. Among them, Solute carrier family 2 facilitated glucose transporter member 1 (SLC2A1), Isoform 3 of Core histone macro-H2A.1 (H2AFY), Spermine synthase (SMS) and Podocalyxin-like protein 1 precursor (PODXL) were predicted targets of miR-148a based on TargetScanHuman 5.1 database. All proteins were analyzed in biological replicate and the expression ratio of these identified proteins between the two experiments were compared (Figure 9).

Furthermore, we used a total of these 57 identified significantly expressed proteins to analyze regulated biological processes by miR-148a by using IPA 9.0 software. Our results showed miR-148a regulated many key functions, mainly classified as three categories, including cancer, cell morphology and development and metabolism (Figure

10) and all these identified proteins involved in these functions were shown in Table 9. For cancer category, it includes gastrointestinal disease, genetic disorder, cell-mediated immune response, cell cycle, cell death, movement and growth as well as proliferation. For cell morphology and development category, it includes hair and skin development and function, organ development, development disorder, hematopoiesis, cardiovascular disease, neuron system development, function and neurological disease. For metabolism category, it includes carbohydrate, drug and vitamin mineral metabolism as well as metabolic disease. Interestingly, our previous data supported these key miR-148a-regulated functions that miR-148a was a potential tumor suppressor in gastric cancer and could repress migration (Figure 6B) and growth of tumor cells (Figure 7), as well as induce cell apoptosis (Figure 8).

3.9 14-3-3β Is a Direct Target of miR-148a

Our results uncovered that miR-148a was a potential tumor suppressor that could suppress metastasis-related abilities of gastric cancer cells. In addition, we found that 14-3-3β was a predicted target gene of miR-148a from TargetScanHuman 5.1 and Pictar databases. 14-3-3β has been reported to be associated with various types of cancer. For example, 14-3-3β is abundant in human lung cancer relative to normal tissues [32] and mutated chronic lymphocytic leukemia (M-CLL) relative to unmutated chronic lymphocytic leukemia (UM-CLL) [33]. Over-expression of 14-3-3β in NIH 3T3 cells (mouse embryonic fibroblast cell line) stimulated cell growth and supported anchorage-independent growth in soft agar medium and tumor formation in nude mice [34], while reducing 14-3-3β expression led to an inhibition of tumor progression due to decreased vascular endothelial growth factor (VEGF) production, inhibition of

angiogenesis and increased apoptosis. In addition, it has been shown that 14-3-3β promotes cell migration by interacting with integrin β1 [35] and activating the MAPK pathway, causing tumor cell metastasis [29, 30]. Thus, these studies support the idea that 14-3-3β could function as an oncogene. Chan *et al.* reported that 14-3-3β showed stronger expression in gastric cancer cells than in paired normal cells by using immunohistochemical staining analysis [30]. Taken together, these reports indicate that 14-3-3β is a potential oncogene in cancers and associated with cancer metastasis. To elucidate whether miR-148a suppresses metastasis of gastric cancer cells through regulating 14-3-3β expression, we first used luciferase assay to check their correlation. Our results indicated that miR-148a over-expressing tumor cells had decreased 14-3-3β expression, whereas 14-3-3β expression was elevated in anti-miR-148a inhibitor-treated tumor cells (Figure 11A and 11B). We also used western blotting method (Figure 11C) to confirm their correlation and the results were consistent with luciferase reporter assay that 14-3-3β was a direct target of miR-148a. These results implied that miR-148a may suppress tumor metastasis through regulating 14-3-3β expression.

3.10 14-3-3β Expression Is Positively Correlated with Aggressive Phenotypes of Gastric Cancer Cells

A key question is whether 14-3-3β affects malignant progression of gastric cancer cells. To address this possibility, we first detected expression profiles of gastric cancer cells by using 2-DE and MS approaches, including non-metastatic AGS and N87 cells and poor differentiated SC-M1 cells as well as high metastatic TSGH cells. A total of 125 differentially expressed proteins were chosen for further analysis by MALDI-TOF and identified from MS/MS data using the MASCOT search engine and the Swiss-Prot

database. We successfully identified 62 significantly differentially expressed proteins. Twenty six proteins among these 62 identified proteins were reported to be associated with cancer progression or they had cancer-relevant functions based on GO analysis (Table 10). Thus, we selected these 26 proteins for further investigation. Interestingly, 14-3-3β (spot 21) was expressed higher in metastatic TSGH and poor differentiated SC-M1 cells than non-metastatic AGS and N87 cells (Figure 12A-12D), and the 3-D profiles of 14-3-3β were shown in Figure 12E. Additionally, we further checked the endogenous 14-3-3β expression in four gastric cancer cell lines, including two non-metastatic cell lines AGS and N87, one poorly differentiated cell line SC-M1 and one high-metastatic cell line TSGH (Figure 13), by using western blotting method. We found that the expression levels of 14-3-3β were positively associated with aggressive phenotypes of gastric cancer cell lines. The results suggest that 14-3-3β may be associated with malignant progression of gastric cancer cells.

On the other hand, we also analyzed molecular functions of these identified proteins and found that their related functions were involved in cancer progression. For example, 78kDa glucose-regulated protein (GRP78), heat shock protein beta-1 (HSPB1), 60kDa heat shock protein, mitochondrial (CH60), annexin A5 (ANXA5), glutathione S-transferase P (GSTP1), 14-3-3 protein epsilon (YWHAE) and heat shock 70kDa protein 1A/1B (HSP71) were associated with apoptosis. Proteins involved in cell migration and angiogenesis and adhesion included annexin A3 (ANXA3) and ezrin (EZRI). Other proteins were involved in cytoskeleton and signal transduction. Additionally, we used the identified proteins in TSGH (metastatic cells) and SC-M1 (poor differential cells) to construct PIN and analyze related functions. PIN and the enriched functions in AGS and N87 (non-metastatic cells) were also performed. PIN in TSGH and SC-M1 cells was visualized in Figure 14A and the enriched biological

processes of this network were shown in Figure 14B. The significantly over-represented GO functional term was negative regulation of apoptosis ($P < 0.05$). There was no enriched function identified in AGS and N87 cells ($P > 0.05$). The results are consistent with those in Figure 12 and Figure 13 that 14-3-3β is expressed higher in malignant TSGH and SC-M1 tumor cells and involved in the negative regulation of apoptosis. Taken together, these results suggest that the identified proteins in TSGH and SC-M1 cells are related to tumor cell progression (Table 10, Figure 12) and 14-3-3β is likely to regulate malignant progression of gastric cancer cells.

3.11 Over-expression of 14-3-3β Enhances Cancer Cell Invasion, Migration and Growth

To further evaluate the regulatory effects of 14-3-3β on gastric cancer cells, we first used Boyden Chamber assay to observe invasiveness and migratory abilities of 14-3-3β-over-expressing tumor cells, including AGS, N87, SC-M1 and TSGH cells. Our findings revealed that 14-3-3β-over-expressing AGS cells had significantly greater invasiveness and migratory capabilities (Figure 15A and 15B) and higher cell growth (Figure 15C) than control cells. The functional studies of 14-3-3β in other gastric cancer cell lines, including N87, SC-M1 and TSGH, were shown in Figure 16. Taken together, these results suggest that 14-3-3β may regulate malignant progression of gastric cancer cells.

3.12 14-3-3β Expression in Tumor Tissues and Serum from Gastric Cancer Patients

In order to elucidate the roles of 14-3-3β in gastric cancer, we analyzed its expression levels in tumor tissues. Western blot analysis of 14-3-3β expression levels in paired tumor and tumor-adjacent normal tissues demonstrated that 14-3-3β expression was significantly increased in tumor tissues compared with normal tissues ($P < 0.01$; Figure 17A). Since 14-3-3β was over-expressed in gastric cancer tissues, its potential release into the periphery was assessed to determine whether it can be detected as a serologic biomarker for the disease. For this purpose, serum 14-3-3β levels were detected by ELISA. Serum 14-3-3β levels in 63 control subjects ranged from 89.4 to 969.9 ng/mL, and the mean and median values were 308.1 and 213.3 ng/mL, respectively. However, serum 14-3-3β levels in cancer patients ($N = 145$) ranged from 186.8 to 1846.2 ng/mL with mean and median values of 625.5 and 494.4 ng/mL respectively. In addition, pre-operative serum 14-3-3β levels in gastric cancer patients were significantly higher than those in controls ($P < 0.0001$, Figure 17B). Serum 14-3-3β levels in stage I gastric cancer patients were significantly higher than those in controls ($P = 0.005$) and ROC curve analysis determined serum 14-3-3β level of 262 ng/mL was the cut off value ($P < 0.001$). These results strongly suggest that serum 14-3-3β may be used as a potential biomarker for gastric cancer.

3.13 Serum 14-3-3β Levels and Overall and Recurrence-free Survival

Survival analysis was conducted in 142 available gastric cancer cases and survival curves were generated according to the Kaplan-Meier method. At the serum level of 349 ng/mL, 14-3-3β had high sensitivity (86%) and specificity (67%) for the detection of gastric cancer; thus, it was defined as the cut-off value. The patients were divided into

two groups, i.e. those that showed low expression of serum 14-3-3β and those with high expression of serum 14-3-3β. The 5-year overall survival rates for those with low and high serum 14-3-3β levels were 72.7% and 46.1% respectively, while the 5-year recurrence-free survival rates for those with low and high serum 14-3-3β levels were 59.9% and 35.0% respectively ($P = 0.038$ and $P = 0.037$, respectively, Figure 17C). Overall, the overall and recurrence-free survival rates of patients with 14-3-3β levels greater than 349 ng/mL were shown to be significantly lower, indicating that 14-3-3β serum levels are suitable as a prognostic marker in gastric cancer patients.

3.14 Serum 14-3-3β Levels Decrease after Gastrectomy with D2 Lymphadenectomy

Among 31 patients with abnormally high 14-3-3β levels, the mean and median of pre-operative serum 14-3-3β levels were 579 ng/mL and 515 ng/mL respectively. In contrast, the mean and median of post-operative serum 14-3-3β levels were 427 ng/mL and 378 ng/mL respectively (Figure 17D). Thus, serum 14-3-3β levels were significantly decreased after gastrectomy ($p < 0.0001$).

3.15 ROC Curves of 14-3-3β in Gastric Cancer

In this study, a ROC curve was used to evaluate serum 14-3-3β concentrations as diagnostic for gastric cancer by plotting sensitivity versus 1-specificity. AUC value was then used as an indicator of the capacity of 14-3-3β to act as a diagnostic marker, with higher AUC values reflecting higher diagnostic capacities. The AUC values for gastric cancer patients versus normal controls at different cancer stages were illustrated in Figure 18. The AUC of 14-3-3β was 0.776 for stage I (A), 0.843 for stage II (B), 0.822

for stage III (C), 0.882 for stage IV (D), and 0.83 for all gastric cancer samples (E). On the other hand, ROC curve analysis determined the cut-off value of serum 14-3-3β for the diagnosis of gastric cancer. A serum 14-3-3β level of 420 ng/mL was defined as the optimal cut-off value for differentiating between patients and controls. When using the cut-off value for the detection of gastric cancer, the serum 14-3-3β sensitivity, specificity and accuracy were 78%, 71% and 76%, respectively. Additionally, we compared the AUC between 14-3-3β and the other existing serum biomarkers such as CEA (Figure 19) and the results showed that 14-3-3β appeared to outperform the established tumor marker CEA.

3.16 The Relationship Between 14-3-3β Expression Level and Metastatic Lymph Node Number, Tumor Size and Cancer Stage

Our clinical analyses showed that pre-operative serum 14-3-3β levels were significantly associated with the number of metastatic lymph nodes ($r = 0.166$, $P = 0.045$) and tumor size ($r = 0.452$, $P < 0.0001$) (Figure 20A and 20B). 14-3-3β serum levels positively correlated with 14-3-3β expression in tumor tissues ($r = 0.385$, $P = 0.033$) (Figure 20C). Pre-operative serum 14-3-3β levels also increased with the depth of tumor invasion ($P = 0.043$), distance of metastasis from the primary site ($P = 0.03$) and peritoneal invasion ($P = 0.049$) (Table 11). These results provide evidence that 14-3-3β plays a crucial role in the migration and invasion of gastric adenocarcinoma.

Chapter 4   Discussion

miRNAs are known to function as gene silencers and their expression profiles have been reported to be negatively correlated with those of their target genes [60]. In particular, up-regulated target genes were found to be specific targets of down-regulated miRNAs in gastric cancer. To find out the miRNA-regulated PINs in gastric cancer, the expression profiles of miRNAs were integrated and analyzed within the human PIN. Twenty three down-regulated miRNA-regulated PINs were identified based on their up-regulated target genes in gastric cancer. Among these, sixteen PINs were activated. The results suggest that repressing these miRNAs in gastric cancer can activate their regulated PINs. This may be due to miRNA-mediated regulation of pivot genes, such as hubs [20], or differentially expressed genes in the biological networks. Therefore, we suggest that these 16 down-regulated miRNAs act as oncomirs and function as tumor suppressors. Additionally, these 16 oncomirs were associated with increased tumor suppression potential and increased survival rates compared with the 7 remaining down-regulated miRNAs, suggesting that these oncomirs can be effective markers for the diagnosis and prognosis of gastric cancer.

Among 16 down-regulated miRNAs, we found that the miR-148a is down-regulated in gastric cancer and its regulated PIN was associated with tumor metastasis-related functions, such as integrin-mediated signaling, cell-matrix adhesion, wound healing and blood coagulation. These findings were validated by over-expressing miR-148a in AGS, SC-M1 and MKN-45 gastric cancer cell lines. While miR-148a over-expression led to a significant reduction in the invasive, migratory, adhesiveness and growth properties of gastric cancer cells, miR-148a inhibitor-treated tumor cells enhanced these effects. Lujambio *et al.* found miR-148a inhibited metastasis formation in xenograft models

[71].

We next ascertained whether miR-148a-mediated down-regulation of PAI-1, VAV2, ITGA5, and ITGB8 expression resulted in the inhibition of malignant progression of tumor cells. These genes were identified as up-regulated targets of miR-148a within its regulated PIN and have been reported to have a high oncogenic potential and are associated with aggressive tumor cell phenotypes [61-68]. Herein, we showed that their expression levels were reduced in response to miR-148a over-expression but elevated in response to anti-miR-148a inhibitor treatment. Overall, these results suggest that miR-148a influences the tumor progression-related biological functions of cancer cells by regulating a small subset of cancer-relevant genes within its regulated PIN.

Furthermore, we used iTRAQ method to analyze miR-148a-regulated proteome and our findings showed that its regulated biological functions were closely related with cancer, cell morphology and development and metabolism. Our previous data supported these findings that miR-148a had tumor-suppressive functions in gastric cancer that its over-expression could inhibit invasiveness, migratory and adhesive abilities of tumor cells. We also demonstrated that miR-148a over-expression reduce cell growth and induce cell apoptosis. Interestingly, iTRAQ results uncovered novel findings that miR-148a-regulated functions were associated with cellular morphology and development, such as organ development, development disorder, hematopoiesis, cardiovascular disease, neuron system development, function and neurological disease. Studies report that miRNAs play important roles in embryonic development and morphogenesis. For example, maternal-zygotic *dicer* (MZ*dicer*) mutants display abnormal morphogenesis during gastrulation, brain formation, somitogenesis, and heart development in zebrafish. Injection of miR-430 rescues the brain defects in MZ*dicer* mutants [72]. Additionally, miR-107 levels are decreased in Alzheimer's disease

patients compared with healthy individuals, even at early stages of disease progression [73]. Presently, the correlation between miR-148a and cellular development and morphogenesis is still unknown; thus, the regulatory role of miR-148a in cellular development and morphogenesis deserve further investigation.

SLC2A1 was predicted as a target gene of miR-148a. More importantly, we found that SLC2A1 was related with cell apoptosis and neurological disease. Interestingly, some studies display that cell apoptosis in neurological disease often occurs [74, 75]. There are evidences suggest that caspases have important roles in Alzheimer's disease and Parkinson's disease [74, 76, 77]. These results indicate that cell apoptosis is closely associated with neurological disease. On the other hand, SLC2A1 is also called glucose transporter type 1 (Glut1), which mediates glucose transport across blood-brain barrier (BBB) [78]. Patients with Alzheimer's disease have decreased BBB glucose transporter [79] and some reports reveal that Glut1 deficiency correlates with neurological disease [78] and low concentration of Glut1 and Glut3 were measured in the patients with Alzheimer's disease [79, 80]. Taken together, these findings suggest that SLC2A1 may be closely related with neurological disease. In this study, we detected miR-148a induced apoptosis-related protein expression, including the activation of caspase-9 and release of cytochrome c (Figure 8). In conclusion, whether miR-148a regulates neural development through mediating SLC2A1 target gene expression deserve further investigation.

Here, our findings revealed that miR-148a was a potential tumor suppressor in gastric cancer and could suppress metastasis-related functions of tumor cells, including invasion, migration, adhesion and growth. On the other hand, 14-3-3β was predicted as a target of miR-148a and reported to be associated with cancer metastasis [29, 30, 34, 35]. A key question is whether miR-148a suppresses metastasis of gastric cancer cells

through regulating 14-3-3β expression. To address this possibility, we first analyzed their correlation and our results indicated that miR-148a could directly regulate 14-3-3β expression. We then ascertained the regulatory mechanism of that miR-148a affected cancer metastasis through regulating 14-3-3β expression. Thus, we analyzed 14-3-3β expression and regulatory roles in gastric cancer. Our findings showed that 14-3-3β was expressed higher in tumor tissues than normal tissues ($P < 0.01$). Moreover, we also found that 14-3-3β was expressed highest in poor differentiated SC-M1 cells and high metastatic TSGH cells when compared with non-metastatic AGS and N87 cells from protein profiles and western blotting method, suggesting that 14-3-3β expression was related to malignant progression of tumor cells. We further verified that 14-3-3β over-expression could promote invasiveness, migration and growth of tumor cells. Our clinical analyses indicated that serum 14-3-3β levels were significantly associated with increases in the depth of tumor invasion, peritoneal invasion, tumor size, the number of metastatic lymph nodes, enhanced cancer stage progression (stage III and IV) and the presence of invasive phenotypes. Taken together, these results indicate that 14-3-3β has oncogenic potential and is associated with malignant progression of gastric cancer cells.

Several biomarkers for gastric cancer have been reported, including CEA, CA19-9 and CA72-4 [39, 40]; however, these were neither sensitive nor specific enough for disease detection [41, 42]. In this study, the 14-3-3β was assessed as a serologic biomarker for gastric cancer and it was confirmed that 14-3-3β levels in pre-operative serum were significantly elevated in cancer patients compared with controls ($P < 0.0001$) and also positively correlated to 14-3-3β expression levels in tumor tissues ($r = 0.385$, $P = 0.033$). Moreover, serum 14-3-3β levels in stage I gastric cancer patients were significantly higher than in controls ($P = 0.005$). These results suggest that 14-3-3β can be used as a potential serum marker for the detection of gastric cancer. Additionally,

overall and recurrence-free survival rates based on 14-3-3β serum levels were also investigated and patients with higher 14-3-3β levels showed a marked reduction in overall and recurrence-free survival. These results therefore demonstrate that 14-3-3β can be used as a potential biomarker for the detection and prognosis of human gastric cancer.

Recently, Xia *et al.* reported that serum macrophage migration-inhibitory factor (MMIF) was a better biomarker than CEA in diagnosing gastric cancer in patients presenting with dyspepsia [81]. Here, we further demonstrate serum 14-3-3β levels as a biomarker in differentiating between gastric cancer patients and controls. Additional prospective studies deserve further investigation where serum 14-3-3β assessment may be combined with other useful serum markers, such as MMIF, to increase the overall sensitivity, specificity and diagnostic accuracy of gastric cancer detection.

Helicobacter pylori (*H. pylori*) infection is a crucial factor in the pathogenesis of gastric cancer and induces disease-specific protein expression in gastric cancer [30]. To elucidate the effects of *H. pylori* infection on 14-3-3β expression, we analyzed their correlation. We found that patients with *H. pylori* infection had higher 14-3-3β levels than those with no *H. pylori* infection (Figure 21), suggesting that 14-3-3β might be involved in the pathogenesis of *H. pylori* in gastric cancer. Some studies are similar with our results that 14-3-3β is up-regulated in *H. pylori*-infected gastric cancer cells [30, 82].

Chapter 5   Conclusion

In conclusion, a novel integrative network-based approach was used to discover the potential functions of these miRNAs in gastric cancer. Furthermore, this approach facilitated the identification of 16 activated oncomir-regulated PINs which might be used as possible diagnostic and prognostic markers of gastric cancer. In particular, miR-148a was identified as a potential prognostic marker in gastric cancer patients, with the ability to function as a tumor suppressor through its regulated PIN. This study not only provides an insight into the miRNA-regulated PINs that are involved in the pathogenesis of gastric cancer; it also shows that a network-based approach can be used to identify novel diagnostic and prognostic markers of disease.

iTRAQ data further indicated that miR-148a-regulated proteome was associated with cancer progression, including cell development, migration and cell death. Our findings uncovered that miR-148a induced cell apoptosis and inhibited cell growth.

On the other hand, we revealed that miR-148a could directly regulate 14-3-3β expression levels. We further demonstrated 14-3-3β was associated with malignant progression of gastric cancer cells; and provided a new insight into the role of 14-3-3β in gastric cancer cell progression. Furthermore, we evaluated clinical significance of serum 14-3-3β in diagnosing gastric cancer. We have identified that serum 14-3-3β could be used for differentiating between gastric cancer patients and controls, and was a poor prognostic factor for survival in gastric cancer. The 14-3-3β ELISA also has the added advantage of being commercially available, easily reproducible, and inexpensive. Thus, it is useful to assay serum 14-3-3β concentration for the diagnosis of gastric cancer.

Taken together, miR-148a is a potential tumor suppressor in gastric cancer and

suppresses tumor metastasis through regulating 14-3-3β expression.

Chapter 6   References

[1] Bartel, D. P., MicroRNAs: genomics, biogenesis, mechanism, and function. *Cell* 2004, *116*, 281-297.

[2] Guo, H., Ingolia, N. T., Weissman, J. S., Bartel, D. P., Mammalian microRNAs predominantly act to decrease target mRNA levels. *Nature* 2010, *466*, 835-840.

[3] Doench, J. G., Sharp, P. A., Specificity of microRNA target selection in translational repression. *Genes Dev* 2004, *18*, 504-511.

[4] Esquela-Kerscher, A., Slack, F. J., Oncomirs - microRNAs with a role in cancer. *Nat Rev Cancer* 2006, *6*, 259-269.

[5] Asangani, I. A., Rasheed, S. A., Nikolova, D. A., Leupold, J. H.*, et al.*, MicroRNA-21 (miR-21) post-transcriptionally downregulates tumor suppressor Pdcd4 and stimulates invasion, intravasation and metastasis in colorectal cancer. *Oncogene* 2008, *27*, 2128-2136.

[6] Meng, F., Henson, R., Wehbe-Janek, H., Ghoshal, K.*, et al.*, MicroRNA-21 regulates expression of the PTEN tumor suppressor gene in human hepatocellular cancer. *Gastroenterology* 2007, *133*, 647-658.

[7] Lee, S. T., Chu, K., Oh, H. J., Im, W. S.*, et al.*, Let-7 microRNA inhibits the proliferation of human glioblastoma cells. *J Neurooncol* 2011, *102*, 19-24.

[8] Park, S. M., Shell, S., Radjabi, A. R., Schickel, R.*, et al.*, Let-7 prevents early cancer progression by suppressing expression of the embryonic gene HMGA2. *Cell Cycle* 2007, *6*, 2585-2590.

[9] Ohshima, K., Inoue, K., Fujiwara, A., Hatakeyama, K.*, et al.*, Let-7 microRNA family is selectively secreted into the extracellular environment via exosomes in a metastatic gastric cancer cell line. *PLoS One* 2010, *5*, e13247.

[10] Huang, J. C., Babak, T., Corson, T. W., Chua, G., *et al.*, Using expression profiling data to identify human microRNA targets. *Nat Methods* 2007, *4*, 1045-1049.

[11] Li, J., Min, R., Bonner, A., Zhang, Z., A probabilistic framework to improve microrna target prediction by incorporating proteomics data. *J Bioinform Comput Biol* 2009, *7*, 955-972.

[12] Bartel, D. P., MicroRNAs: target recognition and regulatory functions. *Cell* 2009, *136*, 215-233.

[13] Baek, D., Villen, J., Shin, C., Camargo, F. D., *et al.*, The impact of microRNAs on protein output. *Nature* 2008, *455*, 64-71.

[14] Selbach, M., Schwanhausser, B., Thierfelder, N., Fang, Z., *et al.*, Widespread changes in protein synthesis induced by microRNAs. *Nature* 2008, *455*, 58-63.

[15] Yu, X., Lin, J., Zack, D. J., Mendell, J. T., Qian, J., Analysis of regulatory network topology reveals functionally distinct classes of microRNAs. *Nucleic Acids Res* 2008, *36*, 6494-6503.

[16] Liang, H., Li, W. H., MicroRNA regulation of human protein protein interaction network. *RNA* 2007, *13*, 1402-1408.

[17] Cusick, M. E., Klitgord, N., Vidal, M., Hill, D. E., Interactome: gateway into systems biology. *Hum Mol Genet* 2005, *14 Spec No. 2*, R171-181.

[18] Rual, J. F., Venkatesan, K., Hao, T., Hirozane-Kishikawa, T., *et al.*, Towards a proteome-scale map of the human protein-protein interaction network. *Nature* 2005, *437*, 1173-1178.

[19] Sharan, R., Ulitsky, I., Shamir, R., Network-based prediction of protein function. *Mol Syst Biol* 2007, *3*, 88.

[20] Hsu, C. W., Juan, H. F., Huang, H. C., Characterization of microRNA-regulated protein-protein interaction network. *Proteomics* 2008, *8*, 1975-1979.

[21] Zhang, H., Li, Y., Lai, M., The microRNA network and tumor metastasis. *Oncogene* 2010, *29*, 937-948.

[22] Lee, Y., Yang, X., Huang, Y., Fan, H.*, et al.*, Network modeling identifies molecular functions targeted by miR-204 to suppress head and neck tumor metastasis. *PLoS Comput Biol* 2010, *6*, e1000730.

[23] Ross, P. L., Huang, Y. N., Marchese, J. N., Williamson, B.*, et al.*, Multiplexed protein quantitation in Saccharomyces cerevisiae using amine-reactive isobaric tagging reagents. *Mol Cell Proteomics* 2004, *3*, 1154-1169.

[24] Han, C. L., Chien, C. W., Chen, W. C., Chen, Y. R.*, et al.*, A multiplexed quantitative strategy for membrane proteomics: opportunities for mining therapeutic targets for autosomal dominant polycystic kidney disease. *Mol Cell Proteomics* 2008, *7*, 1983-1997.

[25] Yang, Y., Chaerkady, R., Beer, M. A., Mendell, J. T., Pandey, A., Identification of miR-21 targets in breast cancer cells using a quantitative proteomic approach. *Proteomics* 2009, *9*, 1374-1384.

[26] Takei, Y., Takigahira, M., Mihara, K., Tarumi, Y., Yanagihara, K., The metastasis-associated microRNA miR-516a-3p is a novel therapeutic target for inhibiting peritoneal dissemination of human scirrhous gastric cancer. *Cancer Res* 2011, *71*, 1442-1453.

[27] Lewis, B. P., Burge, C. B., Bartel, D. P., Conserved seed pairing, often flanked by adenosines, indicates that thousands of human genes are microRNA targets. *Cell* 2005, *120*, 15-20.

[28] Krek, A., Grun, D., Poy, M. N., Wolf, R.*, et al.*, Combinatorial microRNA target predictions. *Nat Genet* 2005, *37*, 495-500.

[29] Komiya, Y., Kurabe, N., Katagiri, K., Ogawa, M.*, et al.*, A novel binding factor of

14-3-3beta functions as a transcriptional repressor and promotes anchorage-independent growth, tumorigenicity, and metastasis. *J Biol Chem* 2008, *283*, 18753-18764.

[30] Chan, C. H., Ko, C. C., Chang, J. G., Chen, S. F*., et al.*, Subcellular and functional proteomic analysis of the cellular responses induced by Helicobacter pylori. *Mol Cell Proteomics* 2006, *5*, 702-713.

[31] Morrison, D. K., The 14-3-3 proteins: integrators of diverse signaling cues that impact cell fate and cancer development. *Trends Cell Biol* 2009, *19*, 16-23.

[32] Qi, W., Liu, X., Qiao, D., Martinez, J. D., Isoform-specific expression of 14-3-3 proteins in human lung cancer tissues. *Int J Cancer* 2005, *113*, 359-363.

[33] Cochran, D. A., Evans, C. A., Blinco, D., Burthem, J*., et al.*, Proteomic analysis of chronic lymphocytic leukemia subtypes with mutated or unmutated Ig V(H) genes. *Mol Cell Proteomics* 2003, *2*, 1331-1341.

[34] Takihara, Y., Matsuda, Y., Hara, J., Role of the beta isoform of 14-3-3 proteins in cellular proliferation and oncogenic transformation. *Carcinogenesis* 2000, *21*, 2073-2077.

[35] Han, D. C., Rodriguez, L. G., Guan, J. L., Identification of a novel interaction between integrin beta1 and 14-3-3beta. *Oncogene* 2001, *20*, 346-357.

[36] Jemal, A., Bray, F., Center, M. M., Ferlay, J*., et al.*, Global cancer statistics. *CA Cancer J Clin* 2011, *61*, 69-90.

[37] Macdonald, J. S., Gastric cancer--new therapeutic options. *N Engl J Med* 2006, *355*, 76-77.

[38] Yamazaki, H., Oshima, A., Murakami, R., Endoh, S., Ubukata, T., A long-term follow-up study of patients with gastric cancer detected by mass screening. *Cancer* 1989, *63*, 613-617.

[39] Kodama, I., Koufuji, K., Kawabata, S., Tetsu, S*., et al.*, The clinical efficacy of CA

72-4 as serum marker for gastric cancer in comparison with CA19-9 and CEA. *Int Surg* 1995, *80*, 45-48.

[40] Ohuchi, N., Takahashi, K., Matoba, N., Sato, T*., et al.*, Comparison of serum assays for TAG-72, CA19-9 and CEA in gastrointestinal carcinoma patients. *Jpn J Clin Oncol* 1989, *19*, 242-248.

[41] Hao, Y., Yu, Y., Wang, L., Yan, M*., et al.*, IPO-38 is identified as a novel serum biomarker of gastric cancer based on clinical proteomics technology. *J Proteome Res* 2008, *7*, 3668-3677.

[42] Ychou, M., Duffour, J., Kramar, A., Gourgou, S., Grenier, J., Clinical significance and prognostic value of CA72-4 compared with CEA and CA19-9 in patients with gastric cancer. *Dis Markers* 2000, *16*, 105-110.

[43] D'Errico, M., de Rinaldis, E., Blasi, M. F., Viti, V*., et al.*, Genome-wide expression profile of sporadic gastric cancers with microsatellite instability. *Eur J Cancer* 2009, *45*, 461-469.

[44] Tusher, V. G., Tibshirani, R., Chu, G., Significance analysis of microarrays applied to the ionizing radiation response. *Proc Natl Acad Sci U S A* 2001, *98*, 5116-5121.

[45] Saeed, A. I., Bhagabati, N. K., Braisted, J. C., Liang, W*., et al.*, TM4 microarray software suite. *Methods Enzymol* 2006, *411*, 134-193.

[46] Friedman, R. C., Farh, K. K., Burge, C. B., Bartel, D. P., Most mammalian mRNAs are conserved targets of microRNAs. *Genome Res* 2009, *19*, 92-105.

[47] Keshava Prasad, T. S., Goel, R., Kandasamy, K., Keerthikumar, S*., et al.*, Human Protein Reference Database--2009 update. *Nucleic Acids Res* 2009, *37*, D767-772.

[48] Ashburner, M., Ball, C. A., Blake, J. A., Botstein, D*., et al.*, Gene ontology: tool for the unification of biology. The Gene Ontology Consortium. *Nat Genet* 2000, *25*, 25-29.

[49] Maere, S., Heymans, K., Kuiper, M., BiNGO: a Cytoscape plugin to assess

overrepresentation of gene ontology categories in biological networks. *Bioinformatics* 2005, *21*, 3448-3449.

[50] Shannon, P., Markiel, A., Ozier, O., Baliga, N. S.*, et al.*, Cytoscape: a software environment for integrated models of biomolecular interaction networks. *Genome Res* 2003, *13*, 2498-2504.

[51] Chang, C. C., Shih, J. Y., Jeng, Y. M., Su, J. L.*, et al.*, Connective tissue growth factor and its role in lung adenocarcinoma invasion and metastasis. *J Natl Cancer Inst* 2004, *96*, 364-375.

[52] Papagiannakopoulos, T., Shapiro, A., Kosik, K. S., MicroRNA-21 targets a network of key tumor-suppressive pathways in glioblastoma cells. *Cancer Res* 2008, *68*, 8164-8172.

[53] Lauren, P., The Two Histological Main Types of Gastric Carcinoma: Diffuse and So-Called Intestinal-Type Carcinoma. An Attempt at a Histo-Clinical Classification. *Acta Pathol Microbiol Scand* 1965, *64*, 31-49.

[54] Sobin LH, W. C., eds., TNM classification of malignant tumors. 1997, *5th ed*.

[55] Xiao, T., Ying, W., Li, L., Hu, Z.*, et al.*, An approach to studying lung cancer-related proteins in human blood. *Mol Cell Proteomics* 2005, *4*, 1480-1486.

[56] Chen, G., Gharib, T. G., Wang, H., Huang, C. C.*, et al.*, Protein profiles associated with survival in lung adenocarcinoma. *Proc Natl Acad Sci U S A* 2003, *100*, 13537-13542.

[57] Katayama, M., Sanzen, N., Funakoshi, A., Sekiguchi, K., Laminin gamma2-chain fragment in the circulation: a prognostic indicator of epithelial tumor invasion. *Cancer Res* 2003, *63*, 222-229.

[58] Juan, H. F., Wang, I. H., Huang, T. C., Li, J. J.*, et al.*, Proteomics analysis of a novel compound: cyclic RGD in breast carcinoma cell line MCF-7. *Proteomics* 2006, *6*,

2991-3000.

[59] Lin, L. L., Chen, C. N., Lin, W. C., Lee, P. H.*, et al.*, Annexin A4: A novel molecular marker for gastric cancer with Helicobacter pylori infection using proteomics approach. *Proteomics Clin Appl* 2008, *2*, 619-634.

[60] Lim, L. P., Lau, N. C., Garrett-Engele, P., Grimson, A.*, et al.*, Microarray analysis shows that some microRNAs downregulate large numbers of target mRNAs. *Nature* 2005, *433*, 769-773.

[61] Bajou, K., Noel, A., Gerard, R. D., Masson, V.*, et al.*, Absence of host plasminogen activator inhibitor 1 prevents cancer invasion and vascularization. *Nat Med* 1998, *4*, 923-928.

[62] Liu, G., Shuman, M. A., Cohen, R. L., Co-expression of urokinase, urokinase receptor and PAI-1 is necessary for optimum invasiveness of cultured lung cancer cells. *Int J Cancer* 1995, *60*, 501-506.

[63] Chambers, S. K., Ivins, C. M., Carcangiu, M. L., Plasminogen activator inhibitor-1 is an independent poor prognostic factor for survival in advanced stage epithelial ovarian cancer patients. *Int J Cancer* 1998, *79*, 449-454.

[64] Lai, S. Y., Ziober, A. F., Lee, M. N., Cohen, N. A.*, et al.*, Activated Vav2 modulates cellular invasion through Rac1 and Cdc42 in oral squamous cell carcinoma. *Oral Oncol* 2008, *44*, 683-688.

[65] Bourguignon, L. Y., Zhu, H., Zhou, B., Diedrich, F.*, et al.*, Hyaluronan promotes CD44v3-Vav2 interaction with Grb2-p185(HER2) and induces Rac1 and Ras signaling during ovarian tumor cell migration and growth. *J Biol Chem* 2001, *276*, 48679-48692.

[66] Koike, T., Kimura, N., Miyazaki, K., Yabuta, T.*, et al.*, Hypoxia induces adhesion molecules on cancer cells: A missing link between Warburg effect and induction of selectin-ligand carbohydrates. *Proc Natl Acad Sci U S A* 2004, *101*, 8132-8137.

[67] Landemaine, T., Jackson, A., Bellahcene, A., Rucci, N.*, et al.*, A six-gene signature predicting breast cancer lung metastasis. *Cancer Res* 2008, *68*, 6092-6099.

[68] Sultmann, H., von Heydebreck, A., Huber, W., Kuner, R.*, et al.*, Gene expression in kidney cancer is associated with cytogenetic abnormalities, metastasis formation, and patient survival. *Clin Cancer Res* 2005, *11*, 646-655.

[69] Chen, J., De, S., Brainard, J., Byzova, T. V., Metastatic properties of prostate cancer cells are controlled by VEGF. *Cell Commun Adhes* 2004, *11*, 1-11.

[70] Patel, V., Rosenfeldt, H. M., Lyons, R., Servitja, J. M.*, et al.*, Persistent activation of Rac1 in squamous carcinomas of the head and neck: evidence for an EGFR/Vav2 signaling axis involved in cell invasion. *Carcinogenesis* 2007, *28*, 1145-1152.

[71] Lujambio, A., Calin, G. A., Villanueva, A., Ropero, S.*, et al.*, A microRNA DNA methylation signature for human cancer metastasis. *Proc Natl Acad Sci U S A* 2008, *105*, 13556-13561.

[72] Giraldez, A. J., Cinalli, R. M., Glasner, M. E., Enright, A. J.*, et al.*, MicroRNAs regulate brain morphogenesis in zebrafish. *Science* 2005, *308*, 833-838.

[73] Christensen, M., Schratt, G. M., microRNA involvement in developmental and functional aspects of the nervous system and in neurological diseases. *Neurosci Lett* 2009, *466*, 55-62.

[74] Friedlander, R. M., Apoptosis and caspases in neurodegenerative diseases. *N Engl J Med* 2003, *348*, 1365-1375.

[75] Yuan, J., Yankner, B. A., Apoptosis in the nervous system. *Nature* 2000, *407*, 802-809.

[76] Gervais, F. G., Xu, D., Robertson, G. S., Vaillancourt, J. P.*, et al.*, Involvement of caspases in proteolytic cleavage of Alzheimer's amyloid-beta precursor protein and amyloidogenic A beta peptide formation. *Cell* 1999, *97*, 395-406.

[77] Garden, G. A., Budd, S. L., Tsai, E., Hanson, L.*, et al.*, Caspase cascades in human immunodeficiency virus-associated neurodegeneration. *J Neurosci* 2002, *22*, 4015-4024.

[78] Klepper, J., Wang, D., Fischbarg, J., Vera, J. C.*, et al.*, Defective glucose transport across brain tissue barriers: a newly recognized neurological syndrome. *Neurochem Res* 1999, *24*, 587-594.

[79] Mooradian, A. D., Chung, H. C., Shah, G. N., GLUT-1 expression in the cerebra of patients with Alzheimer's disease. *Neurobiol Aging* 1997, *18*, 469-474.

[80] Simpson, I. A., Chundu, K. R., Davies-Hill, T., Honer, W. G., Davies, P., Decreased concentrations of GLUT1 and GLUT3 glucose transporters in the brains of patients with Alzheimer's disease. *Ann Neurol* 1994, *35*, 546-551.

[81] Xia, H. H., Yang, Y., Chu, K. M., Gu, Q.*, et al.*, Serum macrophage migration-inhibitory factor as a diagnostic and prognostic biomarker for gastric cancer. *Cancer* 2009, *115*, 5441-5449.

[82] Lim, J. W., Kim, H., Kim, J. M., Kim, J. S.*, et al.*, Cellular stress-related protein expression in Helicobacter pylori-infected gastric epithelial AGS cells. *Int J Biochem Cell Biol* 2004, *36*, 1624-1634.

Figures
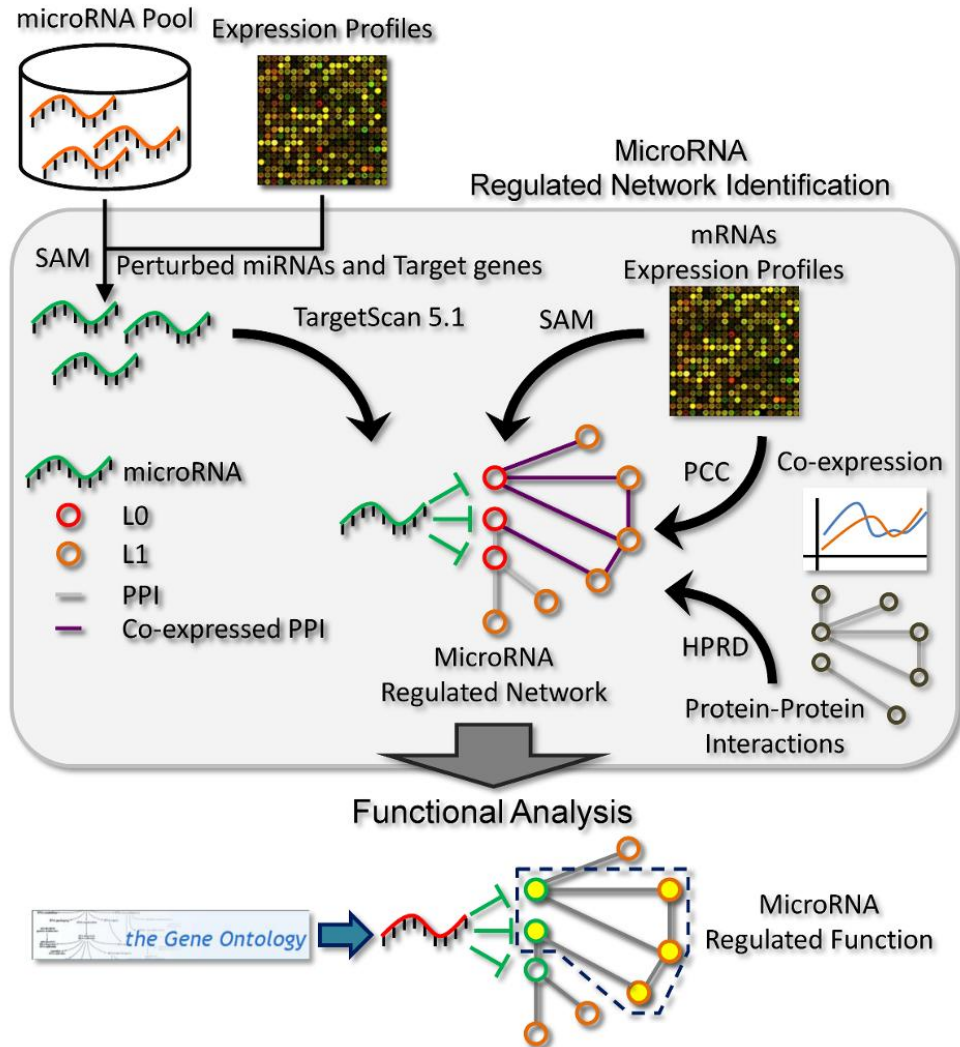
Figure 1 Expression profiles of miRNAs and genes were used to discover condition-specific targets of miRNAs. The miRNA-regulated PINs were denoted as the PIN which is formed by their differentially expressed targets (L0) and interacting partners (L1). The enrichment of CePPIs involved in the miRNA-regulated PIN was utilized to evaluate the activity of the network. The potential miRNA-regulated functions were predicted by functional enrichment analysis.
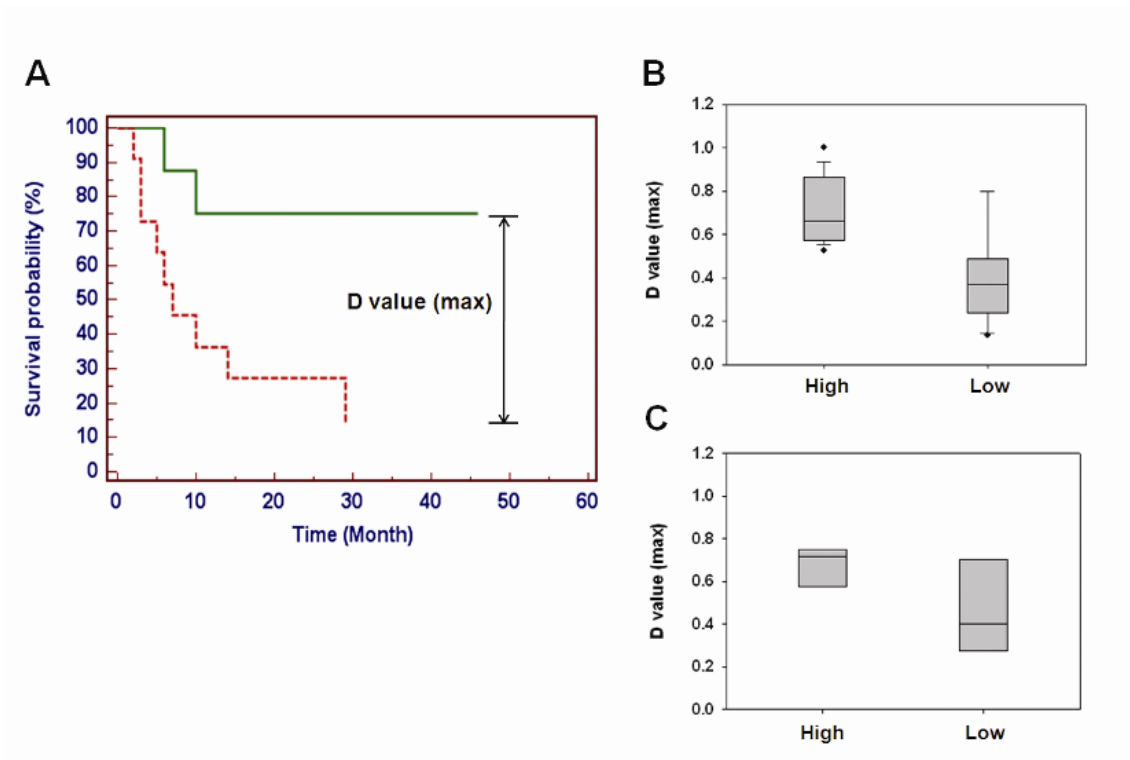
Figure 2 Kaplan-Meier survival curves of 23 downregulated miRNAs in gastric cancer. (A) The median of 22 paired miRNA expression values that was obtained by miRNA microarray was defined as the cutoff value. The green line represents high miRNA expressing patients and the red line represents low miRNA expressing patients. The D value was calculated by analyzing the maximum difference in survival rate between high and low groups. The difference in D values between high and low groups for the 16 oncomir in Table 2 was more significant ($P < 0.0001$, B) than in the 7 remaining down-regulated miRNAs ($P = 0.016$, C) (paired Wilcoxon rank sum test).
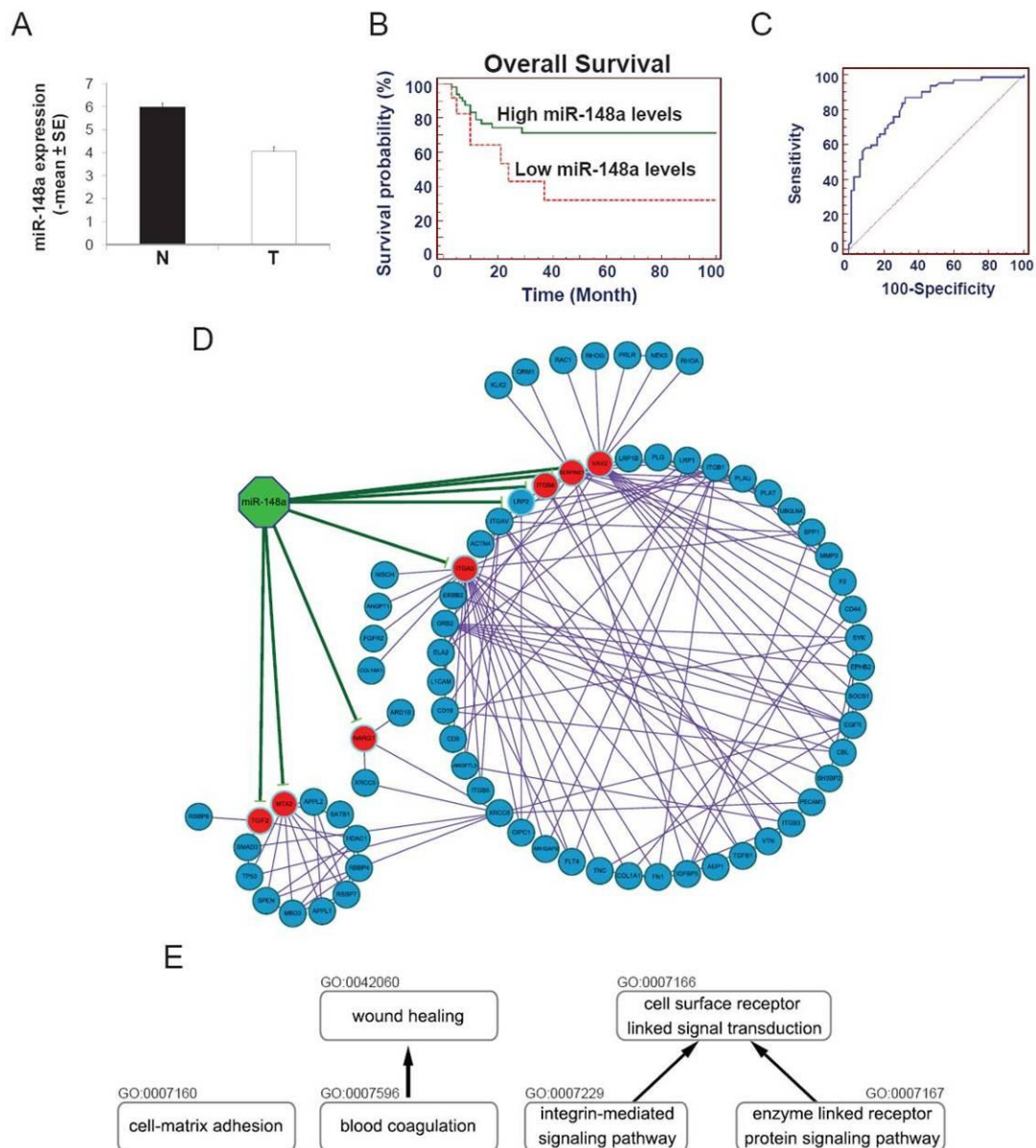
Figure 3 miR-148a and its regulated PIN. (A) miR-148a expression levels (Mean ± standard error) were detected and normalized to U6 snRNA by qRT-PCR ($P < 0.0001$, paired t-test). (B) The effect of miR-148a expression levels on patient survival was measured. Cut-off value of 0.101 was determined based on the finding that miR-148a expression levels in 60% of patients (37 out of 62) that survived for a period of 2 to 140 months after surgical resection were above 0.101. Solid and dotted lines represent high ($\geq$0.101, N = 50) and low (<0.101, N = 12) miR-148a levels. (C) The AUC of miR-148a was 0.84 (0.76-0.90, 95% confidence interval) (ROC curves analysis, $P = 0.0001$). (D) Red nodes represent up-regulated target genes and blue nodes represent their interacting partners within the human PIN. Green edges represent predicted interactions between miRNAs and targets and purple edges represent PPIs between proteins. (E) Nodes represent enriched GO terms in the miR-148a-regulated PIN and edges represent the relationships in the GO.

59
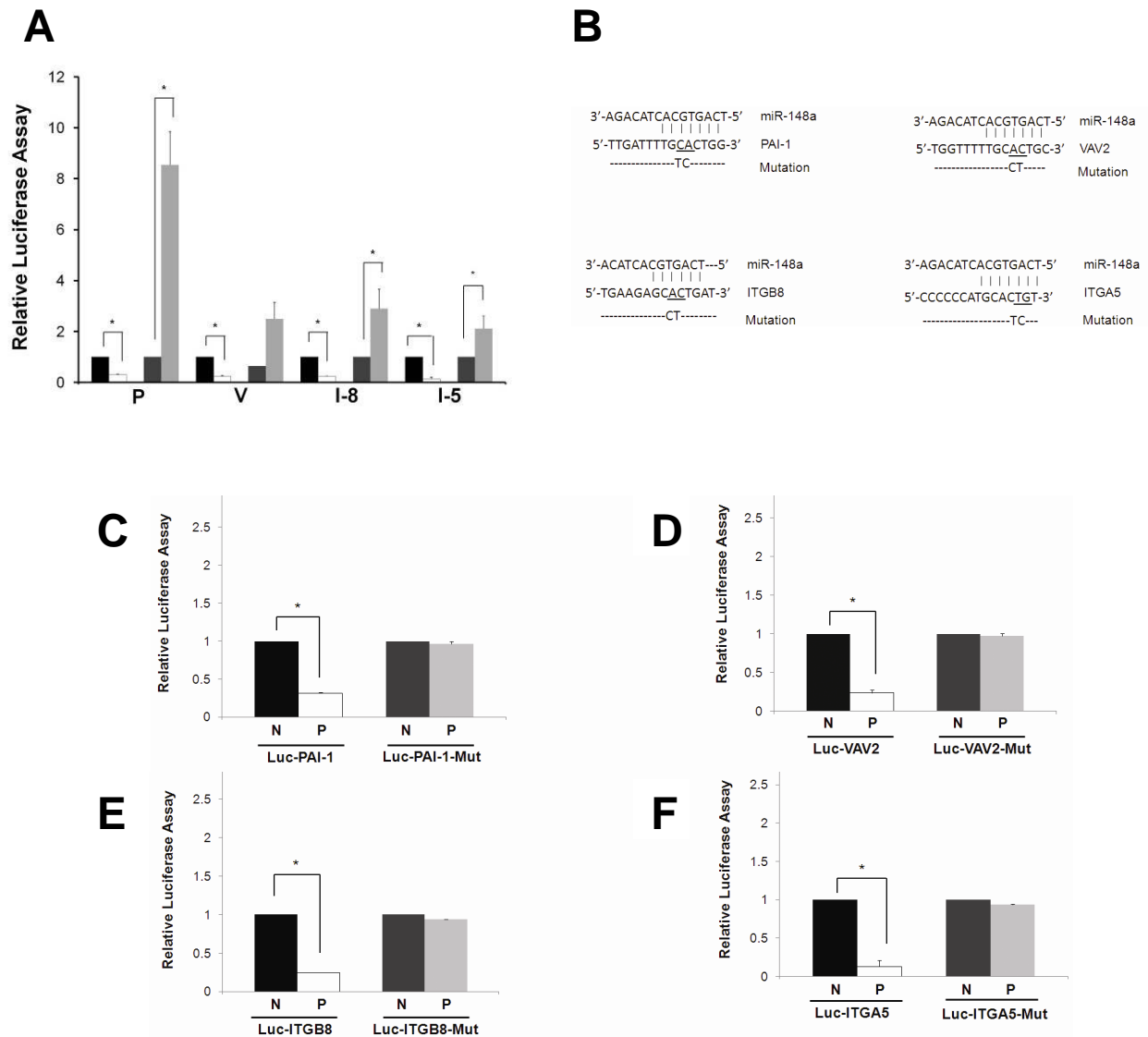
Figure 4 The relationship between miR-148a and PAI-1 (P), VAV2 (V), ITGB8 (I-8) and ITGA5 (I-5). (A) White and light gray bars represent miR-148a precursor and inhibitor, respectively. Black and dark gray represent precursor and inhibitor negative controls, respectively. (B) Schematic diagram of miR-148a-target sites and sites mutation in PAI-1, VAV2, ITGB8 and ITGA5. (C-F) Luc-PAI-1, Luc-VAV2, Luc-ITGB8 and Luc-UTGA5 represented AGS cells were transfected with pMIR-REPORT luciferase expression vector containing each putative miR-148a target sites. Mut represented their sites mutation in sequences. P and N represent miR-148a precursor and negative control, respectively (*$P < 0.05$).
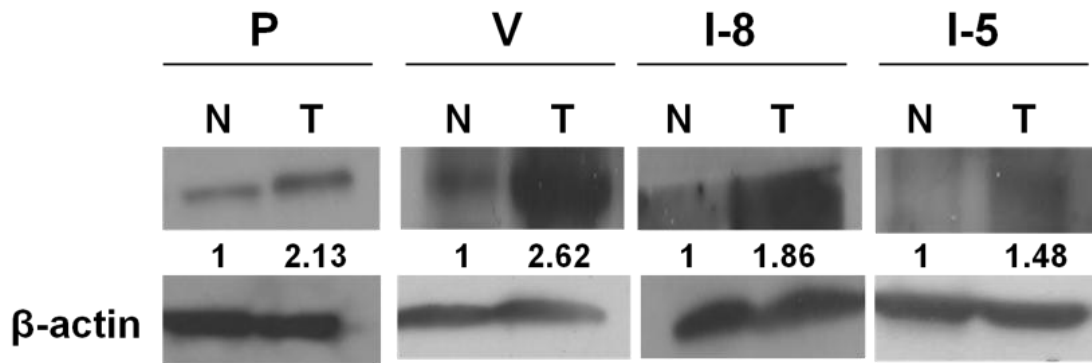
Figure 5 The expression levels of PAI-1 (P, 50kDa), VAV2 (V, 95kDa), ITGB8 (I-8, 85kDa) and ITGA5 (I-5, 150kDa) in paired tumor (T) and normal (N) tissues were measured by immunoblotting. β-actin was used for normalization.
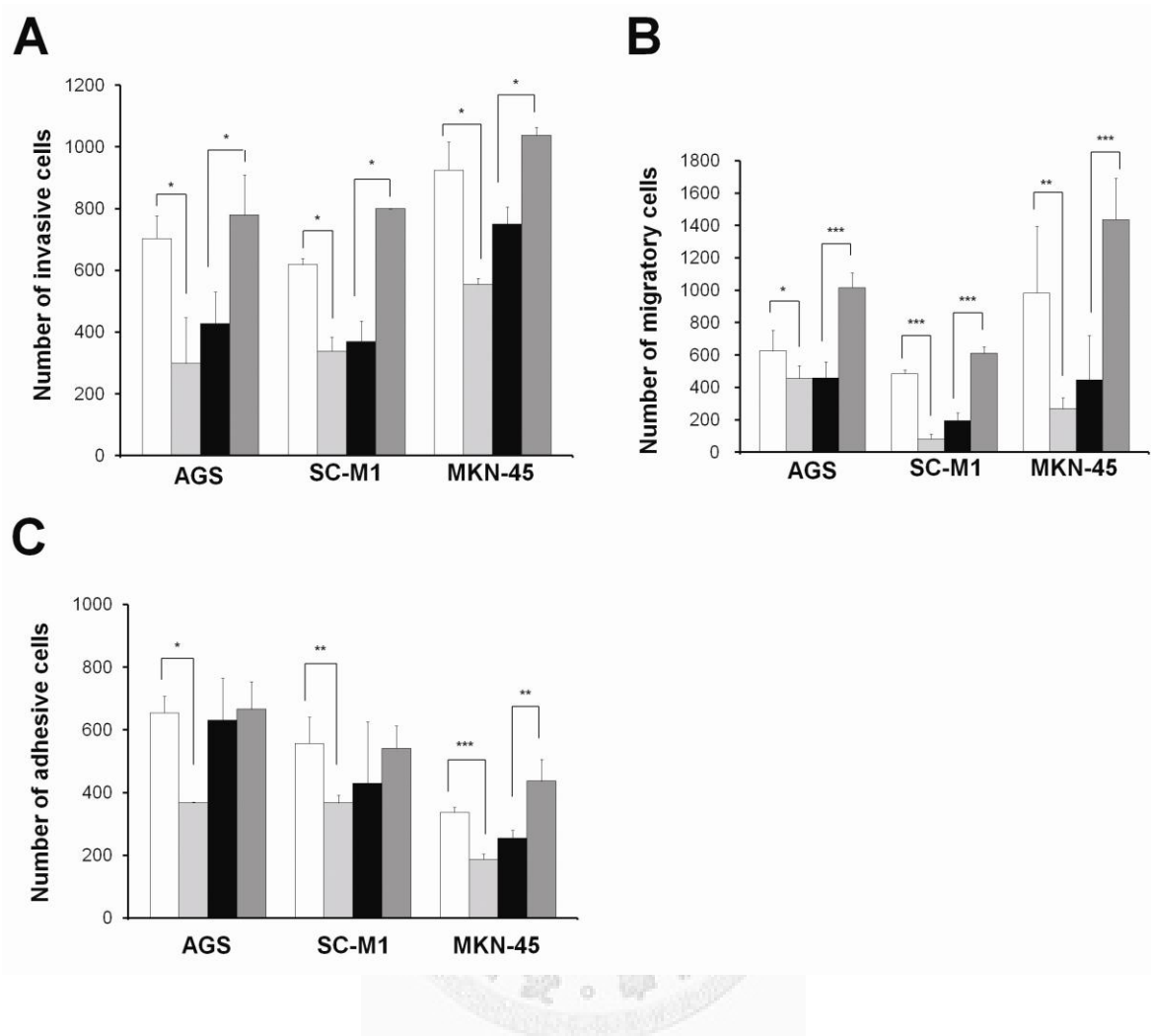
Figure 6 miR-148a reduces invasion, migration and adhesion of tumor cells. Over-expressed miR-148a reduces invasion (A), migration (B) and adhesion (C) of tumor cells. Invasive, migratory and adhesive activities of tumor cells were measured after transfection for 48hr with miR-148a precursor (light gray bar) and inhibitor-treated (dark gray bar) AGS, SC-M1 and MKN-45 cell lines. Precursor (white bar) and inhibitor (black bar) negative controls were used (*t*-test, *$P < 0.05$; **$P < 0.01$; ***$P < 0.001$).
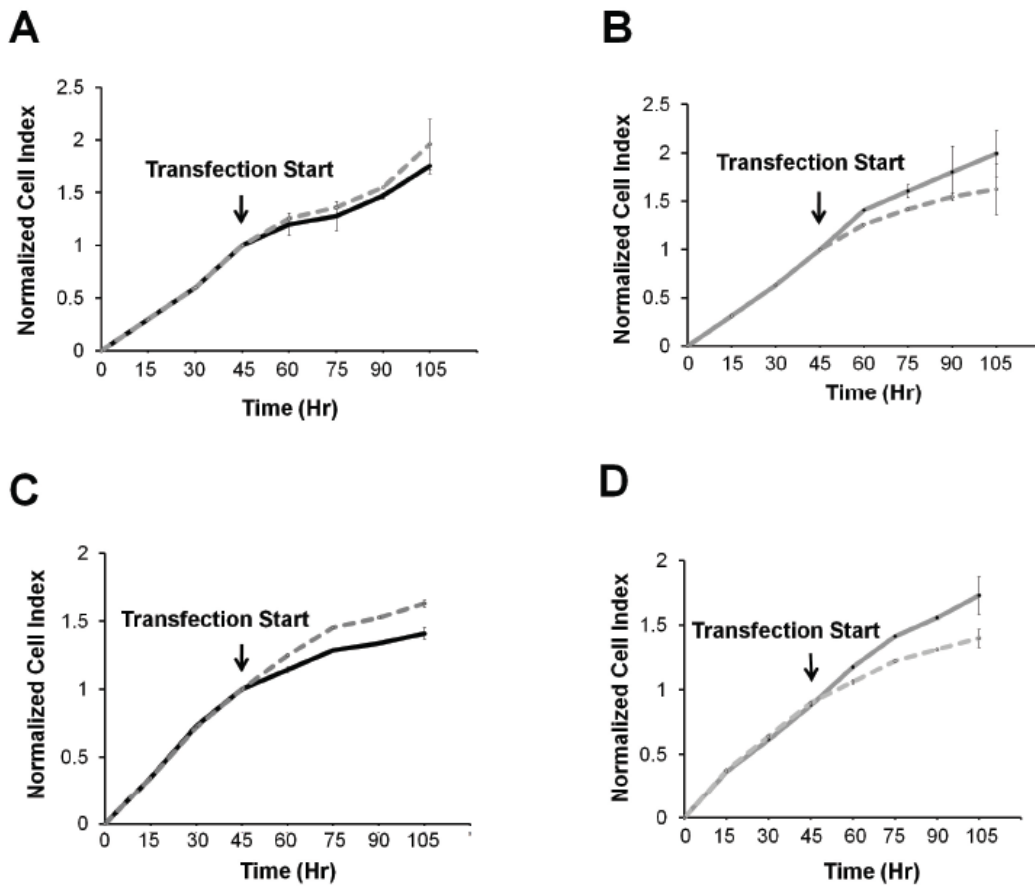
Figure 7 Over-expressed miR-148a reduces cells growth. Cell growth was monitored in real-time using the xCELLigence system. (A, B) AGS and (C, D) SC-M1 tumor cells were transfected with either miR-148a precursor or inhibitor and compared to their respective negative controls. The results indicated that miR-148a reduced tumor cell growth (*t*-test, $P = 0.23$, A and $P < 0.001$, C), while miR-148a inhibitor-transfected tumor cells showed increased cell growth (*t*-test, $P < 0.001$, B and $P < 0.001$, D). Black and gray solid lines represent miR-148a precursor and inhibitor, respectively. Dashed lines represent their negative controls. The *P*-value was calculated using a paired *t*-test.
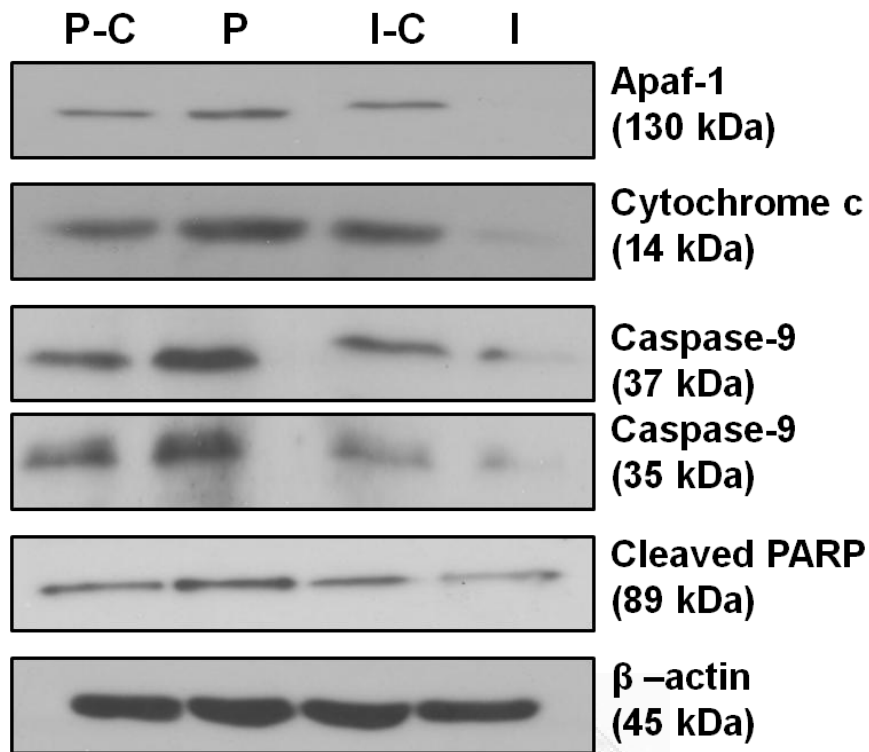
Figure 8 Over-expressed miR-148a induces cells apoptosis. The expression levels of apoptosis-related proteins, including Apaf-1, cytochrome c, caspase-9 and cleaved PARP, were detected in miR-148a over-expressing AGS cells using western blotting. P and I represent miR-148a precursor and anti-miR-148a inhibitor; P-C and I-C represent their negative controls, respectively. β-actin was used as internal control.
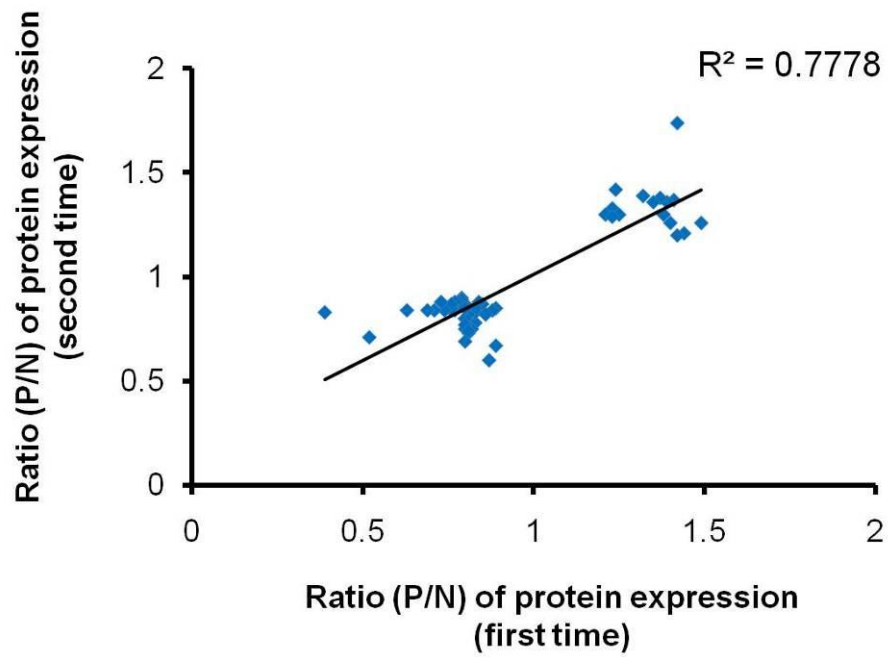
Figure 9 Scatter plot showing the comparison of expression ratio of all identified significantly expressed proteins between the biological replicate. P and N represent miR-148a precursor and its negative control, respectively.
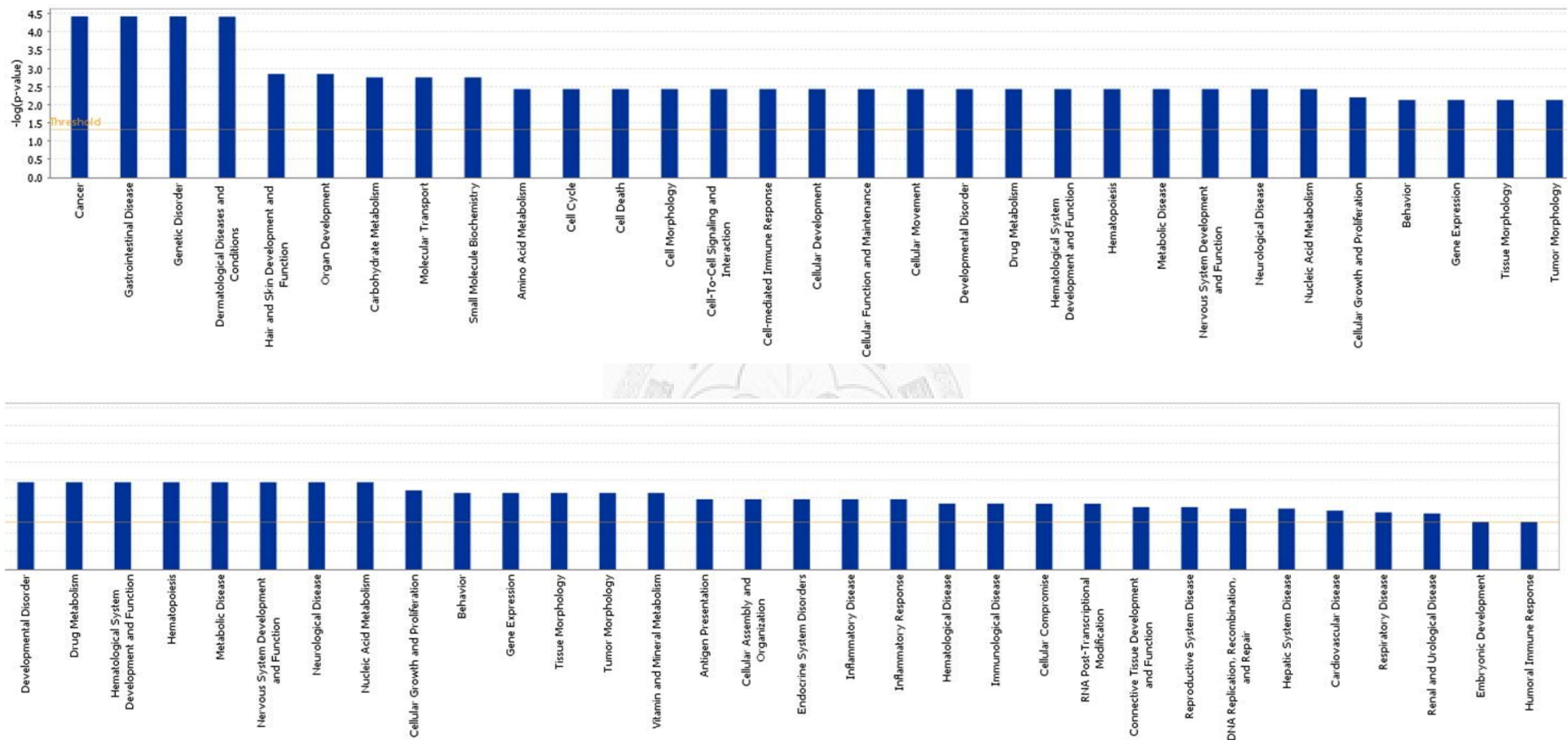
Figure 10 Associated biological functions of miR-148a-regulated proteome. A total of 57 identified significantly expressed proteins from iTRAQ data were used to analyze associated biological functions using IPA 9.0 software. All shown functions were significant ($P < 0.05$).

A

Position 1693-1699 of YWHAB 3'-UTR   5' ......GAAAAGAAAAAUUUAUGCACUGA...

　　　　　　　　　　　　　　　　　　　　　　　　　　│ │ │ │ │ │ │

hsa-miR-148a   3'   UGUUUCAAGACAUCACGUGACU
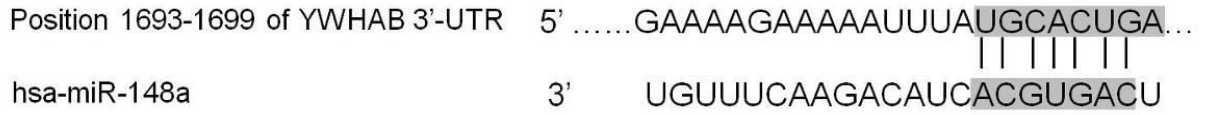
B
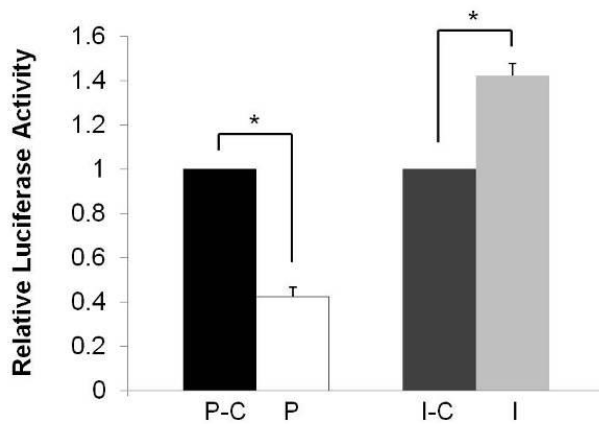
C
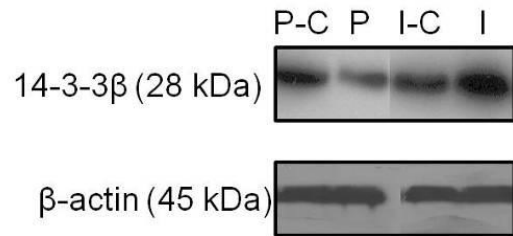
Figure 11 14-3-3β is a direct target of miR-148a. (A) 14-3-3β is a predicted target of miR-148a based on TargetScanHuman 5.1 database. (B) Luciferase assay was used to analyze their correlation between miR-148a and 14-3-3β. P and I represent miR-148a precursor and anti-miR-148a inhibitor; P-C and I-C represent their negative controls, respectively (*$P < 0.05$, *t*-test). (C) Western blotting assay was used to confirm their correlation. β-actin was used as internal control.
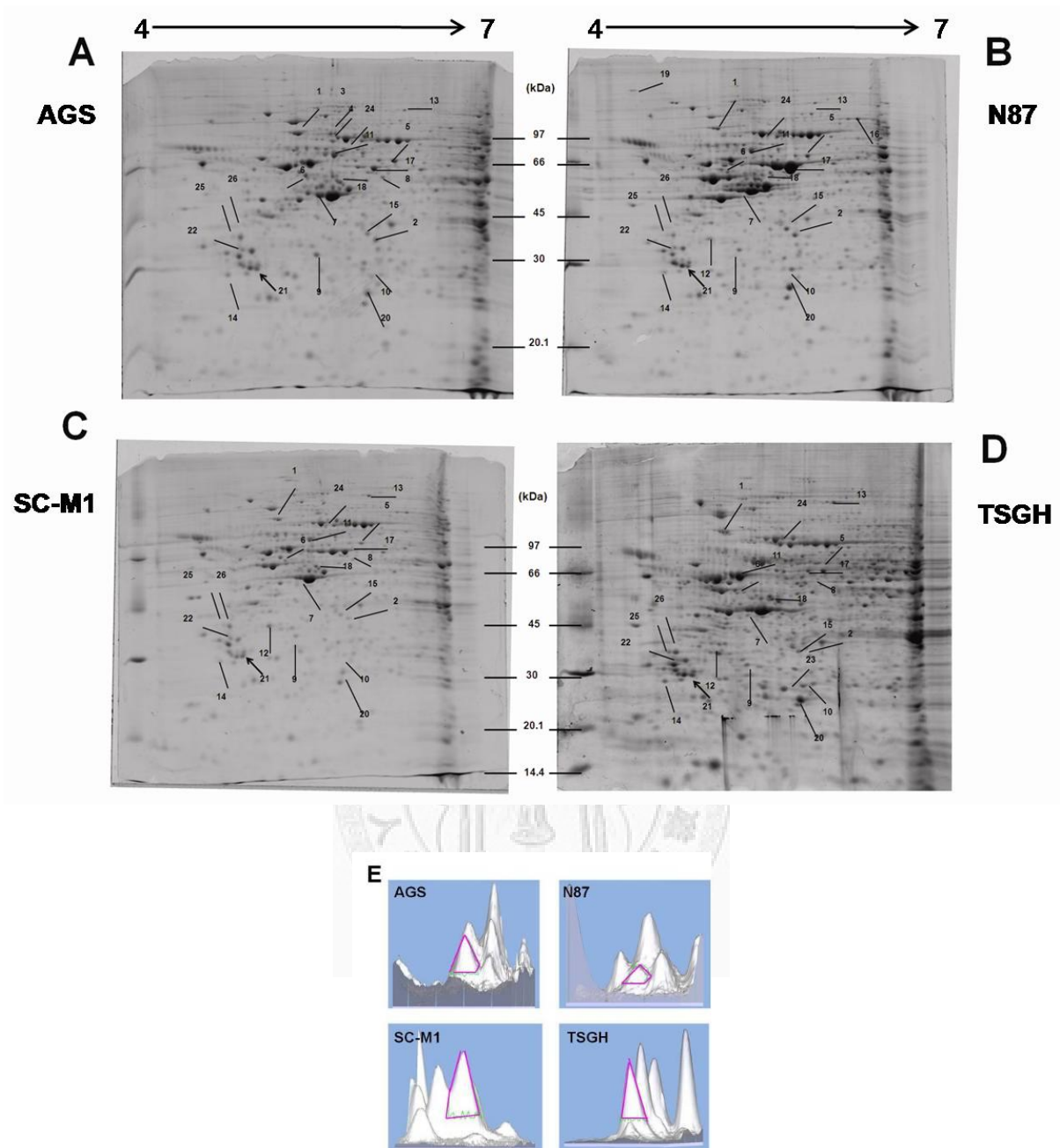
Figure 12 Expression profiles of gastric cancer cells. The expression profile of SC-M1 (C) was compared with those of other gastric cancer cell lines, including AGS (A), N87 (B) and TSGH (D). 500 μg of total protein was separated by 2-DE. For separation in the first dimension, isoelectric focusing (IEF) was performed using an 18cm strip (pH 4-7) at 8000V for a total of 91.2 KVhr at 20°C. The strips were then transferred onto a 12.5% non-gradient SDS-PAGE gel for second dimensional separation. The 2-D images were analyzed using ImageMaster software version 6.0 (Amersham Pharmacia Biotech) to detect and quantify protein spots. A total of 26 significant expressed cancer-relevant proteins ($P < 0.05$) were identified after Mascot search and shown in Table 10. 3-D profiles of 14-3-3β on the gels were shown in E. The expression profiles of these tumor cells were performed in triplicate.
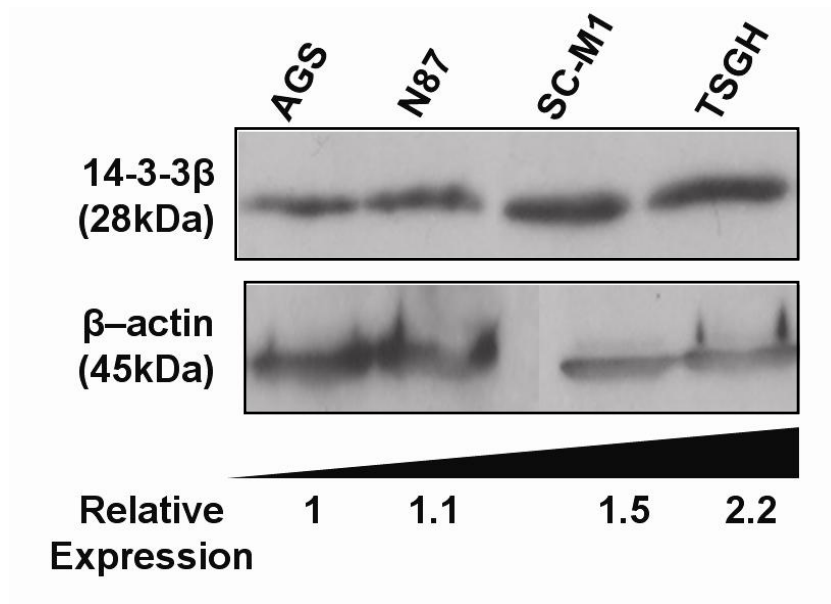
Figure 13 Endogenous 14-3-3β expression levels in gastric cancer cells. Endogenous 14-3-3β expression was detected in different gastric cancer cell lines, including non-metastatic AGS and N87 cells, poor differentiated AGS cells and high metastatic TSGH cells. β-actin was used as internal control.
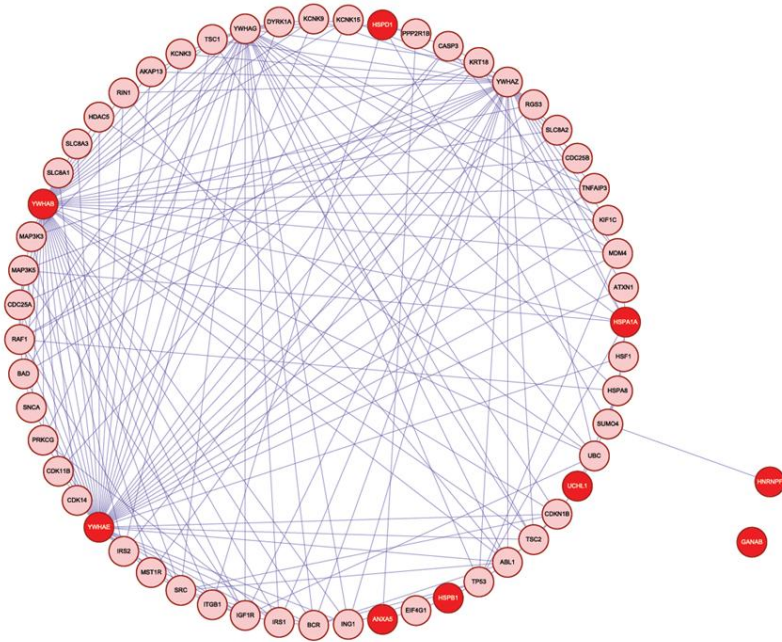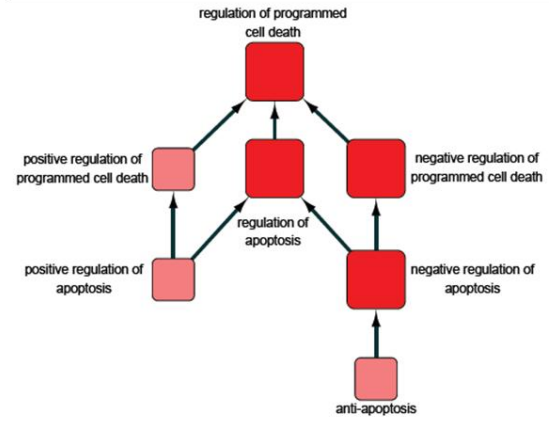
Figure 14 PIN in malignant cell lines. The identified proteins in TSGH and SC-M1 cells were used to construct PIN and analyzed related functions of the network. (A) Dark red nodes represent the identified proteins in TSGH and SC-M1 cells (Table 10) and light red nodes represent their interacting partners within the human PIN. Purple edges represent PPIs between proteins. (B) Nodes represent enriched GO terms in the PIN and edges represent the relationships in the GO.
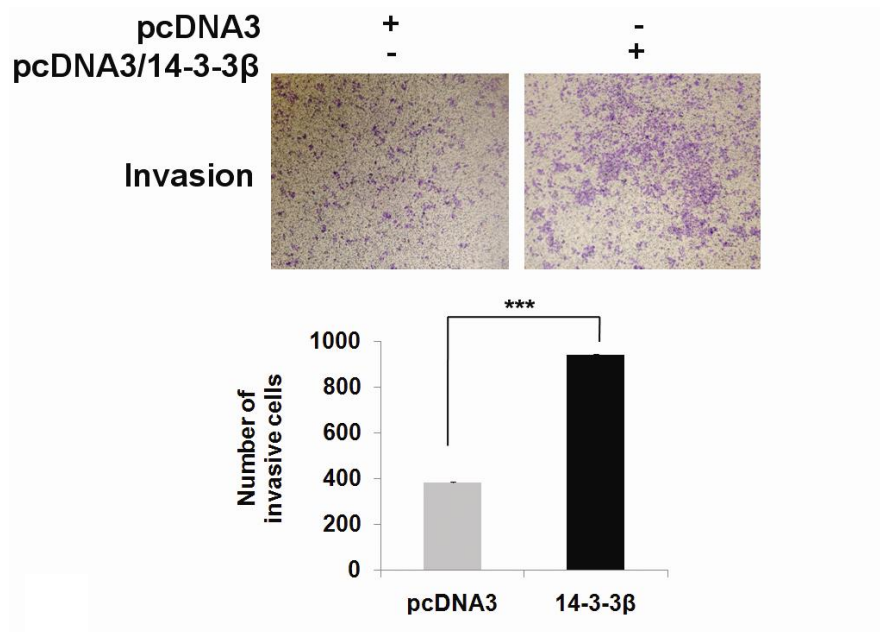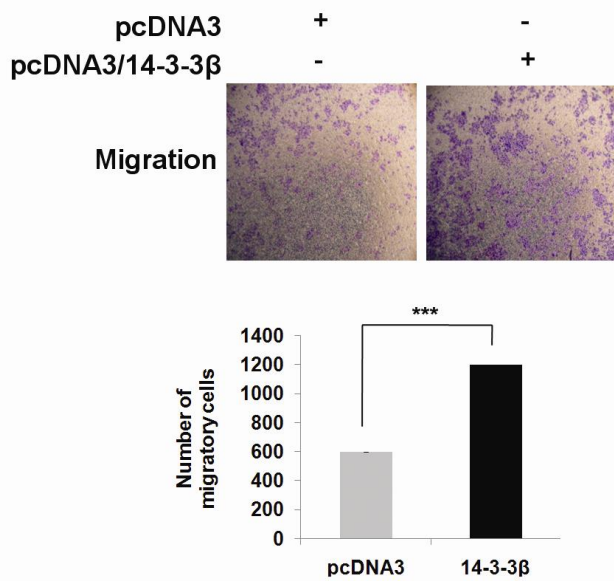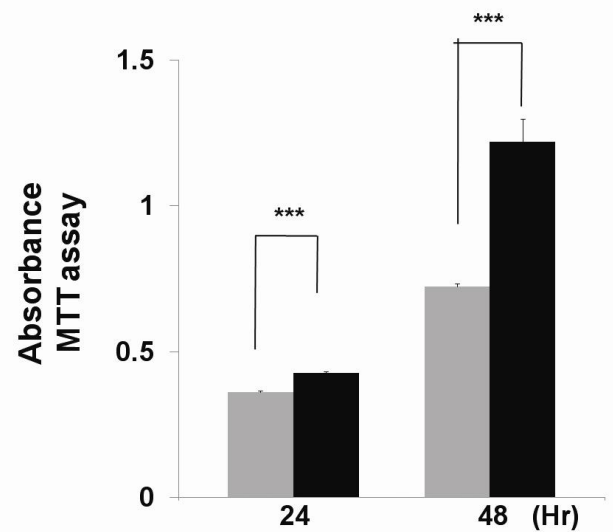
Figure 15 Over-expressed 14-3-3β enhances tumor cell invasion, migration and growth. (A and B) Invasive and migratory activities were measured after transfection with 14-3-3β plasmid into AGS cells for 48hr, respectively. (C) Cell growth was measured after transfection with 14-3-3β plasmid into AGS cells for 24 hr and 48hr by MTT assay. *** indicates $P < 0.001$.
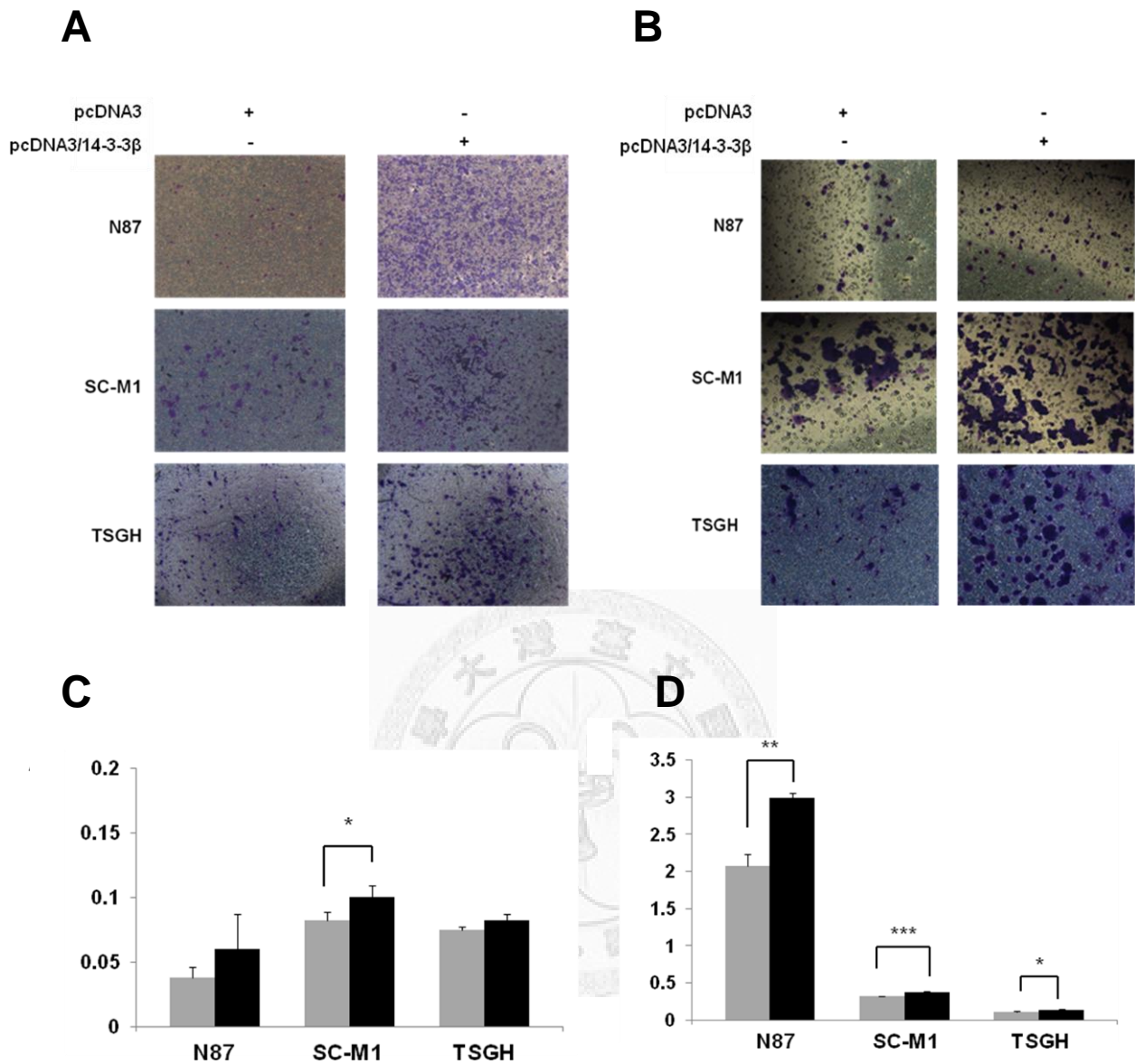
Figure 16 Over-expressed 14-3-3β enhances invasion, migration and growth of N87, SC-M1 and TSGH cells. Invasiveness (A) and migratory (B) activities were measured after transfection with pcDNA3/14-3-3β or pcDNA3 control vectors into N87, SC-M1 and TSGH cells for 48hr. Each experiment was performed in triplicate. Cell growth was measured after transfection with pcDNA3/14-3-3β or pcDNA3 control plasmid into gastric cancer cells, including N87, SC-M1 and TSGH, for 24 hr (C) and 48hr (D) by MTT assay. Black and gray bars represent pcDNA3/14-3-3β and pcDNA3 control vectors, respectively. Each experiment was performed in triplicate (*$P < 0.05$; **$P < 0.01$; ***$P < 0.001$).
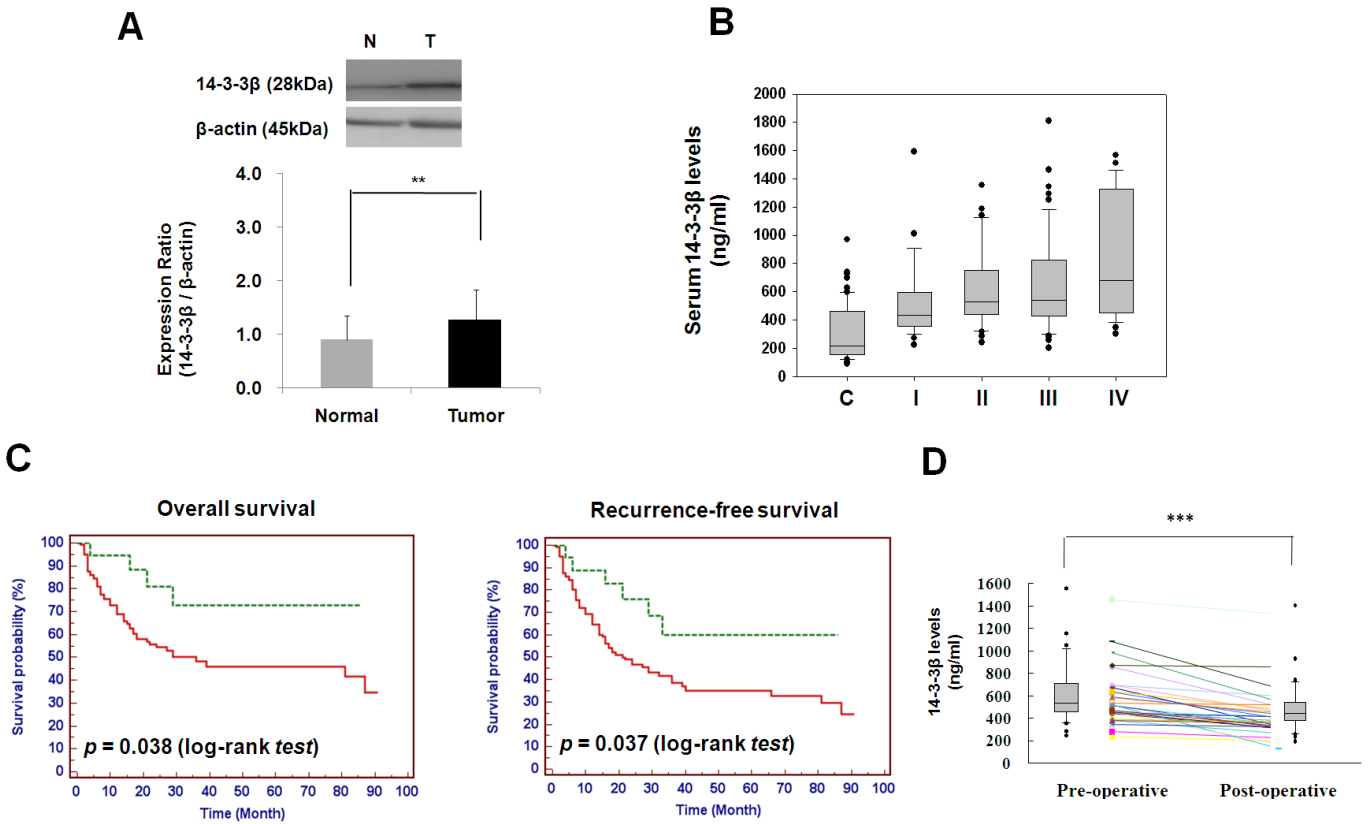
Figure 17 14-3-3β reduced patient survival. (A) 14-3-3β expression in 40 paired tumor and normal tissues was analyzed. β-actin served as a loading control (**, $P < 0.01$). (B) Comparison of serum 14-3-3β levels in controls ($N = 63$), stage I ($N = 28$), stage II ($N = 32$), stage III ($N = 56$) and stage IV ($N = 29$). (C) The relationship between serum 14-3-3β levels and patient survival. Solid line: higher 14-3-3β levels (≥ 349 ng/mL) ($N = 122$); dotted line: lower 14-3-3β levels (< 349 ng/mL) ($N = 20$). Patients with higher 14-3-3β values showed poorer overall ($P = 0.038$) and recurrence-free survival ($P = 0.037$). (D) 14-3-3β levels in pre- and post-operative patients (***, $P < 0.0001$) ($N = 31$).

14-3-3β, AUC = 0.776
Stage I (n =28) *vs* normal controls (n = 63)
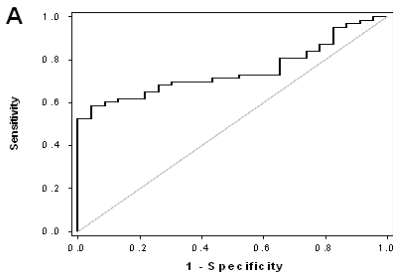
14-3-3β, AUC = 0.843
Stage II (n = 32) *vs* normal controls (n = 63)
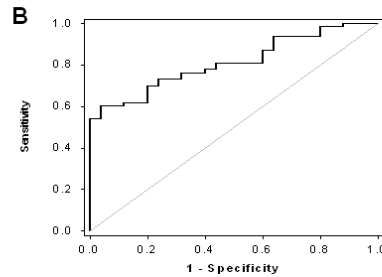
14-3-3β, AUC = 0.822
Stage III (n = 56) *vs* normal controls (n = 63)
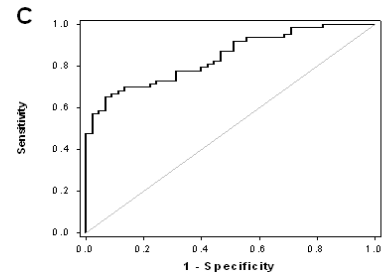
14-3-3β, AUC = 0.882
Stage IV (n = 29) *vs* normal controls (n = 63)
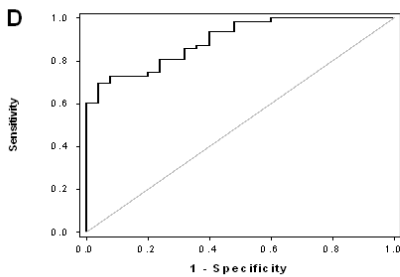
14-3-3β, AUC = 0.83
All Gastric Ca (n = 145) *vs* normal controls (n = 63)
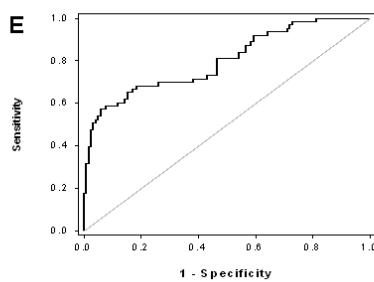
Figure 18 14-3-3β reduced patient survival. ROC curves of 14-3-3β. Serum concentrations of 14-3-3β from 145 gastric cancer patients and 63 control samples were determined by ELISA. The area under the curve (AUC) was 0.776 for stage I (95% CI, 0.676 to 0.857, A), 0.843 for stage II (95% CI, 0.753 to 0.909, B), 0.822 for stage III (95% CI, 0.741 to 0.886, C), 0.882 for stage IV (95% CI, 0.798 to 0.94, D), and 0.83 for all gastric cancer samples (95% CI, 0.772 to 0.878, E).
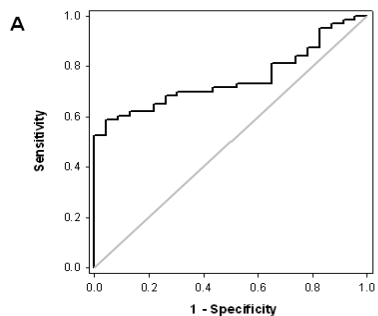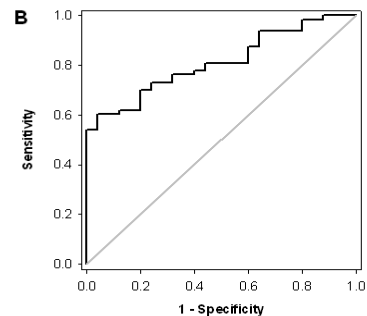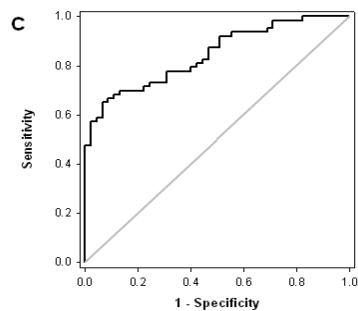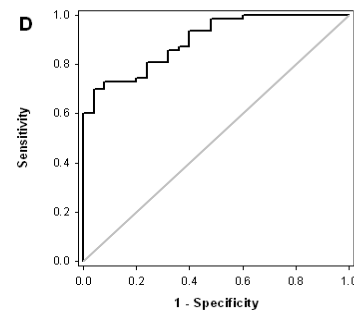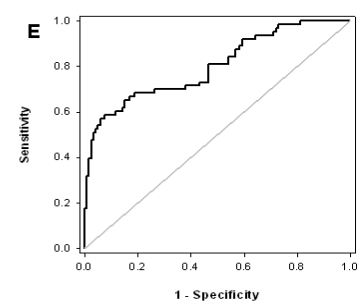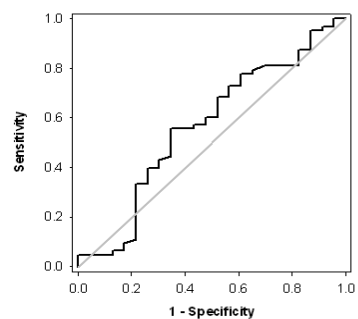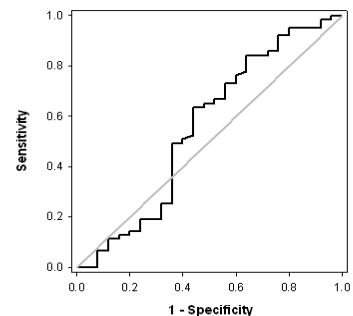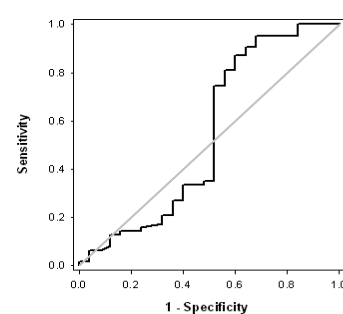
Figure 19 ROC curves of 14-3-3β and CEA. ROC curves of 14-3-3β and CEA at stage I (A, *P* = 0.023); stage II (B, *P* = 0.001); stage III (C, *P* < 0.001); stage IV (D, *P* < 0.001); all tumor samples (E, *P* < 0.001) were compared.
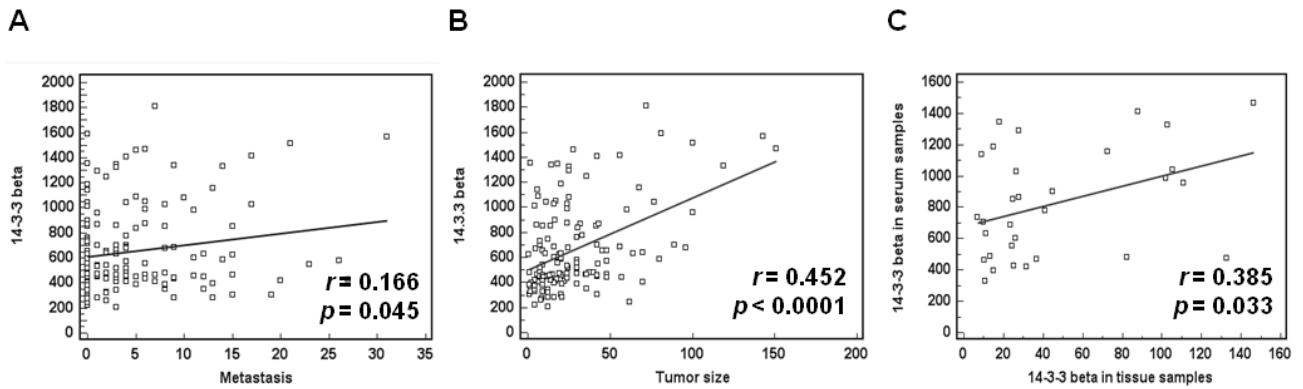
Figure 20 Serum 14-3-3β levels correlated with specific clinical features. Patient pre-operative serum 14-3-3β levels correlated with (A) the number of lymph node metastases ($N = 145$); (B) tumor size ($N = 139$) and (C) 14-3-3β expression in tumor tissues ($N = 31$).
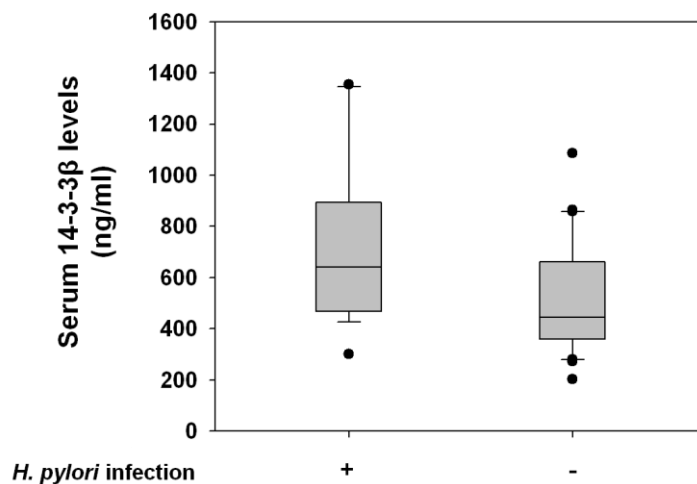
Figure 21 Correlation between H. pylori infection and 14-3-3β expression. Correlation between serum 14-3-3β levels and *H. pylori* was analyzed from available clinical data. The results showed that patients with *H. pylori* infection had higher 14-3-3β levels ($N = 18$) than those with no *H. pylori* infection ($N = 33$) ($P = 0.016$, *t*-test).

Tables

Table 1. Demographics of gastric cancer patients

	No. of patients	%
Age, years		
Median	67	
Range	29-89	
Gender		
Male	89	61
Female	56	39
Stage		
I and II	60	41
III and IV	85	59
Depth of tumor invasion		
T1	17	12
T2	42	29
T3	80	55
T4	6	4
Lymph node metastasis		
N0	42	29
N1	63	43
N2	30	21
N3	10	7
Distant metastasis		
M0	120	83
M1	25	17
Lauren classification		
Diffuse type	75	52
Intestinal type	68	48
Organ invasion		
Negative	106	73
Positive	39	27

Table 1. (Continued)

	No. of patients	%
Vascular invasion		
Negative	30	23
Positive	100	77
Peritoneal invasion		
Negative	124	86
Positive	21	14

Table 2. Activities of the 23 down-regulated miRNA-regulated PINs in normal and tumor tissues

Down-regulated miRNAs	Fold Change	T-test *P*-value	Normal		Tumor	
			P-value	Activity	*P*-value	Activity
miR-143	0.0397	1.52E-06	1	-	0.01	activated
miR-29c	0.0630	2.92E-11	0.08	-	0.01	activated
let-7b	0.1075	8.32E-13	0.96	-	< 0.001	activated
let-7a	0.1079	6.71E-11	0.96	-	< 0.001	activated
miR-29a	0.1224	1.64E-12	0.08	-	0.01	activated
miR-26a	0.1436	1.08E-10	0.21	-	< 0.001	activated
let-7f	0.1718	1.81E-08	0.96	-	< 0.001	activated
miR-22	0.1908	4.20E-09	0.56	-	< 0.001	activated
miR-141	0.1912	6.65E-10	0.08	-	0.01	activated
miR-142-3p	0.1930	3.10E-05	0.35	-	0.02	activated
miR-29b	0.2186	4.13E-10	0.08	-	0.01	activated
miR-148a	0.2201	1.51E-05	1	-	0.07	activated
miR-768-3p	0.2990	1.04E-05	0.12	-	< 0.001	activated
let-7g	0.3555	3.63E-06	0.96	-	< 0.001	activated
let-7c	0.3696	7.83E-11	0.96	-	< 0.001	activated
miR-200a	0.3805	3.22E-06	0.08	-	0.01	activated
miR-16	0.3378	4.59E-10	0	activated	0.03	activated
miR-145	0.0207	2.08E-07	0.01	inactivated	0.2	-
miR-23b	0.1874	2.27E-12	< 0.001	inactivated	0.93	-
miR-27b	0.4324	1.39E-09	< 0.001	inactivated	0.8	-
miR-638	0.1357	7.04E-07	0.93	-	0.68	-
miR-200c	0.1689	1.16E-11	0.52	-	0.28	-
miR-24	0.2120	2.25E-11	0.47	-	0.54	-

Table 3. Activities of the 39 unchanged miRNA-regulated PINs in normal and tumor tissues

Unchanged microRNAs	Normal		Tumor	
	P-value	Activity	*P*-value	Activity
miR-21	< 0.001	activated	< 0.001	activated
miR-107	0.01	activated	0.04	activated
miR-195	< 0.001	activated	0.03	activated
miR-103	0.01	activated	0.04	activated
miR-15b	< 0.001	activated	0.03	activated
miR-194	0.91	-	< 0.001	activated
miR-19b	0.43	-	0.01	activated
miR-324-3p	0.12	-	0.01	activated
let-7d	0.96	-	< 0.001	activated
let-7e	0.96	-	< 0.001	activated
let-7i	0.96	-	< 0.001	activated
miR-34a	0.74	-	0.03	activated
miR-193b	0.72	-	0.03	activated
miR-222	0.50	-	< 0.001	activated
miR-370	0.01	activated	0.13	-
miR-130a	0.00	activated	0.30	-
miR-23a	< 0.001	inactivated	0.93	-
miR-27a	< 0.001	inactivated	0.80	-
miR-30d	0.01	inactivated	0.20	-
miR-494	0.56	-	0.32	-
miR-192	1.00	-	1.00	-
miR-200b	0.52	-	0.28	-
miR-375	1.00	-	1.00	-
miR-215	1.00	-	1.00	-
miR-146a	1.00	-	1.00	-
miR-125b	0.34	-	0.33	-
miR-126	1.00	-	1.00	-

miR-768-5p	1.00	-	1.00	-
miR-142-5p	0.33	-	0.13	-
miR-575	1.00	-	1.00	-
miR-106b	0.73	-	0.69	-
miR-214	0.36	-	1.00	-
miR-25	0.81	-	0.18	-
miR-572	1.00	-	1.00	-
miR-31	1.00	-	1.00	-
miR-223	0.08	-	0.12	-
miR-93	0.73	-	0.69	-
miR-106a	0.73	-	0.69	-
miR-451	1.00	-	1.00	-

Table 4. Receiver operating characteristic (ROC) curves of the 23 down-regulated miRNAs in gastric cancer to classify tumor and normal samples

miRNAs	AUC	95% Cl of AUC	Overall correct classification (%)
16 oncomirs			
miR-29c	0.831[***]	0.687-0.927	77
miR-29b	0.661[*]	0.503-0.797	66
miR-29a	0.645	0.486-0.783	61
miR-200a	0.502	0.348-0.656	57
miR-141	0.620	0.461-0.762	64
miR-768-3p	0.715[**]	0.559-0.841	70
miR-26a	0.711[**]	0.555-0.837	70
miR-142-3p	0.599	0.441-0.744	57
miR-22	0.589	0.430-0.735	59
let-7c	0.655	0.497-0.792	68
let-7g	0.661[*]	0.503-0.797	66
let-7b	0.671[*]	0.514-0.805	64
let-7a	0.645	0.486-0.783	59
let-7f	0.618	0.459-0.760	59
miR-143	0.783[***]	0.633-0.893	75
miR-148a	0.785[***]	0.635-0.894	73
7 down-regulated miRNAs only			
miR-16	0.851	0.361-0.670	45
miR-23b	0.669[*]	0.511-0.804	66
miR-27b	0.655	0.497-0.792	61
miR-145	0.822[***]	0.678-0.921	80
miR-24	0.539	0.383-0.690	39
miR-200c	0.597	0.439-0.742	59
miR-638	0.680[*]	0.522-0.812	66
Combinations[†]			
All 16 oncomirs	0.981[****]	0.886-1.000	93
All 7 down-regulated miRNAs	0.888[****]	0.757-0.963	82

1. These data were obtained by miRNA microarray from 22 gastric cancer patients.

2. AUC, area under the receiver operating curve.

3. Cl, confidence interval.

4. Significant values of AUC, [*]$P < 0.05$; [**]$P < 0.01$; [***]$P < 0.001$; [****]$P < 0.0001$.

5. [†]Analyzed by stepwise logistic regression (enter variable if $P < 0.05$; remove variable if $P > 0.1$).

Table 5. The over-represented functions of oncomir-regulated PINs in gastric cancer

miRNA Family	Enriched Functions
miR-29abc	Ras protein signal transduction, phosphate metabolism, post-translational protein modification, intracellular signaling
miR-141/200a	RNA elongation from RNA polymerase II promoter, transcription initiation from RNA polymerase II promoter, post-translational protein modification, interphase of mitotic cell cycle, ectoderm development, intracellular signaling
miR-768-3p	Negative regulation of cell growth, DNA replication, cell cycling
miR-26a	RNA elongation from RNA polymerase II promoter, interphase of mitotic cell cycle, post-translational protein modification, transcription initiation from RNA polymerase II promoter, ectoderm development, intracellular signaling
miR-142-3p	Apoptosis, apoptotic mitochondrial changes, regulation of protein homo-/hetero-dimerization activity, regulation of mitochondrial membrane potential, negative regulation of developmental processes
miR-22	Actin cytoskeleton organization and biogenesis, actin filament polymerization, negative regulation of endocytosis, signal transduction
let-7/98	Ras protein signal transduction, anterior/posterior pattern formation, interphase of mitotic cell cycle, apoptosis, negative regulation of gene expression
miR-143	Regulation of chemokine biosynthetic processes, regulation of blood coagulation, blood coagulation, acute-phase response, positive regulation of transcription, wound healing
miR-148a	Integrin-mediated signaling, cell-matrix adhesion, blood coagulation, wound healing

Table 6. Cox proportional hazards regression: significance of clinicopathologic factors on overall survival

Variable	Univariate analysis		Multivariate analysis	
	HR (95% Cl)	*P*	HR (95% Cl)	*P*
miR-148a[†]	0.27 (0.08 to 0.88)	0.03	1.69 (0.61 to 2.77)	0.002
Stage: early (I + II) vs advanced (III + IV)	0.10 (0.07 to 0.42)	< 0.001	2.43 (0.84 to 4.02)	0.003
Peritoneal invasion	0.02 (0.002 to 0.25)	0.002	0.46 (-1.26 to 2.17)	0.601
Organ invasion	0.66 (0.19 to 2.34)	0.518	-1.04 (-2.05 to -0.02)	0.047
Vascular invasion	0.27 (0.1 to 0.69)	0.006	1.71 (-0.38 to 3.79)	0.11

Abbreviation: HR, hazard ratio; 95% Cl, Confidence interval of the estimated HR.

[†]Cutoff = 0.101

Table 7. The relationship between miR-148a expression levels and clinical factors

	No. of Patients	%	Mean (2-ΔΔCt)	P-value
Fold change (T/N)	62		0.524	
Gender				0.183[*]
Male	39	63	0.415	
Female	23	37	0.710	
Stage				0.283[**]
I	12	19	0.946	
II	14	23	0.204	
III	26	42	0.528	
IV	10	16	0.459	
Depth of tumor invasion				0.279[**]
T1	8	13	1.153	
T2	9	15	0.390	
T3	43	69	0.439	
T4	2	3	0.456	
Lymph node metastasis				0.237[**]
N0	21	34	0.235	
N1	25	40	0.809	
N2	11	18	0.255	
N3	5	8	0.650	
Distant metastasis				0.043[*]
Negative	58	94	0.549	
Positive	4	6	0.238	
Lauren classification				0.179[*]
Intestinal-type	58	94	0.549	
Diffuse-type	4	6	0.238	
Organ invasion				0.013[*]
Negative	27	44	0.630	
Positive	35	56	0.415	
Vascular invasion				0.305[*]
Negative	51	82	0.588	
Positive	11	18	0.230	
Peritoneal invasion				0.040[*]
Negative	17	27	0.676	
Positive	45	73	0.467	

T and N represent tumor and normal tissues, respectively. [*]t-test analysis. [**]One-way ANOVA analysis.

Table 8. Identification of significantly differentiated expressed proteins in miR-148a-overexpressing AGS cells

Gene name	Protein name	Accession number[a]	Protein score	Quantified peptides	Ratio (P/N)[b] (Mean[+-]SD)
Up-regulation					
CPOX	Coproporphyrinogen-III oxidase	IPI00093057	155	3	1.49 [+-] 0.16
			345	3	1.26 [+-] 0.18
ACBD3	Golgi resident protein GCP60	IPI00009315	44	1	1.44 [+-] 0
			148	2	1.21 [+-] 0.15
POLRMT	DNA-directed RNA polymerase	IPI00251989	56	2	1.42 [+-] 0.14
			94	2	1.20 [+-] 0
STK39	STE20/SPS1-related proline-alanine-rich protein kinase	IPI00004363	106	1	1.42 [+-] 0
			51	2	1.74 [+-] 0
RRM2	Ribonucleoside-diphosphate reductase subunit M2	IPI00011118	69	1	1.41 [+-] 0.01
			57	1	1.37 [+-] 0.35
GRWD1	Glutamate-rich WD repeat-containing protein 1	IPI00027831	105	1	1.40 [+-] 0
			327	2	1.26 [+-] 0
UBE2O	Ubiquitin-conjugating enzyme E2 O	IPI00783378	108	1	1.39 [+-] 0.34
			79	1	1.36 [+-] 0.14
NCAPD2	Condensin complex subunit 1	IPI00299524	133	1	1.38 [+-] 0.12
			304	6	1.30 [+-] 0.27
ANP32E	Acidic leucine-rich nuclear phosphoprotein 32 family member E	IPI00165393	186	2	1.37 [+-] 0.13
			943	3	1.38 [+-] 0.42
PRSS1	Trypsin-1	IPI00011694	197	1	1.35 [+-] 0.49
			532	2	1.36 [+-] 0.3
DIDO1	Isoform 1 of Death-inducer obliterator 1	IPI00249982	43	1	1.32 [+-] 0
			54	1	1.39 [+-] 0
PMM2	Phosphomannomutase 2	IPI00006092	108	1	1.24 [+-] 0.39
			136	3	1.42 [+-] 0.23
RBM39	Isoform 1 of RNA-binding protein 39	IPI00163505	368	3	1.23 [+-] 0.23
			794	3	1.33 [+-] 0.23
STAT3	Isoform Del-701 of Signal transducer and activator of transcription 3	IPI00306436	237	1	1.25 [+-] 0.25
			277	5	1.24 [+-] 0.1
UBE2V1	Isoform 1 of Ubiquitin-conjugating enzyme E2 variant 1	IPI00007847	52	1	1.21 [+-] 0
			69	2	1.30 [+-] 0.03
SARS	Seryl-tRNA synthetase	IPI00220637	57	1	1.23 [+-] 0.11
			1337	11	1.29 [+-] 0.3
Down-regulation					
MGST3	Microsomal glutathione S-transferase 3	IPI00647044	237	2	0.85 [+-] 0.15
			559	2	0.84 [+-] 0.18

Table 8. (Continued)

Gene name	Protein name	Accession number[a]	Protein score	Quantified peptides	Ratio (P/N)[b] (Mean[+-]SD)
RPL37A	60S ribosomal protein L37a	IPI00414860	47	1	0.85 [+-] 0.06
			84	1	0.87 [+-] 0
PYCR2	Pyrroline-5-carboxylate reductase 2	IPI00470610	61	1	0.84 [+-] 0
			425	2	0.88 [+-] 0.14
SNRPA1	U2 small nuclear ribonucleoprotein A' Galectin-3-binding protein	IPI00297477	413	2	0.83 [+-] 0.15
			697	3	0.78 [+-] 0.11
LGALS3BP	Solute carrier family 2 U2 small nuclear ribonucleoprotein A'	IPI00023673	200	3	0.83 [+-] 0.13
			187	2	0.87 [+-] 0.14
SLC2A1	Galectin-3-binding protein	IPI00220194	111	1	0.83 [+-] 0.13
			811	6	0.83 [+-] 0.15
ATP5O	ATP synthase subunit O	IPI00007611	237	4	0.83 [+-] 0.07
			294	4	0.85 [+-] 0.19
ELOVL1	Elongation of very long chain fatty acids protein 1	IPI00010187	141	2	0.82 [+-] 0.11
			76	1	0.88 [+-] 0
ANXA4	annexin IV	IPI00793199	2250	7	0.81 [+-] 0.14
			866	6	0.82 [+-] 0.12
C3orf31	MMP37-like protein	IPI00060287	121	1	0.81 [+-] 0.14
			58	1	0.73 [+-] 0
RTN4	Isoform 2 of Reticulon-4	IPI00298289	608	4	0.81 [+-] 0.11
			501	3	0.82 [+-] 0.19
POLR1E	Isoform 1 of DNA-directed RNA polymerase I subunit RPA49	IPI00251989	96	1	0.81 [+-] 0.03
			89	1	0.74 [+-] 0
DCI	Isoform 1 of 3 2-trans-enoyl-CoA isomerase mitochondrial	IPI00300567	401	2	0.80 [+-] 0.19
			204	1	0.75 [+-] 0.11
CTSD	Cathepsin D	IPI00011229	571	4	0.80 [+-] 0.14
			210	4	0.80 [+-] 0.11
H2AFY	H2A histone family	IPI00059366	437	2	0.80 [+-] 0.09
			1322	8	0.80 [+-] 0.14
GSK3A	Glycogen synthase kinase-3 alpha	IPI00292228	46	1	0.80 [+-] 0
			213	3	0.86 [+-] 0.11
MRPL38	39S ribosomal protein L38	IPI00783656	45	1	0.80 [+-] 0
			65	2	0.77 [+-] 0
RQCD1	Cell differentiation protein RCD1 homolog	IPI00023101	87	2	0.80 [+-] 0
			71	1	0.69 [+-] 0
SMS	Spermine synthase	IPI00642393	82	1	0.79 [+-] 0.08
			162	1	0.90 [+-] 0

Table 8. (Continued)

Gene name	Protein name	Accession number[a]	Protein score	Quantified peptides	Ratio (P/N)[b] (Mean[+-]SD)
HIBCH	Isoform 2 of 3-hydroxyisobutyryl-CoA hydrolase	IPI00377161	64	1	0.79 [+-] 0
			102	3	0.89 [+-] 0.07
PHF6	Isoform 1 of PHD finger protein 6	IPI00395568	76	1	0.78 [+-] 0
			45	1	0.88 [+-] 0
RAB10	Ras-related protein Rab-10	IPI00016513	680	4	0.77 [+-] 0.14
			362	5	0.88 [+-] 0.1
VASP	Vasodilator-stimulated phosphoprotein	IPI00301058	469	3	0.77 [+-] 0.03
			397	6	0.84 [+-] 0.11
KRT2	Keratin	IPI00021304	306	6	0.76 [+-] 0.02
			219	3	0.84 [+-] 0.11
IFIT3	Interferon-induced protein with tetratricopeptide repeats 3	IPI00024254	107	1	0.76 [+-] 0
			79	2	0.85 [+-] 0.02
RPRD1B	Regulation of nuclear pre-mRNA domain-containing protein 1B	IPI00009659	44	1	0.76 [+-] 0
			236	2	0.87 [+-] 0.15
GNPDA1	Glucosamine-6-phosphate isomerase 1	IPI00009305	44	1	0.74 [+-] 0
			270	3	0.84 [+-] 0.12
SUCLG1	Succinyl-CoA ligase [GDP-forming] subunit alpha	IPI00872762	46	1	0.73 [+-] 0
			66	1	0.88 [+-] 0
TAP2	HLA-DOB transporter 2	IPI00001382	50	1	0.71 [+-] 0
			196	2	0.84 [+-] 0.06
PODXL	Podocalyxin-like protein 1 precursor	IPI00299116	193	2	0.69 [+-] 0.07
			208	2	0.84 [+-] 0
FAF2	FAS-associated factor 2	IPI00172656	44	1	0.63 [+-] 0
			373	3	0.84 [+-] 0.14
KRT1	Keratin	IPI00220327	250	6	0.52 [+-] 0.1
			262	6	0.71 [+-] 0.11
KRT10	Keratin	IPI00009865	116	2	0.39 [+-] 0
			177	4	0.83 [+-] 0.03
GGH	Gamma-glutamyl hydrolase	IPI00023728	144	2	0.88 [+-] 0.01
			141	2	0.85 [+-] 0.29
FKBP2	Peptidyl-prolyl cis-trans isomerase FKBP2	IPI00002535	50	1	0.89 [+-] 0
			67	1	0.85 [+-] 0
SAMHD1	Isoform 1 of SAM domain and HD domain-containing protein 1	IPI00943982	479	4	0.88 [+-] 0.13
			608	6	0.84 [+-] 0.18
UQCRC2	Cytochrome b-c1 complex subunit 2	IPI00305383	113	2	0.88 [+-] 0
			690	4	0.84 [+-] 0.18

Table 8. (Continued)

Gene name	Protein name	Accession number[a]	Protein score	Quantified peptides	Ratio (P/N)[b] (Mean[+-]SD)
COX4I1	Cytochrome c oxidase subunit 4 isoform 1	IPI00006579	242	3	0.86 [+-] 0.11
			398	3	0.82 [+-] 0.09
POLR1E	Isoform 1 of DNA-directed RNA polymerase I subunit RPA49	IPI00251989	96	1	0.81 [+-] 0.03
			89	1	0.74 [+-] 0
HSDL2	Isoform 1 of Hydroxysteroid dehydrogenase-like protein 2	IPI00031107	102	1	0.87 [+-] 0.09
			512	3	0.68 [+-] 0
KRAS	Isoform 2A of GTPase KRas	IPI00423568	72	1	0.89 [+-] 0
			112	2	0.67 [+-] 0.05

The data are analyzed from iTRAQ results. Each sample is analyzed in biological duplicate and Mean [+-] SD value is obtained based on expression value of all identified peptides in each protein.

[a]Accession number is obtained from International protein index (IPI) database.

[b]P and N represent miR-148a precursor and its negative control, respectively.
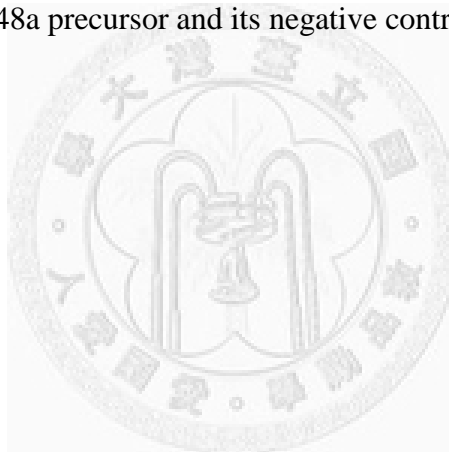
Table 9. Associated biological functions of all identified proteins from iTRAQ

Biological Functions	Proteins
Cancer	SLC2A1, RRM2, ANXA4, KRAS, STAT3, PRPF38B, KRT10, CTSD, SMS, PRSS1/PRSS3, LGALS3BP, KRT2, RBM39, COX4I1
Gastrointestinal Disease	CTSD, PRSS1/PRSS3, RRM2, KRAS, KRT10, TAP2, MGST3
Genetic Disorder	IFIT3, SLC2A1, RRM2, KRAS, GSK3A, STAT3, KRT10, CTSD, HIBCH, PRSS1/PRSS3, H2AFY, LGALS3BP, KRT2, KRT1, TAP2, MGST3,
Dermatological Diseases and Conditions	IFIT3, PRSS1/PRSS3, H2AFY, LGALS3BP, KRT2, GSK3A, KRT1, KRT10
Hair and Skin Development and Function	KRT2, KRT10, KRT1
Organ Development	KRT2, KRT10, KRT1
Carbohydrate Metabolism	GNPDA1, SLC2A1, GSK3A
Molecular Transport	SLC2A1, GGH, RRM2, GSK3A, TAP2
Small Molecule Biochemistry	SMS, GNPDA1, SLC2A1, GGH, RRM2, GSK3A, KRT1
Amino Acid Metabolism	SMS, GGH
Cell Cycle	KRAS, STAT3, NCAPD2, TAP2
Cell Death	CTSD, SLC2A1, LGALS3BP, UBE2V1, RRM2, RTN4, GSK3A, KRAS, STAT3
Cell Morphology	CTSD, RTN4, KRT2
Cell-To-Cell Signaling and Interaction	PRSS1/PRSS3, LGALS3BP, KRT2, KRAS, VASP
Cell-mediated Immune Response	CTSD
Cellular Development	CTSD, STK39, KRAS, STAT3
Cellular Function and Maintenance	CTSD
Cellular Movement	CTSD, PODXL, PRSS1/PRSS3, SLC2A1, RRM2, RTN4, KRT2, STAT3, SARS, VASP
Developmental Disorder	PHF6, KRAS
Drug Metabolism	GGH
Hematological System Development and Function	CTSD, STAT3
Hematopoiesis	CTSD
Metabolic Disease	HIBCH, CTSD, SLC2A1, SUCLG1, PMM2
Nervous System Development and Function	RTN4
Neurological Disease	CTSD, PHF6, SLC2A1, SAMHD1
Nucleic Acid Metabolism	RRM2
Cellular Growth and Proliferation	CTSD, SLC2A1, RRM2, KRAS, STAT3, KRT10
Behavior	PRSS1/PRSS3, STAT3
Gene Expression	KRAS, STAT3, POLRMT
Tissue Morphology	STAT3, VASP
Tumor Morphology	KRAS
Vitamin and Mineral Metabolism	GGH, KRT1
Antigen Presentation	STAT3, KRT1

Table 9. (Continued)

Biological Functions	Proteins
Cellular Assembly and Organization	RTN4, NCAPD2, TAP2
Endocrine System Disorders	PRSS1/PRSS3
Inflammatory Disease	PRSS1/PRSS3, KRT10
Inflammatory Response	STAT3, KRT1
Hematological Disease	RRM2, KRAS, STAT3
Immunological Disease	RRM2, KRAS, STAT3
Cellular Compromise	CTSD, RTN4, KRAS, STAT3, COX4I1
RNA Post-Transcriptional Modification	SARS
Connective Tissue Development and Function	SMS, GNPDA1, SLC2A1, GGH, RRM2, GSK3A, KRT1
Reproductive System Disease	LGALS3BP, RTN4
DNA Replication, Recombination, and Repair	KRAS, RBM39, COX4I1
Hepatic System Disease	KRAS, NCAPD2, TAP2
Cardiovascular Disease	CTSD, SLC2A1, RRM2, STAT3, TAP2, MGST3
Respiratory Disease	STK39, ACBD3, RRM2, ANXA4, GSK3A, STAT3, UBE2O, HIBCH, C3orf31, POLR3A, SUCLG1, RTN4, FAF2, RBM39, COX4I1
Renal and Urological Disease	KRAS
Embryonic Development	RRM2, KRAS, STAT3
Humoral Immune Response	RQCD1

Biological functions are obtained based on IPA analysis.

Table 10. Identification of differentially expressed proteins in gastric cancer cells

Spot	Gene Name[a]	Accession Number[a]	Protein Name[b]	m/z[b]	PI[b]	Matched Peptides[c]	Coverage (%)	Ion Score[d]	AGS/SC-M1 (Mean±SD)[e]	N87/SC-M1 (Mean±SD)[e]	TSGH/SC-M1 (Mean±SD)[e]	Molecular function[f]
1	GRP78	P11021	78 kDa glucose-regulated protein	72288/1	5.07	5	12	351	1.30±0.10	0.66±0.18	0.87±0.02	Anti-apoptosis
2	ANXA3	P12429	Annexin A3	36353/1	5.63	2	7	52	2.18±0.17	2.12±0.5	1.60±0.16	Positive regulation of angiogenesis and endothelial cell migration
3	ACTB	P60709	Actin, cytoplasmic 1	41710/1	5.29	2	9	94	A	-	-	Cytoskeleton
4	ACTA	P62736	Actin, aortic smooth muscle	41982/1	5.23	1	4	35	A	-	-	Protein binding
5	PDIA3	P30101	Protein disulfide-isomerase A3	56747/1	5.98	4	10	347	1.10±0.57	0.84±0.36	0.43±0.02	Protein binding and folding
6	PDIA6	Q15084	Protein disulfide-isomerase A6	48091/1	4.95	4	17	148	1.45±0.22	0.87±0.16	1.38±0.03	Protein binding and folding
7	ACTB	P60709	Actin, cytoplasmic 1	41710/1	5.29	3	14	115	0.98±0.12	0.76±0.24	0.91±0.09	Cytoskeleton
8	ARP3	P61158	Actin-related protein 3	47341/1	5.61	3	11	99	1.51±0.17	1.38±0.14	0.91±0.02	Cytoskeleton
9	CLIC1	O00299	Chloride intracellular channel protein 1	26906/1	5.09	1	3	32	1.66±0.25	0.98±0.26	1.37±0.28	Signal transduction
10	HSPB1	P04792	Heat shock protein beta-1	22768/1	5.98	2	13	114	1.76±0.21	3.14±1.01	4.24±1.27	Anti-apoptosis
11	CH60	P10809	60 kDa heat shock protein, mitochondrial	61016/1	5.70	3	7	252	1.07±0.37	1.00±0.30	1.11±0.39	Negative regulation of apoptosis
12	ANXA5	P08758	Annexin A5	35914/1	4.94	3	18	128	0.76±0.02	0.90±0.02	1.50±0.02	Anti-apoptosis; negative regulation of coagulation
13	GANAB	Q14697	Neutral alpha-glucosidase AB	106807/1	5.74	4	6	86	0.47±0.03	0.61±0.17	1.05±0.02	carbohydrate metabolic process
14	IF6	P56537	Eukaryotic translation initiation factor 6	26582/1	4.56	2	17	232	1.36±0.06	0.83±0.13	2.05±0.11	translation initiation factor activity; ribosome binding
15	IPYR	Q15181	Inorganic pyrophosphatase	32639/1	5.54	3	14	50	1.33±0.09	1.58±0.33	1.63±0.18	inorganic diphosphatase activity
16	EZRI	P15311	Ezrin	69370/1	5.94	2	1	71	1.32±0.06	1.01±0.31	1.11±0.02	cell adhesion molecule binding
17	GFAP	P14136	Glial fibrillary acidic protein	49850/1	5.42	1	2	61	1.20±0.59	1.03±0.27	0.26±0.02	Cytoskeleton

Table 10. (Continued)

Spot	Gene Name[a]	Accession Number[a]	Protein Name[b]	m/z[b]	PI[b]	Matched Peptides[c]	Coverage (%)	Ion Score[d]	AGS/SC-M1 (Mean±SD)[e]	N87/SC-M1 (Mean±SD)[e]	TSGH/SC-M1 (Mean±SD)[e]	Molecular function[f]
18	HNRPF	P52597	Heterogeneous nuclear ribonucleoprotein F	45643/1	5.38	2	8	119	0.84±0.20	0.73±0.18	1.19±0.16	Protein binding; RNA splicing
19	INVO	P07476	Involucrin	68437/1	4.62	3	9	256	-	N	-	Protein binding
20	GSTP1	P09211	Glutathione S-transferase P	23341/1	5.43	3	22	132	2.01±1.42	3.05±1.50	3.60±0.02	Anti-apoptosis
21	YWHAB	P31946	14-3-3 protein beta/alpha	28065/1	4.76	14	40	170	0.54±0.11	0.45±0.06	1.18±0.13	Ras signal transduction
22	YWHAE	P62258	14-3-3 protein epsilon	29155/1	4.63	3	19	129	0.78±0.04	0.42±0.07	0.86±0.07	Apoptosis
23	UCHL1	P09936	Ubiquitin carboxyl-terminal hydrolase isozyme L1	24808/1	5.33	1	9	52	-	-	T	negative regulation of MAP kinase activity
24	HSP71	P08107	Heat shock 70 kDa protein 1A/1B	70009/1	5.48	2	4	67	0.75±0.21	0.71±0.24	1.27±0.53	Anti-apoptosis
25	CH60	P10809	60 kDa heat shock protein, mitochondrial	61016/1	5.70	2	6	90	0.82±0.21	0.95±0.02	1.95±0.65	Negative regulation of apoptosis
26	CH60	P10809	60 kDa heat shock protein, mitochondrial	61016/1	5.70	2	6	98	3.22±1.51	0.51±0.02	4.69±1.62	Negative regulation of apoptosis

These differentially expressed protein spots are identified by MS/MS and then selected after Mascot database searching ($P < 0.05$).

[a] Gene name and accession number are obtained from SWISS-PROT database.

[b] The data are identified after Mascot database searching (m/z, m = mass; z = +1).

[c] The number of trypsic peptides which match to peptides of the identified proteins.

[d] Ion score was obtained based on MS/MS analysis.

[e] A, N and T represent AGS, N87 and TSGH gastric cancer cell lines.

[f] Molecular function is based on GO database.

Table 11. The relationship between 14-3-3β and clinical factors

	Mean (ng/ml)	Median (ng/ml)	P-value
Stage[a]			0.015[*]
I and II ($N = 60$)	576.38 ± 283.98	472.44	
III and IV ($N = 85$)	712.03 ± 375.94	578.83	
Depth of tumor invasion[b]			0.043[*]
T1 ($N = 17$)	467.44 ± 177.08	427.17	
T2 ($N = 42$)	620.24 ± 353.53	482.44	
T3 ($N = 80$)	716.55 ± 353.18	633.28	
T4 ($N = 6$)	637.57 ± 407.00	467.17	
Lymph node metastasis[b]			0.218
N0 ($N = 42$)	607.61 ± 315.28	525.22	
N1 ($N = 63$)	654.56 ± 321.93	532.17	
N2 ($N = 30$)	656.76 ± 376.48	471.33	
N3 ($N = 10$)	864.53 ± 486.74	716.06	
Distant metastasis[a]			0.030[*]
M0 ($N = 120$)	620.23 ± 318.04	518.00	
M1 ($N = 25$)	827.11 ± 425.80	681.19	
Lauren classification[a]			0.957
Diffuse-type ($N = 75$)	656.60 ± 373.71	488.28	
Intestinal-type ($N = 68$)	659.74 ± 318.91	554.77	
Organ invasion[a]			0.088
Negative ($N = 106$)	624.88 ± 323.36	516.06	
Positive ($N = 39$)	745.17 ± 393.14	602.72	
Vascular invasion[a]			0.125
Negative ($N = 30$)	595.70 ± 294.35	481.89	
Positive ($N = 100$)	698.92 ± 371.42	573.56	
Peritoneal invasion[a]			0.049[*]
Negative ($N = 124$)	625.31 ± 318.57	516.06	
Positive ($N = 21$)	836.54 ± 453.08	631.61	

Serum 14-3-3β levels were measured by ELISA, and mean (mean ± SD) and median values are given for each group.

[a]t-test analysis. [b]One-way ANOVA analysis. [*]$P < 0.05$.

Appendix

Journal Papers

1. **<u>Chien-Wei Tseng</u>**, Jyh-Chin Yang, Chiung-Nien Chen, Hsuan-Cheng Huang, Kai-Neng Chuang, Chen-Ching Lin, Hong-Shiee Lai, Po-Huang Lee, King-Jen Chang, Hsueh-Fen Juan. Identification of 14-3-3β in human gastric cancer cells and its potency as a diagnostic and prognostic biomarker. *Proteomics* 2011, *11*, 2423-2439.

2. **<u>Chien-Wei Tseng</u>**, Chen-Ching Lin, Chiung-Nien Chen, Hsuan-Cheng Huang, Hsueh-Fen Juan. Integrative network analysis reveals active microRNAs and their functions in gastric cancer. *BMC Systems Biology* 2011, *5*, 99.

3. Yet-Ran Chen, Hsueh-Fen Juan, Hsuan-Cheng Huang, Hsin-Hung Huang, Ya-Jung Lee, Mei-Yueh Liao, **<u>Chien-Wei Tseng</u>**, Li-Ling Lin, Jeou-Yuan Chen, Mei-Jung Wang, Jenn-Han Chen, Yu-Ju Chen. Quantitative Proteomic and Genomic Profiling Reveals Metastasis-Related Protein Expression Patterns in Gastric Cancer Cells. *Journal of Proteome Research* 2006, *5*, 2727-2742.

Conferences Proceedings

1. **<u>Chien-Wei Tseng</u>**, Chen-Ching Lin, Kai-Neng Chuang, Chiung-Nien Chen, Hsuan-Cheng Huang, and Hsueh-Fen Juan. MicroRNA-148a suppresses cell metastasis through targeting 14-3-3β in gastric cancer. 2011 Translational Medicine Conference and Taiwan Proteomics Society Annual Symposium, Taipei, Taiwan, April 27-28 **(Poster Award)**.

2. **<u>Chien-Wei Tseng</u>**, Chen-Ching Lin, Chiung-Nien Chen, Hsuan-Cheng Huang, and Hsueh-Fen Juan. MicroRNA-148a suppresses cell metastasis through targeting 14-3-3β in gastric cancer. 2011 College of Life Science Symposium, National Taiwan University, Taipei, Taiwan, June 3 **(Poster Award)**.

3. **<u>Chien-Wei Tseng</u>**, Chiung-Nien Chen, Hsueh-Fen Juan. 14-3-3β is a novel biomarker for early detection and prognosis in gastric cancer. 2008 Taiwan-Japan Proteomics Symposium, Taipei, Taiwan, Dec. 3-5 **(Poster Award: 1st prize)**.

RESEARCH ARTICLE

Identification of 14-3-3β in human gastric cancer cells and its potency as a diagnostic and prognostic biomarker

Chien-Wei Tseng[1], Jyh-Chin Yang[2], Chiung-Nien Chen[3,4,5*], Hsuan-Cheng Huang[6], Kai-Neng Chuang[1], Chen-Ching Lin[6,7], Hong-Shiee Lai[3], Po-Huang Lee[3], King-Jen Chang[3,4,8] and Hsueh-Fen Juan[1,7]

[1] Department of Life Science, Institute of Molecular and Cellular Biology, National Taiwan University, Taipei, Taiwan
[2] Department of Internal Medicine, National Taiwan University Hospital and College of Medicine, Taipei, Taiwan
[3] Department of Surgery, National Taiwan University Hospital and College of Medicine, Taipei, Taiwan
[4] Angiogenesis Research Center, National Taiwan University, Taipei, Taiwan
[5] Division of Mechanics, Research Center for Applied Sciences, Academia Sinica, Taipei, Taiwan
[6] Institute of Biomedical Informatics and Center for Systems and Synthetic Biology, National Yang-Ming University, Taipei, Taiwan
[7] Graduate Institute of Biomedical Electronics and Bioinformatics, National Taiwan University, Taipei, Taiwan
[8] Department of Surgery, Cheng Ching Hospital, Taicrang, Taiwan

Gastric cancer is the second most common cause of cancer deaths worldwide and due to its poor prognosis, it is important that specific biomarkers are identified to enable its early detection. Through 2-D gel electrophoresis and MALDI-TOF-TOF-based proteomics approaches, we found that 14-3-3β, which was one of the proteins that were differentially expressed by 5-fluorouracil-treated gastric cancer SC-M1 cells, was upregulated in gastric cancer cells. 14-3-3β levels in tissues and serum were further validated in gastric cancer patients and controls. The results showed that 14-3-3β levels were elevated in tumor tissues ($n = 40$) in comparison to normal tissues ($n = 40$; $p < 0.01$), and serum 14-3-3β levels in cancer patients ($n = 145$) were also significantly higher than those in controls ($n = 63$; $p < 0.0001$). Elevated serum 14-3-3β levels highly correlated with the number of lymph node metastases, tumor size and a reduced survival rate. Moreover, overexpression of 14-3-3β enhanced the growth, invasiveness and migratory activities of tumor cells. Twenty-eight proteins involved in anti-apoptosis and tumor progression were also found to be differentially expressed in 14-3-3β-overexpressing gastric cancer cells. Overall, these results highlight the significance of 14-3-3β in gastric cancer cell progression and suggest that it has the potential to be used as a diagnostic and prognostic biomarker in gastric cancer.

1 Introduction

Gastric cancer is the second leading cause of cancer deaths worldwide (WHO 2009 report) [1], with more than 80% of patients being diagnosed at an advanced stage of tumor progression or experiencing tumor recurrence after surgical resection [2]. Gastric cancer patients diagnosed with

Correspondence: Dr. Hsueh-Fen Juan, Department of Life Science, National Taiwan University, No. 1, Sec. 4, Roosevelt Rd., Taipei 106, Taiwan
E-mail: yukijuan@ntu.edu.tw
Fax: +886-2-23673374

Abbreviations: AUC, area under the curve; **CEA,** carcinoembryonic antigen; **5-FU,** 5-fluorouracil; **MTT,** 3-(4,5-dimethylthiazol-2-yl)-2,5-diphenyltetrazolium bromide; **PPI,** protein–protein interactions; **ROC,** receiver operating characteristics

*Additional corresponding author: Dr. Chiung-Nien Chen
  E-mail: cnchen@ntu.edu.tw
Colour online: See article online to view Figs. 1, 3, 6, 8 in colour

advanced stages have a survival rate of <35% beyond 5 years [3]. The poor prognosis is mainly due to the fact that most patients are diagnosed with advanced stages or tumor recurrence after curative surgery. Thus, identification of serum markers for early detection and prognosis in gastric cancer is critical for prolonged patient survival.

Serological tumor markers are routinely used for the detection and screening of early-stage cancers in asymptomatic patients. Several gastric cancer markers have been discovered, including carcinoembryonic antigen (CEA), carbohydrate antigen 19-9 (CA19-9) and carbohydrate antigen 72-4 (CA72-4) [4, 5]; however, these are not sensitive nor specific enough for disease detection [6, 7]. Therefore, the identification of novel gastric cancer biomarkers that are sensitive and specific enough to facilitate early detection is required.

Proteomic techniques provide powerful high-throughput methods of studying the complete set of proteins (proteome) that is expressed in a cell, tissue, organ or organism at a given time. Oncoproteomics is the study of protein complexes and interactions in cancers and has been increasingly applied to discover novel cancer biomarkers [8]. Recent reports indicate that proteomic approaches can be used to identify altered proteins, potentially cancer biomarkers, with drug treatment in cancer therapy [9, 10]. In this study, we used proteomic methods to identify differentially expressed proteins from 5-fluorouracil (5-FU)-treated and untreated gastric cancer SC-M1 cells. 5-FU is a widely used chemotherapeutic agent in the treatment of gastric cancer. We identified that 14-3-3β was significantly upregulated in untreated cancer cells. Reports indicate that 14-3-3β is abundant in human lung cancer relative to normal tissues [11] and mutated chronic lymphocytic leukemia (M-CLL) relative to unmutated chronic lymphocytic leukemia (UM-CLL) [12]. Overexpression of 14-3-3β in NIH 3T3 cells (mouse embryonic fibroblast cell line) stimulated cell growth and supported anchorage-independent growth in soft agar medium and tumor formation in nude mice [13], while reducing 14-3-3β expression led to an inhibition of tumor progression due to decreased vascular endothelial growth factor (VEGF) production, inhibition of angiogenesis and increased apoptosis. In addition, it has been shown that 14-3-3β promotes cell migration by interacting with integrin β1 [14] and activating the MAPK pathway, causing tumor cell metastasis [15, 16]. Thus, these studies support the idea that 14-3-3β could function as an oncogene. Chan et al. reported that 14-3-3β showed stronger expression in gastric cancer cells than in paired normal cells by using immuno-histochemical staining analysis [16]; however, the roles of 14-3-3β in human gastric cancer are still poorly understood.

In this study, we found a significant reduction of 14-3-3β in tumor cells that were treated with 5-FU. 14-3-3β expression levels in tumor tissues and serum from gastric cancer patients were subsequently measured, evaluated for potential utility as a serological biomarker and studied in the context of specific clinical features. Finally, integration of proteomics and network analysis was performed to reveal the down-

stream regulation of 14-3-3β and determine the enriched functions of its regulated network in gastric cancer. The biological functions of 14-3-3β were also tested by various functional assays, as illustrated in Fig. 1. Overall, our findings reveal the important role that 14-3-3β plays in gastric cancer cell progression and suggests that it can potentially be used as a diagnostic and prognostic biomarker in gastric cancer.

2 Materials and methods

2.1 Cell culture

TSGH, SC-M1, N87 and AGS gastric cancer cells were obtained from the cell line databank at the National Taiwan University Hospital and were cultured in RPMI-1640 medium supplemented with 10% FBS (Invitrogen, Carlsbad, CA, USA) at 37°C in an atmosphere of 5% CO_2.

2.2 Protein extraction

Cell samples were lysed in lysis buffer containing 7 M urea (Boehringer, Mannheim, Germany), 2 M thiourea, 4% CHAPS (J.T. Baker, Phillipsburg, NJ) and 0.002% bromophenol blue (Amersco, OH, USA), sonicated and clarified by centrifugation before the protein concentration of each sample was determined using a protein assay kit (Bio-Rad, Hercules, CA, USA). Tissues were stored in liquid nitrogen until use. All tissue samples were air-dried at −50°C and homogenized by grinding in liquid nitrogen. Protein lysates were extracted, sonicated and centrifuged and the protein concentration was then measured.

2.3 2-D electrophoresis and image analysis

The protein profiles of 14-3-3β-overexpressing and control gastric cancer AGS cells were analyzed using 2-DE. Five hundred micrograms of total protein was separated by 2-DE [17]. For separation in the first dimension, isoelectric focusing (IEF) was performed using an 18-cm strip (pH 4–7) in an IPGphor isoelectric focusing system (Amersham Pharmacia Biotech, Uppsala, Sweden) at 8000 V for a total of 91.2 kV h at 20°C. The strips were then transferred onto a 12.5% non-gradient SDS-PAGE gel for 2-D separation. The 2-D images were analyzed using ImageMaster software version 6.0 (Amersham Pharmacia Biotech) to detect and quantify protein spots. The expression profiles were performed in triplicate.

2.4 In-gel digestion and mass spectrometry

The differentially expressed proteins were excised from 2-D-gels, digested with trypsin and the tryptic peptides were
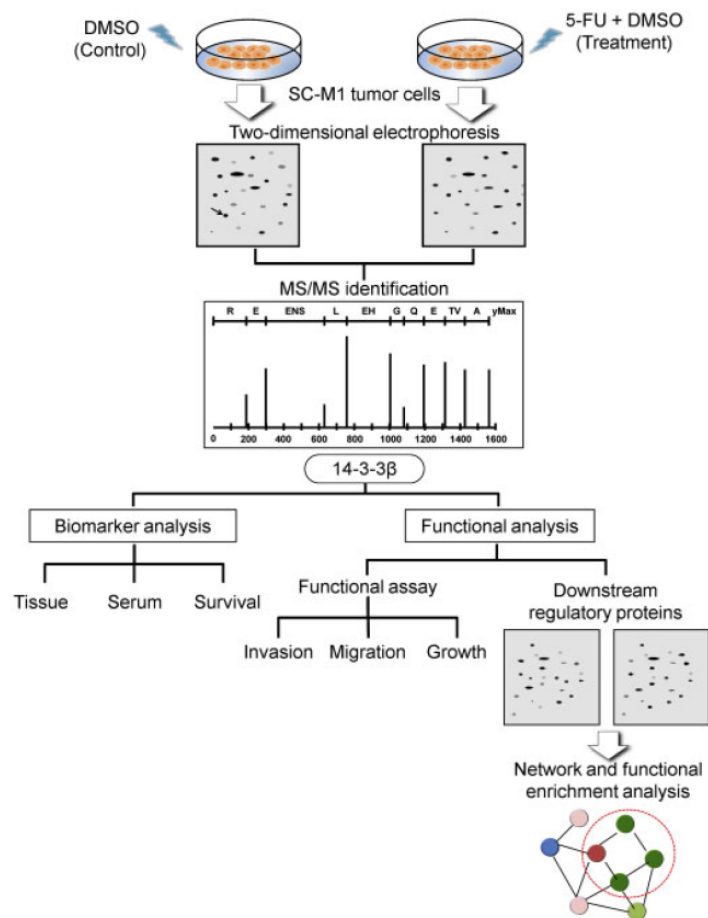
Figure 1. Schematic representation of the experimental design used for comprehensive proteomic and network analysis. The expression of 14-3-3β protein in SC-M1 tumor cells was identified to be reduced after 5-FU treatment by 2-DE and mass spectrometry (MS/MS). 14-3-3β protein expression in tissues was further assayed and subsequently identified as a diagnostic biomarker in serum from gastric cancer patients by using ELISA. Downstream regulation of 14-3-3β in tumor cell progression was displayed by proteomics and network analysis. The biological functions of 14-3-3β were also tested by various functional assays.

extracted from the gel. These protein spots were analyzed according to our previously published method [17]. Samples were resuspended in 0.1% TFA and matrix (5 mg/mL CHCA dissolved in 50% ACN, 0.1% v/v TFA and 2% w/v ammonium citrate). The peptide mixture was then loaded onto a MALDI plate (PerSeptive Biosystems, CA, USA) and samples were analyzed by a MALDI-Q-TOF Ultima MALDI Mass Spectrometer (Micromass, Manchester, UK) that was fully automated with a predefined probe motion pattern and peak intensity threshold for switching over from MS survey scan to MS/MS, and from one MS/MS to another. The peak lists were acquired by the MassLynx^{TM} version 4.0 software, and the raw data were processed to enable a database search using ProteinLynx Global Server 2.2 (PLGS 2.2). From the MS spectrum, the highest five precursors that had a signal-to-noise ratio of more than 50 were selected for subsequent MS/MS analysis. Starting from the peak of greatest intensity, parent ions that met the predefined criteria (any peak within the *m/z* 800–3000 range with an intensity of above a

count of 10 ±include/exclude list) were selected for collision-induced dissociation (CID) MS/MS using argon as a collision gas and a mass-dependent ±5 V rolling collision energy until the end of probe pattern was reached. Both the LM and HM resolution of the quadrupole were set at 10 to give a precursor selection window of approximately 4 Da. The instrument was calibrated to <5 ppm accuracy over the mass range of *m/z* 800–3000 using a sodium iodide and PEG 200, 600, 1000 and 2000 mixture and was further adjusted with Glu-Fibrinopeptide B as the near-point lock mass calibrant during data processing. At a laser firing rate of 10 Hz, individual spectra from a 5 s integration period that was acquired for each of the MS surveys and MS/MS performed were combined, smoothed, deisotoped (fast option) and centroided using the Micromass PKGS 2.2 data processing software. The following MS default parameters were used: background subtract type, normal; background threshold, 35%; background polynomial, 5; perform smoothing, yes; smoothing type, Savitzky–Golay; smoothing

iteration, 1; smoothing window, two channels; combine options, all; but low mass threshold, 1500 Da; intensity range, 2–100 were not used. The following MS/MS default parameters were used: background subtract type, normal; background threshold, 35%; background polynomial, 5; peptide filter; but perform smoothing, no; smoothing type, Savitzky–Golay; smoothing iteration, 2; smoothing window, three channels were not used [18]. The combined peptide mass fingerprinting (PMF) and MS/MS ion meta data were searched in concert against the specified protein database within the PLGS 2.2 workflow [18]. Alternatively or additionally, the PMF and individual MS/MS ion data can be displayed as MASCOT-searchable.txt file and.pkl files for independent searches using MASCOT (version 2.3) against the Swiss-Prot (version 57.11) database (512 994 sequences; 180 531 504 residues) of *Homo sapiens*. The search parameters were as follows: enzyme, trypsin; fixed modifications, carbamidomethylation of cysteines; variable modifications, oxidation of methionine; one missed tryptic peptide cleavage; peptide tolerance, ± 50 ppm; fragment MS/MS tolerance, ± 0.25 Da; mass values, monoisotopic; peptide charge, +1. The cut-off score of MS/MS was approximately 21, and the score values were calculated by MASCOT based on the Mowse algorithm. Peptide matches were analyzed using mass values (MS/MS fragment ion masses) and scores were reported as $-10*\log_{10}(P)$, where P is the absolute probability which is used to measure the significance of a result when a match is random and the size of the searched sequence database is known. The accepted threshold was defined as an event expected to occur at random with a frequency of <5%. Identified proteins with statistically significant protein scores higher than ion scores ($p<0.05$, based on MS/MS spectra) were selected at 95% confidence level for matched peptides.

2.5 Western blot analysis

Primary mouse monoclonal antibodies against 14-3-3β (Abcam, Cambridge, UK) were used at a 1:1000 dilution ratio, and the candidate protein was visualized with the enhanced chemiluminescence (ECL) detection kit (Pierce, Boston Technology, Woburn, MA) and exposed to X-ray film.

2.6 Gastric cancer patients and clinical data

The use of human tissue samples and serum was approved, and the confidentiality of human subjects was protected by the Institute Review Board (IRB, No. 200612109R). A total of 145 gastric cancer patients who had undergone curative intent radical gastrectomy at the National Taiwan University Hospital from July 2001 to March 2006 were included in this study. They were staged according to the World Health Organization, Lauren's classification and International

Union against Cancer (UICC) TNM system (Table 1) [19, 20]. Patients who had undergone curative intent resection were classified according to the following criteria: complete removal of a primary gastric tumor, D2 dissection of regional lymph nodes, absence of any macroscopic tumors remaining at the site of resection and absence of metastases in the liver, lungs or distant organs at the time of surgery. In addition, the patient should have been clear of any concomitant primary cancers and had not received chemotherapy or radiotherapy prior to surgery. Clinicopathologic factors including age, sex, Borrmann and Lauren classifications, depth of tumor invasion, status and number of lymph node metastases, vascular invasion and tumor size (length × width of tumor) were also considered and stored in the patients' database. Organ invasion was defined as direct tumor invasion into at least one adjacent structure such as the duodenum, esophagus, liver, mesocolon or diaphragm. Patient follow-up occurred from 3 to 46 months after surgery, and the follow-up intervals were calculated as

Table 1. Demographics of gastric cancer patients

	No. of patients	%
Age (years)		
Median	67	
Range	29–89	
Gender		
Male	89	61
Female	56	39
Stage		
I and II	60	41
III and IV	85	59
Depth of tumor invasion		
T1	17	12
T2	42	29
T3	80	55
T4	6	4
Lymph node metastasis		
N0	42	29
N1	63	43
N2	30	21
N3	10	7
Distant metastasis		
M0	120	83
M1	25	17
Lauren classification		
Diffuse type	75	52
Intestinal type	68	48
Organ invasion		
Negative	106	73
Positive	39	27
Vascular invasion		
Negative	30	23
Positive	100	77
Peritoneal invasion		
Negative	124	86
Positive	21	14

survival intervals after surgery. Furthermore, the association between serum 14-3-3β levels and the above-mentioned clinical outcomes was evaluated.

2.7 Blood and tissue sample collection

Thirty-one post-operative serum samples were also collected from the 145 gastric cancer patients. Three different control groups were included: 19 endoscopically diagnosed with gastric ulcer, 19 with non-ulcer dyspepsia and 25 healthy controls. Venous blood samples were collected in plain tubes, allowed to clot and then centrifuged at 2000 rpm (Kubota, Bunkyo-Ku, Japan) at room temperature for 10 min. Aliquots of the separated sera were individually stored below −80°C until serum 14-3-3β concentrations were assayed. Forty pairs of tumor and tumor-adjacent normal tissue specimens were also obtained from these 145 gastric cancer patients. The paired tissue samples were dissected within 30 min of gastrectomy and frozen in liquid nitrogen.

2.8 ELISA for 14-3-3β

To detect the serum levels of 14-3-3β, ELISA was performed according to previously published methods [21–23]. Monoclonal anti-14-3-3β antibody (4 μg/mL, Abcam) was incubated on streptavidin-coated 96-well microwell plate overnight at 4°C. After blocking, the 14-3-3β standard antigen and all diluted serum samples (1:400) were incubated on the plate for 3 h. Subsequently, the plate was washed and incubated with polyclonal anti-14-3-3β antibody (0.08 μg/mL, Upstate Biotechnology, Lake Placid, NY, USA) for 2 h. One hundred microliters of polyclonal goat anti-rabbit HRP conjugated IgG antibody (0.04 μg/mL) was added and incubated for 1 h. The plate was washed and added with tetramethylbenzidine (TMB) substrate solution (Bionova Biotechnology, Dartmouth, NS, Canada) for 30 min. The reaction was stopped by adding 2 M sulfuric acid. Protein concentration of 14-3-3β and unknown samples was determined by measuring the absorbance at 450 and 570 nm using an ELISA reader.

2.9 Construction of the 14-3-3β overexpressing plasmid

Reverse transcription-polymerase chain reaction was used to synthesize cDNA from the total RNA extracted from TSGH cells and amplify the 14-3-3β product using specific forward (5′-GGTACGTAAGCTTGCCACCATGACAAT GGATAAAAGT-3′) and reverse (5′-AGTCGAGAATTCTTA GTTCTCTCCCTCCCC-3′) primers. The product was cloned into a pcDNA3 vector (Invitrogen) and verified by sequencing (Mission Biotech).

2.10 Cell invasion and migration assays using Boyden chambers

The pcDNA3/14-3-3β and control vectors were mixed with lipofectamine 2000 and transfected into the AGS cells according to manufacturer's instructions (Invitrogen). Migration assays were performed with modified Boyden chambers with filter inserts (pore size, 8 μm) and invasion assays were also studied by coating the chambers with Matrigel (35 μg, BD Biosciences, CA, USA) based on previously described methods [24]. Approximately 2.5×10^4 cells in 100 μL medium were added on the upper chamber and cells were fixed, stained and counted by a light microscope (Olympus) after 48 h in culture. Each experiment was performed in triplicate.

2.11 3-(4,5-Dimethylthiazol-2-yl)-2,5-diphenyltetrazolium bromide (MTT) assay for cell growth

AGS cells were cultured in a 24-well plate at 5×10^4/well for 24 h and then transfected with 3 μg each of 14-3-3β and control vectors for 24 and 48 h. One hundred microliters of MTT reagent was added to each 1 mL of culture medium and measured at 570 nm using an ELISA reader. Each experiment was performed in quadruplicate.

2.12 Proteomic and network analysis of 14-3-3β-regulated protein–protein interactions (PPI)

To investigate the downstream regulation of 14-3-3β in gastric cancer cells, we integrated proteomic and network analyses to identify the 14-3-3β-regulated protein–protein interaction networks and their enriched biological functions. The human protein interaction network (PIN) was downloaded from Human Protein Reference Database (HPRD) [25] and only the largest connected component, containing 9059 proteins and 34 869 interactions, was studied. The 14-3-3β-related network consisted of proteins that were differentially expressed as a result of 14-3-3β overexpression and at least two of their interacting partners, 14-3-3β-related biological processes, were further predicted by functional enrichment analysis of its related networks. BiNGO [26], a Cytoscape [27] plug-in, was used to determine which Gene Ontology (GO) terms were significantly overrepresented (Hypergeometric test, Benjamini and Hochberg false discovery rate (FDR) correction, $p \leq 0.001$) in 14-3-3β-related networks.

2.13 Statistical analysis

To analyze the correlation between 14-3-3β and clinical outcomes, Student's t-test was used to compare the

differences between two clinicopathological groups. Comparisons between multiple groups were done using one-way ANOVA (SAS 9.1 software). *p*-Values were two-sided and the α level of significance was defined as $p < 0.05$.

Receiver operating characteristics (ROC) curves were used to assess serum 14-3-3β concentrations as diagnostic for gastric cancer by plotting sensitivity versus 1-specificity, and the area under the curve (AUC) was subsequently calculated. The AUC was then used as an indicator of the capacity of 14-3-3β to act as a diagnostic marker, with higher AUC values reflecting higher diagnostic capacities. Recurrence-free survival and overall survival curves were generated according to the Kaplan–Meier method to study the relationship between serum 14-3-3β expression and patient survival and a paired Student's *t*-test was used to compare the changes in 14-3-3β plasma levels between pre-operative and post-operative patients.

3   Results

3.1   Proteomic profiling of 5-FU-treated SC-M1 gastric cancer cells

In this study, we performed a proteomic approach to identify proteins that were differentially expressed in 5-FU-treated (66.5 μM) SC-M1 cells, as illustrated in Fig. 1. After spot detection and quantification was performed on the 2-D gel images, a total of 397 protein spots were observed in 5-FU-treated SC-M1 cells. Among them, 24 differentially expressed proteins were chosen for further analysis by MALDI-TOF and identified using the MASCOT search engine and the Swiss-Prot database. We successfully identified 18 significantly differentially expressed proteins, including 12 that were downregulated and 6 that were

upregulated in 5-FU-treated tumor cells (Fig. 2A and Table 2). The peptide sequences and spectra of these 18 identified proteins are shown in the Supporting Information Fig. S1. These proteins are mainly involved in apoptosis, cell adhesion, cell motility, signal transduction, migration and glycolysis. Downregulated proteins involved in apoptosis included endoplasmin (HSP90B1), annexin A5 (ANXA5), keratin, type I cytoskeletal 18 (KRT18) and glutathione *S*-transferase P (GSTP1), whereas heat shock 70 kDa protein 1 (HSPA1A) was upregulated. Proteins involved in cell motility were downregulated, including F-actin capping protein β subunit (CAPZB) and heat-shock protein β-1 (HSP27 or HSPB1) while proteins participating in signal transduction were significantly downregulated, including 14-3-3 protein epsilon (YWHAE) and 14-3-3 protein β/α (YWHAB). Among them, 14-3-3β was significantly downregulated in 5-FU-treated SC-M1 cells and enlarged images and 3-D profiles of 14-3-3β on the gels are shown in Fig. 2B and C, respectively. This was confirmed by Western blot analysis (Fig. 2D), as 14-3-3β expression was observed to be downregulated by 2.55-fold (2.55 ± 0.27, $p = 0.05$) after 5-FU treatment of SC-M1 cells. These results suggest that 14-3-3β is highly associated with gastric cancer.

3.2   14-3-3β expression in tumor tissues and serum from gastric cancer patients

Western blot analysis of 14-3-3β expression levels in paired tumor and tumor-adjacent normal tissues demonstrated that 14-3-3β expression was significantly increased in tumor tissues compared with normal tissues ($p < 0.01$; Fig. 3A). Since 14-3-3β was overexpressed in gastric cancer tissues, its potential release into the periphery was assessed to determine whether it can be detected as a serologic biomarker for
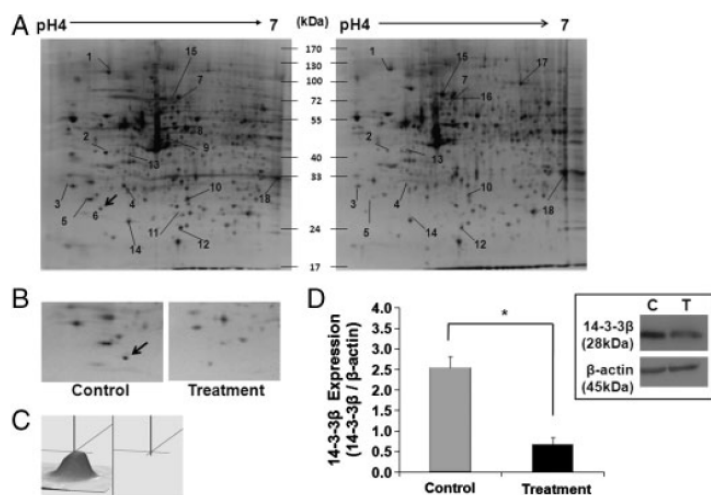
Figure 2. 14-3-3β is differentially expressed after 5-FU treatment of SC-M1 cells. (A) Proteins from the 5-FU-treated (right) SC-M1 cells and the untreated control (left) were compared using 2-DE. Differentially expressed proteins were selected and identified by MS/MS (Table 2). Enlarged images and 3-D profiles of 14-3-3β on the gels are shown in (B) and (C). (D) 14-3-3β expression was significantly reduced after 5-FU treatment (*$p < 0.05$), as confirmed by Western blot. The expression profiles were performed in triplicate.

Table 2. Identification of significantly differentially expressed proteins in 5-FU-treated and control gastric cancer SC-M1 cells

Spot	Gene name[a]	Accession number[a]	Protein name[b]	m/z[b]	pI[b]	Matched peptides[c]	Unmatched peptides[d]	Coverage (%)	Ion score[e]	False discovery rate (%)[f]	Error (ppm)[f]	Fold (T/C)[g]	Peptides identified	Molecular function[h]
Downregulation														
1	HSP90B1	P14625	Endoplasmin	92696/1	4.76	5	77	9	245	0	2.21 4.99 -3.15 0.79 -1.60	0.939	K.FAFQAEVNR.M K.SILFVPTSAPR.G R.RVFITDDFHDMMPK.Y +2 oxidation (M) R.FQSSHHPTDITSLDQYVER.M R.TDDEVVQREEEAIQL DGLNASQIR.E	Apoptosis
2	RPSA	P08865	40S ribosomal protein SA	32347/1	4.79	4	18	16	252	0	-2.53 2.62 -2.83 -5.48	0.453	K.FAAATGATPIAGR.F R.FTPGTFTNQIQAAFR.E R.AIVAIENPADVSVISSR.N R.FTPGTFTNQIQAAFREPR.L	Adhesion
3	C1QBP	Q07021	Component 1Q subcomponent binding protein	31742/1	4.74	2	21	12	155	0	-13.01 -7.56	0.733	K.AFVDFLSDEIKEER.K K.VEEQEPELTSTPNFVVEVIK.N	Immune response
4	ANXA5	P08758	Annexin A5	35971/1	4.94	4	28	14	203	0	-7.12 -0.79 -5.82 -3.32	0.565	R.SEIDLFNIR.E R.GTVTDFPGFDER.A K.GLGTDEESILTLLTSR.S R.GTVTDFPGFDERADAETLR.K	Apoptosis
5	YWHAE	P62258	14-3-3 protein ε	29326/1	4.63	3	21	11	151	0	-1.65 -3.71 -9.69	0.424	R.YLAEFATGNDR.K R.YLAEFATGNDRK.E K.AASDIAMTELPPTHPIR.L +oxidation (M)	Signal
6	YWHAB	P31946	14-3-3 protein β/α	28179/1	4.76	1	22	5	63	0	-2.49	C*	K.AVTEQGHELSNEER.N	Ras signal
7	HNRNPK	P61978	Heterogeneous nuclear ribonucleoprotein K	51230/1	5.39	1	35	2	61	0	-5.31	0.705	R.NLPLPPPPPR.G	mRNA splice
8	KRT18	P05783	Keratin, type I cytoskeletal 18	48029/1	5.34	2	41	5	56	0	-22.48 -0.32	C*	K.VKLEAEIATYR.R R.AQIFANTVDNAR.I	Apoptosis
9	KRT18	P05783	Keratin, type I cytoskeletal 18	48029/1	5.34	2	39	5	53	0	-32.23 0.97	C*	K.VKLEAEIATYR.R R.AQIFANTVDNAR.I	Apoptosis
10	CAPZB	P47756	F-actin capping protein β subunit	31616/1	5.36	2	24	8	109	0	-5.32 2.84	0.653	R.RLPPQQIEK.N R.KLEVEANNAFDQYR.D	Cell motion
11	HSPB1	P04792	Heat-shock protein β-1 (HSP27)	22826/1	5.98	2	17	13	151	0	-10.55 -4.79	C*	R.LFDQAFGLPR.L K.LATQSNEITIPVTFESR.A	Cell motion
12	GSTP1	P09211	Glutathione S-transferase P	23569/1	5.43	4	10	30	290	0	-7.44 -9.28 -11.16 -6.24	0.655	M.PPYTVYFPVR.G R.FQDGDLTLYQSNTILR.H K.ALPGQLKPFETLLSQNQGGK.T K.YISLIYTNYEAGKDDYVK.A	Apoptosis
Upregulation														
13	KRT2	P35908	Keratin, type II cytoskeletal 2	65678/1	8.07	1	53	2	69	0	2.67	1.223	R.HGGGGGGFGGGGFGSR.S	Migration
14	ARHGDIA	P52565	Rho GDP-dissociation inhibitor 1	23250/1	5.02	4	11	27	183	0	-4.47 3.50 -6.10 -8.53	1.275	K.QSFVLKEGVEYR.I K.IDKTDYMVGSYGPR.A +oxidation (M) R.AEEYEFLTPVEEAPK.G K.SIQEIQELDKDDESLR.K	Adhesion

www.proteomics-journal.com

Table 2. Continued

Spot	Gene name[a]	Accession number[a]	Protein name[b]	m/z[b]	pI[b]	Matched peptides[c]	Unmatched peptides[d]	Coverage (%)	Ion score[e]	False discovery rate (%)[f]	Error (ppm)	Fold (T/C)[g]	Peptides identified	Molecular function[h]
15	HSPA8	P11142	Heat shock cognate 71 kDa protein	71082/1	5.37	4	54	10	272	0	−2.55 4.12 −2.47 −11.68	3.262	R.ARFEELNADLFR.G R.TTPSYVAFTDTER.L K.TVTNAVTVPAYFNDSQR.Q K.QTQTFTTYSDNQP GVLIQVYEGER.A	Protein binding
16	HSPA1A	P08107	Heat shock 70 kDa protein 1	70294/1	5.48	5	46	9	254	0	−9.04 −15.45 −5.47 −0.39 −4.34	T*	K.LLQDFFNGR.D K.DAGVIAGLNVLR.I R.LVNHFVEEFKR.K R.TTPSYVAFTDTER.L R.IINEPTAAAIAYGLDR.T	Apoptosis
17	EZR	P15311	Ezrin	69484/1	5.94	5	58	7	174	0	−12.27 −3.12 −6.70 −7.08 −35.65	T*	K.IGFPWSEIR.N K.QRIDEFEAL.- K.APDFVFYAPR.L K.KAPDFVFYAPR.L R.QLLTLSSELSQAR.D	Actin
18	GAPDH	P04406	Glyceraldehyde-3-phosphate dehydrogenase	36201/1	8.57	4	22	16	269	0	−5.49 −2.69 −23.65 −9.49	1.536	K.LVINGNPITIFQER.D K.LISWYDNEFGYSNR.V K.LVINGNPITIFQERDPSK.I K.VIHDNFGIVEGLMTTVHAITATQK.T +Oxidation (M)	Glycolysis

These differentially expressed protein spots are identified by MS/MS and then selected after MASCOT database searching ($p < 0.05$).

a) Gene name and accession number are obtained from Swiss-Prot database.
b) The data are identified after MASCOT database searching (m/z, m = mass; $z = +1$).
c) The number of tryptic peptides that match to peptides of the identified proteins.
d) The number of tryptic peptides that do not match to peptides of the identified proteins.
e) Ion score was obtained based on MS/MS analysis.
f) False discovery rate was determined by the results of randomized database searches.
g) T represents 5-FU-treated SC-M1 cells and C represents untreated control cells. C* represents the protein is only expressed in untreated control cells. T* represents the protein is only expressed in 5-FU-treated SC-M1 cells.
h) Molecular function is based on GO database.

the disease. For this purpose, serum 14-3-3β levels were detected by ELISA. Serum 14-3-3β levels in 63 control subjects ranged from 89.4 to 969.9 ng/mL, and the mean and median values were 308.1 and 213.3 ng/mL, respectively. However, serum 14-3-3β levels in cancer patients ($n = 145$) ranged from 186.8 to 1846.2 ng/mL with mean and median values of 625.5 and 494.4 ng/mL, respectively. In addition, pre-operative serum 14-3-3β levels in gastric cancer patients were significantly higher than those in controls ($p < 0.0001$, Fig. 3B). Serum 14-3-3β levels in stage I gastric cancer patients were significantly higher than those in controls ($p = 0.005$), and ROC curve analysis determined serum 14-3-3β level of 262 ng/mL was the cut-off value ($p < 0.001$). These results strongly suggest that serum 14-3-3β may be used as a potential biomarker for gastric cancer.

3.3 Serum 14-3-3β levels and overall and recurrence-free survival

Survival analysis was conducted in 142 available gastric cancer cases, and survival curves were generated according to the Kaplan–Meier method. At the serum level of 349 ng/mL, 14-3-3β had high sensitivity (86%) and specificity (67%) for the detection of gastric cancer; thus, it was defined as the cut-off value. The patients were divided into two groups, i.e. those that showed low expression of serum 14-3-3β and those with high expression of serum 14-3-3β. The 5-year overall survival rates for those with low and high serum 14-3-3β levels were 72.7 and 46.1% respectively, whereas the 5-year recurrence-free survival rates for those with low and

high serum 14-3-3β levels were 59.9 and 35.0%, respectively ($p = 0.038$ and 0.037, respectively, Fig. 3C). Overall, the overall and recurrence-free survival rates of patients with 14-3-3β levels greater than 349 ng/mL were shown to be significantly lower, indicating that 14-3-3β serum levels are suitable as a prognostic marker in gastric cancer patients.

3.4 Serum 14-3-3β levels decrease after gastrectomy with D2 lymphadenectomy

Among 31 patients with abnormally high 14-3-3β levels, the mean and the median of pre-operative serum 14-3-3β levels were 579 and 515 ng/mL, respectively. In contrast, the mean and the median of post-operative serum 14-3-3β levels were 427 and 378 ng/mL, respectively (Fig. 3D). Thus, serum 14-3-3β levels were significantly decreased after gastrectomy ($p < 0.0001$).

3.5 ROC curves of 14-3-3β in gastric cancer

In this study, a ROC curve was used to evaluate serum 14-3-3β concentrations as diagnostic for gastric cancer by plotting sensitivity versus 1-specificity. AUC value was then used as an indicator of the capacity of 14-3-3β to act as a diagnostic marker, with higher AUC values reflecting higher diagnostic capacities. The AUC values for gastric cancer patients versus normal controls at different cancer stages were illustrated in Fig. 4. The AUC of 14-3-3β was 0.776 for stage I (A), 0.843 for stage II (B), 0.822 for stage III (C), 0.882 for

Figure 3. 14-3-3β reduced patient survival. (A) 14-3-3β expression in 40 paired tumor and normal tissues was analyzed. β-actin served as a loading control (**$p < 0.01$). (B) Comparison of serum 14-3-3β levels in controls ($n = 63$), stage I ($n = 28$), stage II ($N = 32$), stage III ($n = 56$) and stage IV ($n = 29$). (C) The relationship between serum 14-3-3β levels and patient survival. Solid line: higher 14-3-3β levels ($\geqq 349$ ng/mL) ($n = 122$); dotted line: lower 14-3-3β levels (< 349 ng/mL) ($n = 20$). Patients with higher 14-3-3β values showed poorer overall ($p = 0.038$) and recurrence-free survival ($p = 0.037$). (D) 14-3-3β levels in pre- and post-operative patients (***$p < 0.0001$; $n = 31$).

Figure 4. ROC curves of 14-3-3β. Serum concentrations of 14-3-3β from 145 gastric cancer patients and 63 control samples were determined by ELISA. The area under the curve (AUC) was 0.776 for stage I (95% CI: 0.676–0.857, A), 0.843 for stage II (95% CI: 0.753–0.909, B), 0.822 for stage III (95% CI: 0.741–0.886, C), 0.882 for stage IV (95% CI: 0.798–0.94, D) and 0.83 for all gastric cancer samples (95% CI: 0.772–0.878, E).

stage IV (D) and 0.83 for all gastric cancer samples (E). On the other hand, ROC curve analysis determined the cut-off value of serum 14-3-3β for the diagnosis of gastric cancer. A serum 14-3-3β level of 420 ng/mL was defined as the optimal cut-off value for differentiating between patients and controls. When using the cut-off value for the detection of gastric cancer, the serum 14-3-3β sensitivity, specificity and accuracy were 78, 71 and 76, respectively. Additionally, we compared the AUC between 14-3-3β and the other existing serum biomarkers such as CEA and the results showed that 14-3-3β appeared to outperform the established tumor marker CEA (Supporting Information Fig. S2).

3.6 The relationship between 14-3-3β expression level and metastatic lymph node number, tumor size and cancer stage

Our clinical analyses showed that pre-operative serum 14-3-3β levels were significantly associated with the number of metastatic lymph nodes ($r = 0.166$, $p = 0.045$) and tumor size ($r = 0.452$, $p < 0.0001$; Fig. 5A and B). 14-3-3β serum levels positively correlated with 14-3-3β expression in tumor tissues ($r = 0.385$, $p = 0.033$; Fig. 5C). Pre-operative serum 14-3-3β levels also increased with the depth of tumor invasion

($p = 0.043$), distance of metastasis from the primary site ($p = 0.03$) and peritoneal invasion ($p = 0.049$; Table 3). These results provide evidence that 14-3-3β plays a crucial role in the migration and invasion of gastric adenocarcinoma.

3.7 Overexpression of 14-3-3β enhances cancer cell invasion, migration and growth

A key question is whether 14-3-3β affects malignant progression of gastric cancer cells. To address this possibility, we first checked the endogenous 14-3-3β expression in four gastric cancer cell lines, including two non-metastatic cell lines AGS and N87, one poorly differentiated cell line SC-M1 and one high-metastatic cell line TSGH (Fig. 6A). We found that the expression levels of 14-3-3β were positively associated with malignant phenotypes of gastric cancer cell lines. Moreover, 14-3-3β-overexpressing AGS cells had significantly greater invasive and migratory capabilities (Fig. 6B and C) and higher cell growth (Fig. 6D) than control cells. The functional studies of 14-3-3β in other gastric cancer cell lines, including N87, SC-M1 and TSGH, were shown in the Supporting Information Fig. S3. These results suggest that 14-3-3β may regulate malignant progression of gastric cancer cells.
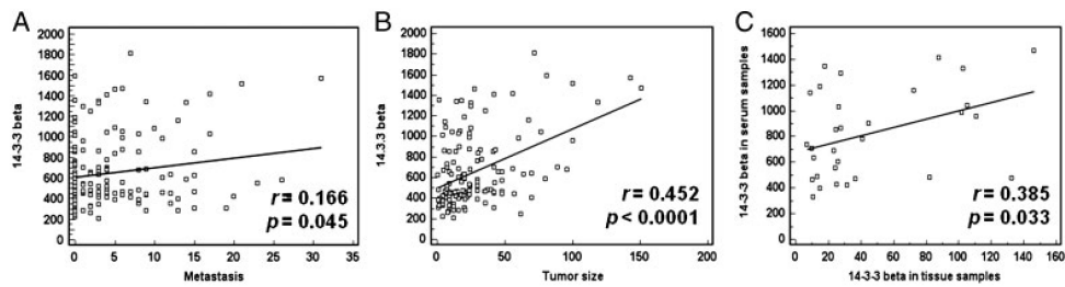
Figure 5. Serum 14-3-3β levels correlated with specific clinical features. Patient pre-operative serum 14-3-3β levels correlated with (A) the number of lymph node metastases ($n = 145$); (B) tumor size ($n = 139$) and (C) 14-3-3β expression in tumor tissues ($n = 31$).

Table 3. The relationship between 14-3-3β and clinical factors

	Mean (ng/mL)	Median (ng/mL)	p-Value[c]
Stage[a]			0.015*
I and II ($n = 60$)	576.38 ± 283.98	472.44	
III and IV ($n = 85$)	712.03 ± 375.94	578.83	
Depth of tumor invasion[b]			0.043*
T1 ($n = 17$)	467.44 ± 177.08	427.17	
T2 ($n = 42$)	620.24 ± 353.53	482.44	
T3 ($n = 80$)	716.55 ± 353.18	633.28	
T4 ($n = 6$)	637.57 ± 407.00	467.17	
Lymph node metastasis[b]			0.218
N0 ($n = 42$)	607.61 ± 315.28	525.22	
N1 ($n = 63$)	654.56 ± 321.93	532.17	
N2 ($n = 30$)	656.76 ± 376.48	471.33	
N3 ($n = 10$)	864.53 ± 486.74	716.06	
Distant metastasis[a]			0.030*
M0 ($n = 120$)	620.23 ± 318.04	518.00	
M1 ($n = 25$)	827.11 ± 425.80	681.19	
Lauren classification[a]			0.957
Diffuse-type ($n = 75$)	656.60 ± 373.71	488.28	
Intestinal-type ($n = 68$)	659.74 ± 318.91	554.77	
Organ invasion[a]			0.088
Negative ($n = 106$)	624.88 ± 323.36	516.06	
Positive ($n = 39$)	745.17 ± 393.14	602.72	
Vascular invasion[a]			0.125
Negative ($n = 30$)	595.70 ± 294.35	481.89	
Positive ($n = 100$)	698.92 ± 371.42	573.56	
Peritoneal invasion[a]			0.049*
Negative ($n = 124$)	625.31 ± 318.57	516.06	
Positive ($n = 21$)	836.54 ± 453.08	631.61	

Serum 14-3-3β levels were measured by ELISA, and mean (mean ± SD) and median values are given for each group.
a) Student's t-test analysis.
b) One-way ANOVA analysis.
c) *$p < 0.05$).

3.8 The downstream regulation of 14-3-3β in gastric cancer cells

To study the regulatory mechanism of 14-3-3β in gastric cancer progression, we integrated proteomics and network analyses to construct a PPI network. A total of 567 protein spots were identified in 14-3-3β-overexpressing AGS cells. Among them, 28 significantly differentially expressed proteins in pcDNA3 control and 14-3-3β-overexpressing tumor cells were identified by 2-DE and mass spectrometry (Fig. 7 and Table 4). The peptide sequences and spectra of these 28 identified proteins are shown in the Supporting Information Fig. S4. These proteins and their interacting partners were used to construct the PPI network (Fig. 8), and all proteins in the network were further analyzed for clustering of functional profiles using BINGO ($p < 0.001$).
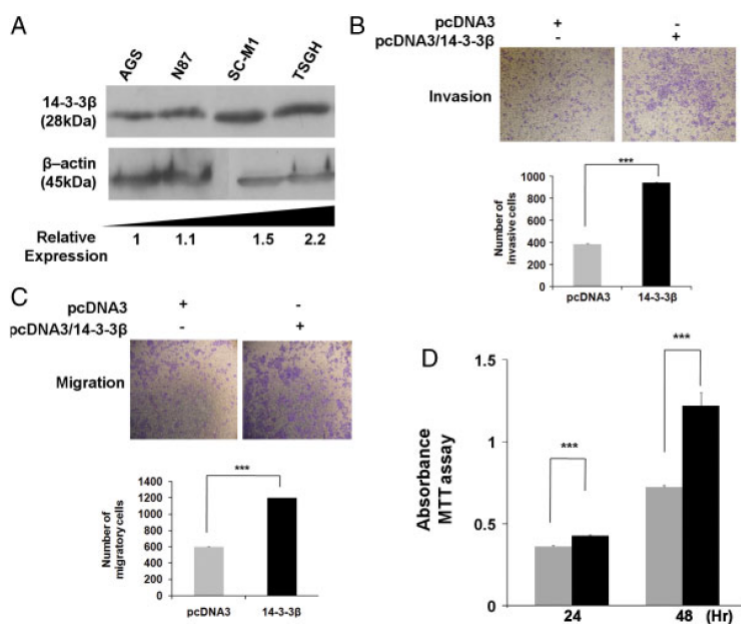
Figure 6. Overexpressed 14-3-3β enhances tumor cell invasion, migration and growth. (A) Endogenous 14-3-3β expression levels in four gastric cancer cell lines, including two non-metastatic cell lines AGS and N87, one poorly differentiated cell line SC-M1 and one high-metastatic cell line TSGH, were detected by Western blot analysis. (B and C) Invasive and migratory activities were measured after transfection with 14-3-3β plasmid into AGS cells for 48 h, respectively. (D) Cell growth was measured after transfection with 14-3-3β plasmid into AGS cells for 24 and 48 h by MTT assay. *** indicates $p < 0.001$.
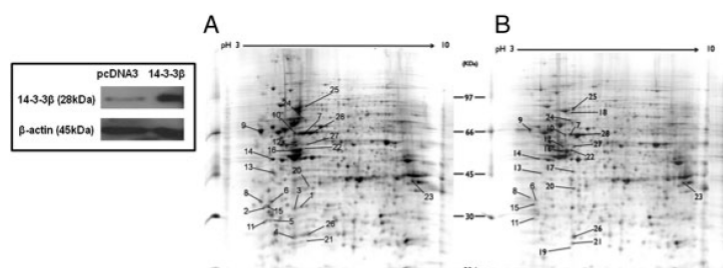
Figure 7. 2-DE map of (A) pcDNA3 control and (B) 14-3-3β-overexpressing tumor AGS cells. After transfection with 14-3-3β plasmid for 48 h, the differentially expressed spots were identified in (A) pcDNA3 control and (B) 14-3-3β-overexpressing tumor cells by 2-DE and then analyzed by mass spectrometry and MASCOT searching. The identified proteins are shown in Table 4 and these proteins were further used to construct the 14-3-3β-regulating PPI network. The expression profiles were performed in triplicate.

Key functional relationships were revealed, including cell death, apoptosis and phosphorylation. Functionally, the identified proteins (L0) were highly associated with the negative regulation of apoptosis and L0 proteins with this function included GSTP1, keratin, type II cytoskeletal 1 (KRT1), calreticulin (CALR), nucleophosmin (NPM1), keratin, type I cytoskeletal 18 (KRT18), heat shock 70 kDa protein 1 (HSPA1A), peroxiredoxin-2 (PRDX2), stress-70 protein, mitochondria (HSPA9). In addition to the negative regulation of apoptosis, the biological functions of their interacting proteins (L1) included the negative regulation of

cellular, developmental and phosphate metabolic processes. These results suggest that 14-3-3β enhances gastric cancer cell progression through the regulation of proteins that are primarily involved in cell development, apoptosis and phosphate metabolic processes. Additionally, in the group with no enriched functions, there were not enough proteins involved in the regulation of same biological functions ($p > 0.001$). However, they might regulate diverse cancer-relevant functions; for example, 40S ribosomal protein SA (RPSA) was involved in cell adhesion; heterogeneous nuclear ribonucleoprotein F (HNRNPF) and heterogeneous

Table 4. Identification of differentially expressed proteins in 14-3-3β-overexpressing and control gastric cancer AGS cells

Spot[a]	Gene name[a]	Accession number[a]	Protein name[b]	m/z[b]	pI[b]	Matched peptides[c]	Unmatched peptides[d]	Coverage (%)	Ion score[e]	False discovery rate (%)[f]	Error (Da)	Fold (T/C)[g]	Peptides identified	Molecular function[h]
Downregulation														
1	ERLIN1	O75477	Prohibitin	29843/1	5.57	3	9	16	120	0	2.14 0.65 −2.38	C*	R.ILFRPVASQLPR.I R.KLEAAEDIAYQLSR.S K.AAELIANSL-ATAGDGLIELR.K	ER-associated protein catabolic process
2	EEF1B2	P24534	Elongation factor 1-β	24919/1	4.5	1	14	6	44	0	0.57	C*	K.SPAGLQVLNDYLADK.S	Translational elongation
3	ERLIN1	O75477	Prohibitin	29843/1	5.57	2	10	8	53	0	7.00 −1.30	C*	R.FDAGELITQR.E R.ILFRPVASQLPR.I	ER-associated protein catabolic process
4	KRT1	P04264	Keratin, type II cytoskeletal 1	66170/1	8.15	2	12	3	56	0	0.59	C*	K.YEELQITAGR.H K.WELLQQVDTSTR.T	Regulation of angiogenesis
5	KRT1	P04264	Keratin, type II cytoskeletal 1	66170/1	8.15	2	12	3	65	0	−1.02 10.0	C*	K.YEELQITAGR.H K.WELLQQVDTSTR.T	Regulation of angiogenesis
6	TPM3	P06753	Tropomyosin α-3 chain	32856/1	4.68	2	31	7	134	0	4.00 5.10	0.45±0.31	R.IQLVEEELDR.A R.KLVIIEGDLER.T	Cell motion
7	KRT8	P05787	Keratin, type II cytoskeletal 8	53671/1	5.52	5	26	11	221	0	−3.82 3.97 2.00 1.61 3.88	0.50±0.37	R.QLYEEEIR.E K.LSELEAALQR.A K.LALDIEIATYR.K R.ASLEAAIADAEQR.G R.LEGLTDEINFLR.Q	Cytoskeleton organization
8	KRT1	P04264	Keratin, type II cytoskeletal 1	66170/1	8.15	4	12	7	192	0	3.39 0.04 9.57 −1.21	0.59±0.37	K.YEELQITAGR.H K.LALDIEIATYR.T K.WELLQQVDTSTR.T R.THNLEPYFESFINNLR.R	Regulation of angiogenesis
9	CALR	P27797	Calreticulin	48283/1	4.29	2	32	5	50	0	−0.98 −0.88	0.59±0.19	K.VHVIFNYK.G R.FYALSASFEPFSNK.G	Regulation of cell cycle
10	KRT8	P05787	Keratin, type II cytoskeletal 8	53671/1	5.52	2	29	4	116	0	2.00 0.63	0.71±0.25	K.LALDIEIATYR.K R.LEGLTDEINFLR.Q	Cytoskeleton organization
11	KRT1	P04264	Keratin, type II cytoskeletal 1	66170/1	8.15	2	20	3	73	0	1.38 9.23	0.68±0.21	K.LALDIEIATYR.T K.WELLQQVDTSTR.T	Regulation of angiogenesis
12	HNRNPF	P52597	Heterogeneous nuclear ribonucleoprotein F	45985/1	5.38	1	14	4	44	0	0.90	0.58±0.06	K.ATENDIYNFFSPLNPVR.V	Signal transduction
13	NPM1	P06748	Nucleophosmin	32726/1	4.64	3	20	18	236	0	−1.29 −1.73 −1.09	0.68±0.19	K.VDNDENEHQLSLR.T K.DELHIVEAEAMNYEGSPIK.V +Oxidation (M) K.MSVQPTVSLGGFEI-TPPVVLR.L +Oxidation (M)	Cell proliferation
14	RPSA	P08865	40S ribosomal protein SA	32947/1	4.79	3	10	15	184	0	2.13 0.03 0.45	0.67±0.13	K.FAAATGATPIAGR.F R.FTPGTFTNQIOAAFR.E R.AIVAIENPADVSVISSR.N	Adhesion
15	YWHAE	P62258	14-3-3 protein ε	29326/1	4.63	2	15	11	88	0	2.22 0.17	0.47±0.18	R.YLAEFATGNDRK.E K.AASDIAMTELPPTHPIR.L +Oxidation (M)	Signal

Table 4. Continued

Spot	Gene name[a]	Accession number[a]	Protein name[b]	m/z[b]	pI[b]	Matched peptides[c]	Unmatched peptides[d]	Coverage (%)	Ion score[e]	False discovery rate (%)[f]	Error (Da)	Fold (T/C)[g]	Peptides identified	Molecular function[h]
16	KRT18	P05783	Keratin, type I cytoskeletal 18	48029/1	5.34	3	18	7	128	0	4.90 / −24.18 / 0.51	0.64±0.06	R.IVLQIDNAR.L / K.VKLEAEIATYR.R / R.AQIFANTVDNAR.I	Apoptosis
Upregulation														
17	EIF3I	Q13347	Eukaryotic translation initiation factor 3 subunit I	36878/1	5.38	1	17	3	55	0	−0.74	T*	R.FFHLAFEEEFGR.V	Translational initiation
18	HSPA1A	P08107	Heat shock 70 kDa protein 1	70294/1	5.48	3	38	6	121	0	−14.95 / −1.61 / 1.06	T*	K.DAGVIAGLNVLR.I / K.AQIHDLVLVGGSTR.I / R.IINEPTAAAIAYGLDR.T	Apoptosis
19	APRT	P07741	Adenine phosphoribosyl-transferase	19766/1	5.78	1	10	7	34	0	−4.41	T*	R.SFPDFFTPGVVFR.D	Adenine salvage
20	PPA1	Q15181	Inorganic pyrophosphatase	33095/1	5.54	1	21	3	33	0	0.34	2.45±1.80	R.AAPPSLEYR.V	Phosphate metabolism
21	PRDX2	P32119	Peroxiredoxin-2	22049/1	5.66	3	13	14	226	0	−0.63 / −1.87 / −2.21	2.11±0.53	R.QITVNDLPVGR.S / K.EGGLGPLNIPLLADVTR.R / R.KEGGLGPLNIPLLADVTR.R	Apoptosis
22	KRT18	P05783	Keratin, type I cytoskeletal 18	48029/1	5.34	2	19	5	58	0	−29.22 / −0.17	2.01±0.39	K.VKLEAEIATYR.R / R.AQIFANTVDNAR.I	Apoptosis
23	KRT1	P04264	Keratin, type II cytoskeletal 1	66170/1	8.15	1	21	2	82	0	2.05	1.71±0.69	R.THNLEPYFESFINNLR.R	Regulation of angiogenesis
24	HNRNPK	P61978	Heterogeneous nuclear ribonucleoprotein K	51230/1	5.39	2	21	5	114	0	1.56 / 1.24	1.53±0.69	R.NLPLPPPPR.G / R.LLIHQSLAGGIIGVK.G	Signal transduction
25	HSPA9	P38646	Stress-70 protein, mitochondrial	73920/1	5.87	4	47	8	293	0	2.69 / 2.52 / 2.53 / 0.62	1.16±0.4	R.AQFEGIVTDLIR.R / K.SDIGEVILVGGMTR.M / K.LLGQFTLIGIPPAPR.G / K.NAVITVPAYFNDSQR.Q	Apoptosis
26	GSTP1	P09211	Glutathione S-transferase P	23569/1	5.43	2	15	12	105	0	0.19 / −0.73	1.65±0.21	M.PPYTVVFPVR.G / K.FQDGDLTLYQSNTILR.H	Apoptosis
27	KRT1	P04264	Keratin, type II cytoskeletal 1	66170/1	8.15	3	51	5	80	0	1.19 / 0.20 / 9.78	1.53±0.26	K.YEELQITAGR.H / K.LALDIEIATYR.T / K.WELLQQVDTSTR.T	Regulation of angiogenesis
28	KRT8	P05787	Keratin, type II cytoskeletal 8	53671/1	5.52	2	29	4	138	0	−0.27 / 0.14	1.28±0.53	K.LALDIEIATYR.K / RLEGLTDEINFLR.Q	Cytoskeleton

These differentially expressed protein spots are identified by MS/MS and then selected after MASCOT database searching ($p < 0.05$).
a) Gene name and accession number are obtained from Swiss-Prot database.
b) The data are identified after MASCOT database searching.
c) The number of tryptic peptides that match to peptides of the identified proteins.
d) The number of tryptic peptides that do not match to peptides of the identified proteins.
e) Ion score was obtained based on MS/MS analysis.
f) False discovery rate was determined by the results of randomized database searches.
g) C represents pcDNA3 control and T represents 14-3-3β-overexpressing tumor cells. C* represents the protein is only expressed in pcDNA3 control cells. T* represents the protein is only expressed in 14-3-3β-overexpressing tumor cells.
h) Molecular function is based on GO database.

110
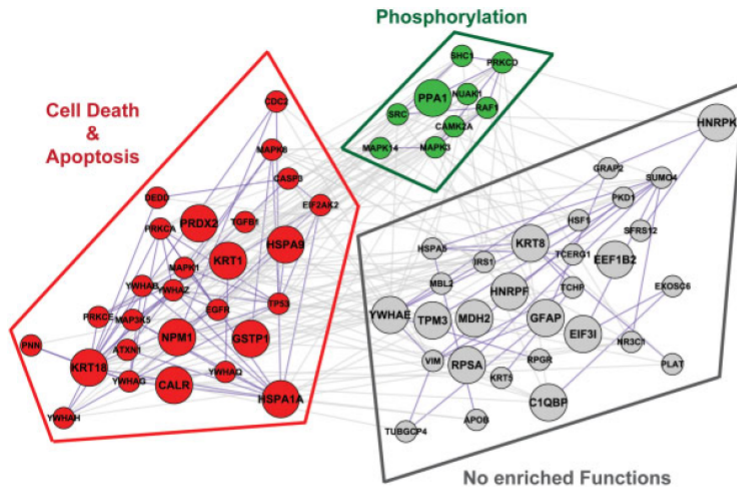
Figure 8. A protein–protein interaction network and the biological functions regulated by 14-3-3β. The significantly differentially expressed proteins in 14-3-3β-overexpressing tumor cells and their interacting proteins were used to construct the PPI network. All proteins in the network were further analyzed for clustering of functional profiles by using BINGO. It uncovered key functional relationships, in particular cell death and apoptosis and phosphorylation in addition to a group of proteins with no enriched function. The large and small circles in their clustering of functional profiles represent the identified proteins (L0) and their interacting proteins (L1), respectively.

nuclear ribonucleoprotein K (HNRNPK) were involved in signal transduction (Table 4).

4 Discussion

Proteomics has been increasingly utilized for the discovery of novel cancer biomarkers and in this study; a proteomics-based approach was used to demonstrate that 14-3-3β expression in gastric cancer cells was significantly reduced after 5-FU treatment. These results suggested that 14-3-3β may be highly associated with the development of gastric cancer. Thus, the level of 14-3-3β expression in tumor tissues was investigated and it was found that 14-3-3β was significantly overexpressed in gastric cancer tissues compared with normal tissues.

Several biomarkers for gastric cancer have been reported, including CEA, CA19-9 and CA72-4 [4, 5]; however, these were not sensitive nor specific enough for disease detection [6, 7]. In this study, the 14-3-3β was assessed as a serologic biomarker for gastric cancer and it was confirmed that 14-3-3β levels in pre-operative serum were significantly elevated in cancer patients compared with controls ($p < 0.0001$) and also positively correlated to 14-3-3β expression levels in tumor tissues ($r = 0.385$, $p = 0.033$). Moreover, serum 14-3-3β levels in stage I gastric cancer patients were significantly higher than in controls ($p = 0.005$). These results suggest that 14-3-3β can be used as a potential serum marker for the

detection of gastric cancer. Additionally, overall and recurrence-free survival rates based on 14-3-3β serum levels were also investigated and patients with higher 14-3-3β levels showed a marked reduction in overall and recurrence-free survival. These results, therefore, demonstrate that 14-3-3β can be used as a potential biomarker for the detection and prognosis of human gastric cancer.

Currently, relatively little is known about the role of 14-3-3β in gastric cancer compared with other types of cancers such as lung cancer, where it was reported that 14-3-3β was abundantly expressed in lung cancer tissues [11] and associated with invasion, migration, metastasis and proliferation of tumor cells [14, 15, 28]. Thus, a key question is whether 14-3-3β also affects malignant progression of gastric cancer cells. Our clinical analyses indicated that serum 14-3-3β levels were significantly associated with increases in the depth of tumor invasion, peritoneal invasion, tumor size, the number of metastatic lymph nodes, enhanced cancer stage progression (stages III and IV) and the presence of invasive phenotypes. We also demonstrated that 14-3-3β enhanced invasion, migration and growth of tumor cells in vitro and these results were consistent with clinicopathological observations. These results suggest that 14-3-3β plays a crucial role in the malignant progression of gastric cancer cells.

To elucidate the downstream regulation of 14-3-3β in gastric cancer cell progression, we identified the differentially expressed proteins regulated by 14-3-3β and

constructed a PPI network for the analysis of their biological functions. Many of the upregulated proteins within the 14-3-3β-regulated network have been reported to be involved in tumor progression. For example, HSPA1A is involved in cancer invasion [29] and promotes tumor cell growth [30]; HSPA9 is associated with hepatocellular carcinoma metastasis [31] and inhibits cell apoptosis through inactivation of p53 expression [32] and PRDX2 overexpression inhibits cisplatin-induced apoptosis [33]. Thus, 14-3-3β may influence biological processes involved in apoptosis, tumor progression and invasion by regulating the expression of a variety of potential downstream interacting partners that also participate in these functions.

Recently, Xia et al. reported that serum macrophage migration-inhibitory factor (MMIF) was a better biomarker than CEA in diagnosing gastric cancer in patients presenting with dyspepsia [34]. Here, we further demonstrate serum 14-3-3β levels as a biomarker in differentiating between gastric cancer patients and controls. Additional prospective studies deserve further investigation where serum 14-3-3β assessment may be combined with other useful serum markers, such as MMIF, to increase the overall sensitivity, specificity and diagnostic accuracy of gastric cancer detection.

Helicobacter pylori infection is a crucial factor in the pathogenesis of gastric cancer and induces disease-specific protein expression in gastric cancer [16]. To elucidate the effects of *H. pylori* infection on 14-3-3β expression, we analyzed their correlation. We found that patients with *H. pylori* infection had higher 14-3-3β levels than those with no *H. pylori* infection (Supporting Information Fig. S5), suggesting that 14-3-3β might be involved in the pathogenesis of *H. pylori* in gastric cancer. Some studies are similar with our results that 14-3-3β is upregulated in *H. pylori*-infected gastric cancer cells [16, 35].

In this study, we evaluated the clinical significance of serum 14-3-3β in diagnosing gastric cancer and elucidated the regulatory roles of 14-3-3β in tumor cell progression. We have identified that serum 14-3-3β could be used for differentiating between gastric cancer patients and controls and was a poor prognostic factor for survival in gastric cancer. The 14-3-3β ELISA also has the added advantage of being commercially available, easily reproducible and inexpensive. Thus, it is useful to assay serum 14-3-3β concentration for the diagnosis of gastric cancer. Furthermore, we have demonstrated that 14-3-3β is associated with malignant progression of tumor cells and provided a new insight into the role of 14-3-3β in gastric cancer cell progression through its regulated network. Thus, these results provide a valuable tool in diagnosis and therapy of gastric cancer.

5   References

[1] Parkin, D. M., Bray, F., Ferlay, J., Pisani, P., Global cancer statistics, 2002. *CA Cancer J. Clin.* 2005, *55*, 74–108.

[2] Macdonald, J. S., Gastric cancer – new therapeutic options. *N. Engl. J. Med.* 2006, *355*, 76–77.

[3] Yamazaki, H., Oshima, A., Murakami, R., Endoh, S., Ubukata, T., A long-term follow-up study of patients with gastric cancer detected by mass screening. *Cancer* 1989, *63*, 613–617.

[4] Kodama, I., Koufuji, K., Kawabata, S., Tetsu, S. et al., The clinical efficacy of CA 72-4 as serum marker for gastric cancer in comparison with CA19-9 and CEA. *Int. Surg.* 1995, *80*, 45–48.

[5] Ohuchi, N., Takahashi, K., Matoba, N., Sato, T. et al., Comparison of serum assays for TAG-72, CA19-9 and CEA in gastrointestinal carcinoma patients. *Jpn. J. Clin. Oncol.* 1989, *19*, 242–248.

[6] Hao, Y., Yu, Y., Wang, L., Yan, M. et al., IPO-38 is identified as a novel serum biomarker of gastric cancer based on clinical proteomics technology. *J. Proteome Res.* 2008, *7*, 3668–3677.

[7] Ychou, M., Duffour, J., Kramar, A., Gourgou, S., Grenier, J., Clinical significance and prognostic value of CA72-4 compared with CEA and CA19-9 in patients with gastric cancer. *Dis. Markers* 2000, *16*, 105–110.

[8] Cho, W. C., Contribution of oncoproteomics to cancer biomarker discovery. *Mol. Cancer* 2007, *6*, 25–37.

[9] Frank, R., Hargreaves, R., Clinical biomarkers in drug discovery and development. *Nat. Rev. Drug Discov.* 2003, *2*, 566–580.

[10] MacKeigan, J. P., Clements, C. M., Lich, J. D., Pope, R. M. et al., Proteomic profiling drug-induced apoptosis in non-small cell lung carcinoma: identification of RS/DJ-1 and RhoGDIalpha. *Cancer Res.* 2003, *63*, 6928–6934.

[11] Qi, W., Liu, X., Qiao, D., Martinez, J. D., Isoform-specific expression of 14-3-3 proteins in human lung cancer tissues. *Int. J. Cancer* 2005, *113*, 359–363.

[12] Cochran, D. A., Evans, C. A., Blinco, D., Burthem, J. et al., Proteomic analysis of chronic lymphocytic leukemia subtypes with mutated or unmutated Ig V(H) genes. *Mol. Cell. Proteomics* 2003, *2*, 1331–1341.

[13] Takihara, Y., Matsuda, Y., Hara, J., Role of the beta isoform of 14-3-3 proteins in cellular proliferation and oncogenic transformation. *Carcinogenesis* 2000, *21*, 2073–2077.

[14] Han, D. C., Rodriguez, L. G., Guan, J. L., Identification of a novel interaction between integrin beta1 and 14-3-3beta. *Oncogene* 2001, *20*, 346–357.

[15] Komiya, Y., Kurabe, N., Katagiri, K., Ogawa, M. et al., A novel binding factor of 14-3-3beta functions as a transcriptional repressor and promotes anchorage-independent growth, tumorigenicity, and metastasis. *J. Biol. Chem.* 2008, *283*, 18753–18764.

[16] Chan, C. H., Ko, C. C., Chang, J. G., Chen, S. F. et al., Subcellular and functional proteomic analysis of the cellular responses induced by *Helicobacter pylori*. *Mol. Cell. Proteomics* 2006, *5*, 702–713.

[17] Juan, H. F., Wang, I. H., Huang, T. C., Li, J. J. et al., Proteomics analysis of a novel compound: cyclic RGD in breast carcinoma cell line MCF-7. *Proteomics* 2006, *6*, 2991–3000.

[18] Lin, L. L., Chen, C. N., Lin, W. C., Lee, P. H. et al., Annexin A4: a novel molecular marker for gastric cancer with *Helicobacter pylori* infection using proteomics approach. *Proteomics Clin. Appl.* 2008, *2*, 619–634.

[19] Lauren, P., The two histological main types of gastric carcinoma: diffuse and so-called intestinal-type carcinoma. An attempt at a histo-clinical classification. *Acta Pathol. Microbiol. Scand.* 1965, *64*, 31–49.

[20] Sobin L. H, Gospodarowicz, M. K., Wittekind, C. (Eds.), *TNM Classification of Malignant Tumors*, 5th Edn, John Wiley and Sons, Inc., New York 1997.

[21] Xiao, T., Ying, W., Li, L., Hu, Z. et al., An approach to studying lung cancer-related proteins in human blood. *Mol. Cell. Proteomics* 2005, *4*, 1480–1486.

[22] Chen, G., Gharib, T. G., Wang, H., Huang, C. C. et al., Protein profiles associated with survival in lung adenocarcinoma. *Proc. Natl. Acad. Sci. USA* 2003, *100*, 13537–13542.

[23] Katayama, M., Sanzen, N., Funakoshi, A., Sekiguchi, K., Laminin gamma2-chain fragment in the circulation: a prognostic indicator of epithelial tumor invasion. *Cancer Res.* 2003, *63*, 222–229.

[24] Chang, C. C., Shih, J. Y., Jeng, Y. M., Su, J. L. et al., Connective tissue growth factor and its role in lung adenocarcinoma invasion and metastasis. *J. Natl. Cancer Inst.* 2004, *96*, 364–375.

[25] Mathivanan, S., Periaswamy, B., Gandhi, T. K., Kandasamy, K. et al., An evaluation of human protein–protein interaction data in the public domain. *BMC Bioinformatics* 2006, *7*, S19.

[26] Maere, S., Heymans, K., Kuiper, M., BiNGO: a cytoscape plugin to assess overrepresentation of gene ontology categories in biological networks. *Bioinformatics* 2005, *21*, 3448–3449.

[27] Shannon, P., Markiel, A., Ozier, O., Baliga, N. S. et al., Cytoscape: a software environment for integrated models of biomolecular interaction networks. *Genome Res.* 2003, *13*, 2498–2504.

[28] Porter, G. W., Khuri, F. R., Fu, H., Dynamic 14-3-3/client protein interactions integrate survival and apoptotic pathways. *Semin. Cancer Biol.* 2006, *16*, 193–202.

[29] Hippo, Y., Taniguchi, H., Tsutsumi, S., Machida, N. et al., Global gene expression analysis of gastric cancer by oligonucleotide microarrays. *Cancer Res.* 2002, *62*, 233–240.

[30] Jaattela, M., Escaping cell death: survival proteins in cancer. *Exp. Cell Res.* 1999, *248*, 30–43.

[31] Yi, X., Luk, J. M., Lee, N. P., Peng, J. et al., Association of mortalin (HSPA9) with liver cancer metastasis and prediction for early tumor recurrence. *Mol. Cell. Proteomics* 2008, *7*, 315–325.

[32] Wadhwa, R., Takano, S., Kaur, K., Deocaris, C. C. et al., Upregulation of mortalin/mthsp70/Grp75 contributes to human carcinogenesis. *Int. J. Cancer* 2006, *118*, 2973–2980.

[33] Chung, Y. M., Yoo, Y. D., Park, J. K., Kim, Y. T., Kim, H. J., Increased expression of peroxiredoxin II confers resistance to cisplatin. *Anticancer Res.* 2001, *21*, 1129–1133.

[34] Xia, H. H., Yang, Y., Chu, K. M., Gu, Q. et al., Serum macrophage migration-inhibitory factor as a diagnostic and prognostic biomarker for gastric cancer. *Cancer* 2009, *115*, 5441–5449.

[35] Lim, J. W., Kim, H., Kim, J. M., Kim, J. S. et al., Cellular stress-related protein expression in *Helicobacter pylori*-infected gastric epithelial AGS cells. *Int. J. Biochem. Cell Biol.* 2004, *36*, 1624–1634.

Integrative network analysis reveals active microRNAs and their functions in gastric cancer

Chien-Wei Tseng (f93b43013@ntu.edu.tw)
Chen-Ching Lin (kdragongo@gmail.com)
Chiung-Nien Chen (ccchen@ntu.edu.tw)
Hsuan-Cheng Huang (hsuancheng@ym.edu.tw)
Hsueh-Fen Juan (yukijuan@ntu.edu.tw)

Quantitative Proteomic and Genomic Profiling Reveals Metastasis-Related Protein Expression Patterns in Gastric Cancer Cells

Yet-Ran Chen,[†] Hsueh-Fen Juan,[‡] Hsuan-Cheng Huang,[§] Hsin-Hung Huang,[†] Ya-Jung Lee,[†] Mei-Yueh Liao,[||] Chien-Wei Tseng,[‡] Li-Ling Lin,[‡] Jeou-Yuan Chen,[⊥] Mei-Jung Wang,[⊥] Jenn-Han Chen,*,[O] and Yu-Ju Chen*,[†,#]

Institute of Chemistry and Genomic Research Center, Academia Sinica, Taipei, Taiwan, Department of Life Science and Institute of Molecular and Cellular Biology, National Taiwan University, Taipei, Taiwan, Institute of Bioinformatics, National Yang-Ming University, Taipei, Taiwan, Institute of Bioscience and Biotechnology, National Taiwan Ocean University, Keelung, Taiwan, Institute of Biomedical Sciences, Academia Sinica, Taipei, Taiwan, School of Dentistry, National Defense Medical Center, National Defense University, Taipei, Taiwan, and Institute of Molecular Biology, National Chung Hsing University, Taichung, Taiwan

Gastric cancer is a leading cause of death worldwide, and patients have an overall 5-year survival rate of less than 10%. Using quantitative proteomic techniques together with microarray chips, we have established comprehensive proteome and transcriptome profiles of the metastatic gastric cancer TMC-1 cells and the noninvasive gastric cancer SC-M1 cell. Our qualitative protein profiling strategy offers the first comprehensive analysis of the gastric cancer cell proteome, identifying 926 and 909 proteins from SC-M1 and TMC-1 cells, respectively. Cleavable isotope-coded affinity tagging analysis allows quantitation of a total of 559 proteins (with a protein false-positive rate of <0.005), and 240 proteins were differentially expressed (>1.3-fold) between the SC-M1 and TMC-1 cells. We identified numerous proteins not previously associated with gastric cancer. Notably, a large subset of differentially expressed proteins was associated with tumor metastasis, including proteins functioning in cell−cell and cell− extracellular matrix (cell−ECM) adhesion, cell motility, proliferation, and tumor immunity. Gene expression profiling by DNA microarray revealed differential expression (of >2-fold) of about 1000 genes. The weak correlation observed between protein and mRNA profiles highlights the important complementarities of DNA microarray and proteomics approaches. These comparative data enabled us to map the disease-perturbed cell−cell and cell−ECM adhesion and Rho GTPase-mediated cytoskeletal pathways. Further validation of a subset of genes suggests the potential use of vimentin and galectin 1 as markers for metastasis. We demonstrate that combining proteomic and genomic approaches not only provides a rapid, robust, and sensitive platform to elucidate the molecular mechanisms underlying gastric cancer metastasis but also may identify candidate diagnostic markers and therapeutic targets.

Keywords: cICAT • 2D-LC−MS/MS • Mass Spectrometry • Gastric Cancer • Metastasis

Introduction

Gastric cancer is one of the most common malignancies and a leading cause of cancer-related deaths worldwide.[1] Although the incidence of and mortality due to gastric cancer have declined over the past 40 years[2] and advances in early diagnosis provide excellent long-term survival probabilities for early stage patients, the overall 5-year survival rate remains less than 10%.[3] The poor prognosis is mainly due to the fact that most patients are diagnosed at an advanced stage. Advanced gastric cancer is accompanied by metastasis to the peritoneum, lymph nodes, or other organs.[4] However, the molecular mechanisms associated with tumor metastasis are still not fully understood. Tumor metastasis is mediated by highly complex, multistep processes beginning with loss of adhesion of the tumor cells to neighboring cells.[5] These cells dissolve the extracellular matrix (ECM), and/or travel via the circulation to invade and proliferate at

* To whom correspondence should be addressed. For Y.-J. C.: e-mail, yjchen@chem.sinica.edu.tw; phone, 886-2-2789-8660, fax, 886-2-2783-1237.
† Institute of Chemistry and Genomic Research Center, Academia Sinica.
‡ National Taiwan University.
§ National Yang-Ming University.
|| National Taiwan Ocean University.
⊥ Institute of Biomedical Sciences, Academia Sinica.
O National Defense University.
National Chung Hsing University.

distant new sites. The detailed molecular and cellular mechanisms of carcinogenesis, cancer invasion, and metastasis remain to be elucidated.

Mapping the cellular networks perturbed during cancer progression by systematic, high-throughput, genome-wide expression analysis at both the mRNA and protein levels will facilitate our understanding of these processes.[6,7] However, it is now generally recognized that mRNA microarray results should be considered preliminary data that require independent follow-up validation. In contrast, a change in protein patterns in a given disease state should reflect the pathologic processes taking place within the cells. The highly complex feedback between the transcriptome and proteome should ideally describe most biochemical processes within and between cells. Thus, a combination of genomic and proteomic analyses is essential.[7]

While substantial efforts have been made to conduct comparative proteomic characterizations of gastric adenocarcinoma,[8–13] most of the efforts to date have used two-dimensional gel electrophoresis (2-DE) and mass spectrometry (MS). Other than the comprehensive account of the proteins thought to have altered expression in gastric cancer, only a limited number of tumor-associated proteins have been observed to be differentially expressed, because of the inherent limitations of detecting extreme pH/mass and low-abundance proteins. Compared to a 2-DE strategy, protein shotgun sequencing based on two-dimensional liquid chromatography tandem mass spectrometry (2D-LC−MS/MS) analysis represents a large-scale, robust, and sensitive technology for protein profiling.[14–16] An alternative proteome profiling approach, isotope-coded affinity tagging (ICAT), combined with the shotgun profiling method, allows quantitative analysis of proteomic changes in response to cellular perturbations with a wide dynamic range and good quantitative accuracy.[16,17] More recently, a second-generation cleavable ICAT (cICAT) reagent was developed to eliminate chromatographic isotope effects caused by hydrogen and deuterium.[18] Furthermore, the combination of cICAT technology and 2D-LC−MS/MS has been shown to be capable of detecting a large number of proteins, allowing more comprehensive coverage of the proteome.[19]

To study gastric cancer metastasis systematically, we performed a quantitative comparison between the nonmetastatic SC-M1 and metastatic TMC-1 gastric cancer cell lines. Although direct analysis of clinical samples is most appropriate in principle, to provide phenotype information, the heterogeneous genetics of clinical samples requires analysis of a large number of patients to guarantee statistical significance. Therefore, well-characterized cell lines may prove more informative because of advantages in reproducibility, availability of large numbers, and genetic homogeneity. SC-M1 is a well-established human gastric carcinoma cell line, originally cultured from a poorly differentiated adenocarcinoma that invaded through the stomach wall but showed no metastasis to lymph nodes or adjacent organs.[20] Another gastric cancer cell line, TMC-1, was derived from the lymph node of an individual with a moderately differentiated adenocarcinoma of the stomach and exhibited highly tumorigenic features.[21] The comparative mRNA and protein profiling of these two cell lines may allow us to study the cellular processes associated with the development of gastric cancer metastasis, facilitating further investigation by clinical specimens.

As shown in Figure 1, we first performed qualitative profiling to define the protein constituents of SC-M1 and TMC-1 cells
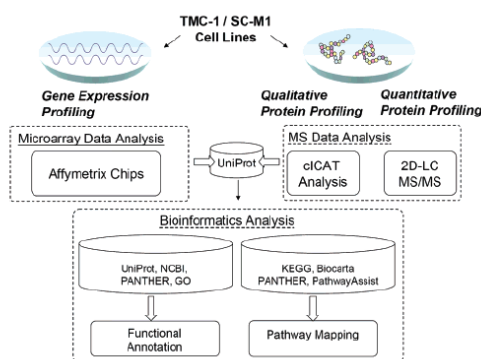
Figure 1. Schematic representation of the experimental design and bioinformatics analysis for comprehensive genomic and proteomic profiling of SC-M1 and TMC-1 cells.

by 2D-LC-−S/MS. We further compared protein and mRNA expression profiles between SC-M1 and TMC-1 cells using cICAT technology and Affymetrix DNA microarrays. To our knowledge, our results offer a more comprehensive proteomic analysis of gastric cancer cells than previously reported. By the complementary analysis of differentially expressed proteins and mRNAs in the two cell lines, we aimed to address the following two issues: (1) the elucidation of the molecular mechanism of metastasis of gastric cancer and (2) the identification of potential markers and/or expression signatures for prognosis and drug discovery for future therapeutic intervention. While the current study focuses on gastric cancer, we expect that the potential markers and pathways uncovered here may be relevant to the metastatic phenotypes of cancer in general.

Materials and Methods

Chemicals. RPMI 1640 medium was purchased from Hy-Clone (Logan, UT). Fetal bovine serum (FBS) was purchased from Gibco BRL (Grand Island, NY). Trypsin was purchased from Promega (Madison, WI). Tris (2-carboxyethyl) phosphine (TCEP) was obtained from Fisher Scientific Corp. (Pittsburgh, PA). The BCA protein assay kit was obtained from Pierce (Rockford, IL). Tris, SDS, Triton X-100, trifluoroacetic acid (TFA), formic acid, and acetonitrile were purchased from Sigma-Aldrich (St. Louis, MO). Iodoacetamide was purchased from Amersham Biosciences (England, U.K.)

Cell Culture and Lysis. The human gastric cancer cell lines SC-M1 and TMC-1 were grown in RPMI 1640 medium supplemented with 25 mM HEPES, 26 mM NaHCO$_3$, 2 mM glutamine, 100 units/mL sodium penicillin G, 100 μg/mL streptomycin sulfate, 0.25 μg amphotericin B (fungizone), and 10% fetal bovine serum (FBS, Invitrogen Corporation, Carlsbad, CA) at 37 °C with 5% CO$_2$. The cells were harvested, washed, divided into aliquots containing about ~2 × 10^7 cells each, and suspended in lysis buffer (50 mM Tris at pH 8.0, 0.1% (w/v) SDS, 0.02% (w/v) Triton X-100). The suspensions were lysed by placement into a sonic water bath for 30 min followed by exposure to three liquid nitrogen freeze−thaw cycles. Total protein concentration of each cell extract was determined using the BCA assay.

Qualitative Protein Profiling by 2D-LC−MS/MS. About 1 mg of total protein from each cell extract was reduced by TECP,

116

alkylated by IAA, and digested by trypsin. Strong cation exchange (SCX) chromatography was used to fractionate the tryptic peptides. The tryptic peptides were fractionated using a 2.1×200 mm polysulfoethyl A SCX column (Poly LC, Columbia, MD). Peptides were eluted with a gradient of 0−25% buffer B (5 mM K_2HPO_4, 25% acetonitrile, and 350 mM, KCl, pH 3.0) over 30 min, followed by a gradient of 25−100% buffer B over 20 min. The SCX fractions (retention time: 20−60 min) were analyzed in duplicate by microcapillary-liquid chromatography MS/MS (μLC−MS/MS).

Quantitative Protein Profiling by cICAT and 2D-LC−MS/MS. About 400 μg of total protein extracted from TMC-1 and SC-M1 cells was labeled with heavy and light isotope-label cICAT, respectively. The cICAT labeling reaction was performed following the manufacturer's protocol (Applied Biosystems, Framingham, MA). The labeled samples were combined and subjected to the trypsin digestion. The digested samples were further fractionated by SCX chromatography, and the cICAT-labeled peptides were isolated by avidin-affinity chromatography for subsequent μLC−MS/MS analysis.

μLC−MS/MS Analysis. Samples were loaded using an autosampler and injected into a 1.5 cm $\times$ 100 μm trapping column and 12 cm $\times$ 75 μm separation column packed in-house (Magic C_{18}; Michrom BioResources, Auburn, CA) and sequentially analyzed by μLC−MS/MS. Peptides were eluted with a linear gradient of 5−40% buffer B over 120 min at ∼200 nL/min (buffer A, 0.1% formic acid in H_2O; buffer B, 0.1% formic acid in acetonitrile). An HP 1100 solvent delivery system (Hewlett-Packard, Palo Alto, CA) was used with precolumn flow splitting. A quadrupole/time-of-flight mass spectrometer (QSTAR Pulsar *i*, Applied Biosystems, Foster City, CA) with an in-house built microspray device was used for all analyses. Peptide fragmentation by collision-induced dissociation was performed in an automated fashion using the information-dependent option.

Data Processing. Uninterpreted MS/MS spectra were searched against the Celera Discovery System (CDS, Celera Genomics, CA) sequence classification protein database (version date 08/13/2003) using the TurboSEQUEST (v.27-rev.12, ThermoFinnigan, San Jose, CA) and validated by the PeptideProphet.[22] The peptides that displayed a PeptideProphet score >0.7 were analyzed by ProteinProphet[23] to calculate the false-positive score of each identified protein. The proteins or related protein groups were identified with a probability score cutoff of $p >$ 0.95. For the qualitative analysis, this value corresponded to a false-positive error rate of 0.005 and 0.004 for SC-M1 and TMC-1, respectively. For the cICAT analysis, this value corresponded to a false-positive error rate of 0.004. The light-to-heavy mass (L/H) ratio resulting from differential expression was calculated and normalized by ASAPRatio.[24] All of the cICAT-labeled peptides quantified by ASAPRatio were also verified manually.

Microarray Analysis. Total cellular RNA was extracted from a minimum of 5×10^6 cells using the TRIZOL reagent (Invitrogen Corp.). RNA was additionally purified by phenol/chloroform/isoamyl alcohol (25:24:1) extraction, and RNA quality was checked using an Agilent 2100 Bioanalyzer (Agilent Technologies, Foster City, CA). RNA processing and hybridization to the Affymetrix HG-U133A GeneChip oligonucleotide microarray (Santa Clara, CA) were performed according to the manufacturer's protocol. Initial data analysis was performed using Microarray Suite v 5.0 software (Affymetrix, Santa Clara, CA), setting the scaling of all probe sets to a constant value of 500 for each GeneChip. Additional data analysis was performed

using GeneSpring v 5.1 (Silicon Genetics Inc., Redwood City, CA). Genes with differential expression levels of 2-fold or more between SC-M1 and TMC-1 cells were selected for further analysis.

Functional Classification and Pathway Annotations. Functional classification of the identified proteins was mainly based on the CDS sequence classification protein database (version date 08/13/2003). The proteins without functional annotation in the CDS database were searched against the UniProt (http://www.pir.uniprot.org/), NCBI (http://www.ncbi.nlm.nih.gov/), PANTHER (http://www.pantherdb.org/), and Gene Ontology (GO) (http://www.geneontology.org/) consortium databases to obtain their biological functions.

For analysis of the perturbed pathway of each differentially expressed gene and protein, we retrieved 314 BioCarta (http://www.biocarta.com) and 155 Kyoto Encyclopedia of Genes and Genome (KEGG, http://www.genome.ad.jp/kegg/pathway.html) pathways. The Unigene accession numbers were used as identifiers to compare with the proteomic and microarray data. The proteomic data is also analyzed by the pathway analysis tool in NCI's Cancer Genome Anatomy Project (CGAP, http://cgap.nci.nih.gov/Pathways).

Immunocytostaining. For immunocytostaining studies, cells grown on coverslips were fixed in 4% paraformaldehyde for 30 min at room temperature, washed twice with TBS (50 mM Tris-HCl and 150 mM NaCl, pH 7.4), and blocked in TBBS (50 mM Tri-HCl, pH 7.4, 150 mM NaCl, 0.1% Triton X-100, and 3% bovine serum albumin) for 1 h at 37 °C. β-Catenin was detected using anti-β-catenin rabbit polyclonal antibody purchased from Sigma (St. Louis, MO) in conjunction with Alexa Fluor 488-conjugated anti-rabbit IgG secondary antibody purchased from Invitrogen. Cells were also counter-stained with 4,6-diamidino-2-phenylindole-dihydrochloride (DAPI, Vector Laboratories, Inc., Burlingame, CA). Cells were analyzed by a laser scanning confocal system (Radiance-2100; Bio-Rad, Hercules, CA).

Flow Cytometry. Cells were seeded at 1×10^5 cells/well in 6-well microplates and incubated overnight in DMEM containing 10% fetal calf serum. Cells were trypsinized; stained with a monoclonal antibody (mAb) against integrin α6 (CD49f, Serotec, Oxford, U.K.), integrin β4 (Serotec), or an isotype IgG; washed with cold PBS three times; labeled with Alexa Fluor 488-conjugated anti-mouse IgG antibody; and subjected to flow cytometry analysis using a FACSCalibur instrument (BD Biosciences). The specific fluorescence index was calculated as the ratio of the mean fluorescence values obtained with the specific Ab and the isotype control Ab.

Alamar Blue Assay for Cell Proliferation and Viability. Cells in a 96-well plate were incubated for 4 h with Alamar Blue dye (Biosource) to measure cellular proliferation and viability. Dye uptake was measured fluorometrically using an ELISA Reader (Molecular Devices Corporation, CA) at an excitation and emission wavelength of 570 and 600 nm, respectively.

Results

Qualitative Protein Profiling of SC-M1 and TMC-1 Cell Lines. As shown in Figure 1, qualitative profiling was performed by 2D-LC−MS/MS to define the protein constituents in SC-M1 and TMC-1 cells prior to quantitative profiling experiments and to facilitate detection of low-abundance proteins and/or cysteine-deficient proteins that cannot be observed by cICAT analysis. Using a stringent identification criterion (protein identification false-positive rate of < 0.005), 926 and 909 protein
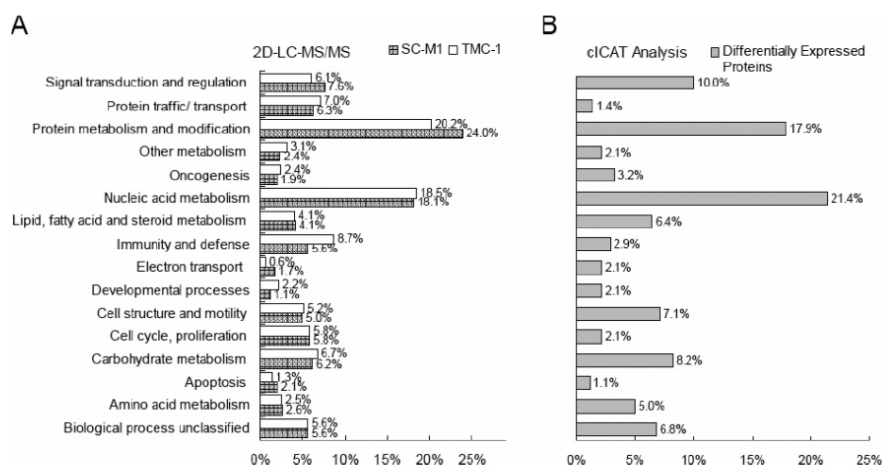
Figure 2. Functional classification of (A) SC-M1 and TMC-1 proteins from 2D-LC−MS/MS. (B) Differentially expressed proteins between SC-M1 and TMC-1 cells from cICAT analysis. The numbers indicate the percentage of proteins that were differentially expressed between the two cell lines for each functional classification.

entries from SC-M1 and TMC-1 cells were identified, respectively (Supplemental Tables 1 and 2, Supporting Information). For those proteins identified in the qualitative profiling, 41 and 48 proteins were cysteine-deficient in SC-M1 and TMC-1, respectively.

To obtain an overview of the similarities and differences in protein expression between the cell lines, functional annotation was performed to compare the protein constituents. Figure 2A compares the functional category distribution of SC-M1 and TMC-1 proteins according to biological processes (also see Supplemental Tables 1 and 2, Supporting Information). As expected, the identified proteins in the two cell lines possess similar functional category patterns. Most proteins fit into two main categories: protein metabolism and modification, and nucleic acid metabolism. A majority of the other proteins participate in signal transduction and regulation, cell structure and mobility, cell cycle and proliferation, immunity and defense, and protein traffic and transport. Several proteins were classified to be oncogenesis-associated, including 14-3-3 protein σ, 14-3-3 protein ζ, 14-3-3 protein τ, annexin I, galectin 1, myc box-dependent interacting protein 1, and T-plastin; these proteins have also been previously found to be differentially expressed in cancer cells.[8,25−27]

Differential Proteomic and Transcriptomic Analyses of SC-M1 and TMC-1 Cell Lines. In cICAT analysis, 1727 cICAT-labeled peptides originated from 615 proteins were identified (with a protein identification false-positive rate of < 0.005), of which 559 could be quantified. From the global mean and standard deviation in this study, we have chosen to highlight proteins that have abundance ratios greater than 1.3-fold. Using this criterion, we identified 240 proteins that displayed more than a 1.3-fold expression difference; 100 proteins were up-regulated and 140 proteins were down-regulated in the TMC-1 cells as compared with the SC-M1 cells. Table 1 lists the summary of these differentially expressed proteins. Figure 2B displays the functional category distribution of differentially expressed proteins. Other than metabolism, prominent among the differential expression findings were proteins involved in

signal transduction and regulation, including down-regulation of the Rho-related GTP-binding protein RhoG, transforming protein RhoA, and transforming protein RhoC in TMC-1 cells. Other significant changes involved proteins related to cell structure and motility. These functional categories showed higher percentage of distributions in comparison with qualitative profiling of SC-M1 and TMC-1 (Figure 2A). Figure 3 shows a differentially expressed protein, β-catenin, quantified by cICAT analysis. The light and heavy cICAT-labeled peptide revealed a 5.9-fold overexpression in TMC-1 cells compared with SC-M1 cells (Figure 3B,C). This observation was confirmed with Western blotting, as shown in Figure 3D.

To examine whether the differential protein expression may be attributable to transcriptional regulation or another regulatory mechanism, mRNA expression profiling was performed on SC-M1 and TMC-1 cells using an Affymetrix HG-U133A Gene-Chip oligonucleotide microarray. The pathways containing differentially expressed genes are listed in Table 2. Among these pathways, three are involved in cancer transformation and proliferation: inhibition of matrix metalloproteinases, multi-drug resistance (MDR) factors, and thrombospondin-1 (TSP-1)-induced apoptosis. Matrix metalloproteinases are a class of proteases secreted by tumor cells that degrade the proteins of the ECM for subsequent tumor cell invasion and metastasis. There are many MDR genes among the mRNAs differentially expressed in SC-M1 and TMC-1 cells, including members of the MDR/TAP subfamily, cytochrome P450 51A1, and glutathione-S-transferase.[28] TSP-1 inhibits angiogenesis and slows tumor growth, apparently by inducing apoptosis of microvascular endothelial cells that line blood vessels.[29] Factors that inhibit angiogenesis might act as cancer therapeutic agents by blocking vessel formation in tumors and starving cancer cells. These pathways may be relevant to the differences between SC-M1 and TMC-1 cells.

Transcriptional versus Translational Regulation of Protein Expression. Changes in protein expression levels between the two cancer cell types were further examined for potential correlations with the changes in mRNA levels. Cross-referencing

Table 1. Summary of Differentially Expressed Proteins and Their Functional Classifications

	UniProt	protein name	peptide number	prob.[a]	cICAT[b]	Affymetrix[c]	molecular function
		Amino Acid Metabolism					
1	P31327	Carbamoyl-phosphate synthase	2	1.00	0.16 ± 0.03	NA[d]	Synthase and synthetase
2	O43175	D-3-phosphoglycerate dehydrogenase	6	1.00	0.31 ± 0.07	0.52	Oxidoreductase
3	P26639	Threonyl-tRNA synthetase, cytoplasmic	2	1.00	0.35 ± 0.04	0.92	Synthase
4	P11586	C-1-tetrahydrofolate synthase	2	1.00	0.43 ± 0.17	0.58	Synthase and synthetase
5	P35520	Cystathionine beta-synthase	2	0.99	0.44 ± 0.07	0.45	Synthase
6	Q9BWD1	Acetyl CoA transferase-like protein	2	1.00	0.52 ± 0.03	1.00	Molecular function unclassified
7	P54886	Delta 1-pyrroline-5-carboxylate synthetase	2	1.00	0.55 ± 0.08	0.58	Kinase
8	P30046	D-dopachrome tautomerase	2	1.00	0.56 ± 0.05	0.59	Isomerase
9	O95671	N-acetylserotonin O-methyltransferase-like protein	1	0.96	1.39 ± 0.12	1.25	Transferase
10	Q9BSE5	Agmatinase, mitochondrial precursor	2	1.00	1.54 ± 0.15	NA[d]	Hydrolase
11	Q9UJ54	DTDP-4-keto-6-deoxy-D-glucose 4-reductase	2	1.00	1.63 ± 0.14	1.27	Oxidoreductase
12	Q9Y617	Phosphoserine aminotransferase	1	0.98	1.78 ± 0.41	1.54	Transferase
13	P00505	Aspartate aminotransferase, mitochondrial precursor	1	0.95	1.84 ± 0.13	0.37	Transferase
14	P27708	CAD protein	3	1.00	2.18 ± 0.53	1.44	Synthase and synthetase
		Apoptosis					
1	O43293	Prostate apoptosis response protein par-4	1	1.00	0.31 ± 0.03	1.27	kinase
2	Q6FI81	PRO0915	1	0.99	0.59 ± 0.20	NA[d]	Select regulatory molecule
3	O95831	Programmed cell death protein 8, mitochondrial precursor	1	1.00	2.77 ± 0.80	1.70	Oxidoreductase
		Carbohydrate Metabolism					
1	P15121	Aldose reductase	2	1.00	0.08 ± 0.04	NA[d]	Reductase
2	P47895	Aldehyde dehydrogenase 6	1	0.99	0.13 ± 0.03	NA[d]	Hydrolase
3	P19367	Hexokinase, type I	3	1.00	0.31 ± 0.08	0.29	Kinase
4	P29401	Transketolase	1	0.99	0.31 ± 0.03	0.45	Transferase
5	P36871	Phosphoglucomutase	1	0.99	0.37 ± 0.34	0.23	Isomerase
6	Q01813	6-phosphofructokinase, type C	3	1.00	0.43 ± 0.09	0.31	Kinase
7	P18669	Phosphoglycerate mutase 1	2	1.00	0.44 ± 0.04	0.47	Isomerase
8	P14786	Pyruvate kinase, M2 isozyme	4	1.00	0.51 ± 0.09	0.52	kinase
9	Q92621	Hypothetical protein KIAA0225	3	1.00	0.51 ± 0.13	0.50	Kinase
10	P00338	L-lactate dehydrogenase A chain	3	1.00	0.65 ± 0.03	0.83	Oxidoreductase
11	P16152	Carbonyl reductase [NADPH] 1	2	1.00	0.65 ± 0.03	NA[d]	Reductase
12	P53396	ATP-citrate synthase	3	1.00	0.69 ± 0.04	0.80	Lyase
13	P48735	Isocitrate dehydrogenase [NADP], mitochondrial precursor	2	1.00	1.33 ± 0.11	0.51	Oxidoreductase
14	P14550	Alcohol dehydrogenase [NADP+]	1	1.00	1.36 ± 0.24	0.86	Oxidoreductase
15	P42330	Aldo-keto reductase family 1 member C3	2	1.00	1.56 ± 0.10	2.68	Oxidoreductase
16	P52789	Hexokinase, type II	3	1.00	1.66 ± 0.16	1.15	Kinase
17	Q02218	2-oxoglutarate dehydrogenase E1 component, mitochondrial precursor	2	1.00	1.67 ± 0.39	2.24	Oxidoreductase
18	P37837	Transaldolase	2	1.00	1.78 ± 0.19	1.29	Transferase
19	Q00796	Sorbitol dehydrogenase	1	1.00	1.90 ± 0.21	3.04	Oxidoreductase
20	P10768	Esterase D	2	1.00	2.21 ± 1.09	1.56	Hydrolase
21	P40925	Malate dehydrogenase, cytoplasmic	2	1.00	2.24 ± 0.12	1.03	Oxidoreductase
22	P40926	Malate dehydrogenase, mitochondrial precursor	11	1.00	4.49 ± 0.60	2.60	Oxidoreductase
23	O60547	GDP-mannose 4,6 dehydratase	1	1.00	6.15 ± 1.02	3.09	Lyase
		Cell Cycle, Proliferation					
1	O75369	Beta-filamin	13	1.00	0.20 ± 0.09	0.08	Cytoskeletal protein
2	P58107	Epiplakin	1	1.00	0.21 ± 0.04	NA[d]	Cytoskeletal protein
3	Q15691	Microtubule-associated protein RP/EB family member 1	1	0.98	0.48 ± 0.09	0.98	Signaling molecule
4	Q14980	NuMA protein	2	1.00	0.68 ± 0.18	0.45	Cytoskeletal protein
5	Q14683	Structural maintenance of chromosome 1-like 1 protein	1	1.00	0.68 ± 0.33	0.77	Nucleic acid binding
6	Q9Y2Z0	Suppressor of G2 allele of SKP1 homolog	1	1.00	2.29 ± 0.20	NA[d]	Molecular function unclassified
		Cell Structure and Motility					
1	Q04695	Cytoskeletal 17	2	1.00	0.03 ± 0.03	NA[d]	Membrane
2	Q96AC1	Hypothetical protein	1	1.00	0.04 ± 0.00	0.04	protein binding
3	Q9NZM1	Myoferlin	2	1.00	0.17 ± 0.08	0.40	Membrane traffic protein
4	Q9P2E9	Ribosome-binding protein 1	4	1.00	0.38 ± 0.26	NA[d]	Receptor
5	P35579	Myosin heavy chain, nonmuscle type A	7	1.00	0.47 ± 0.05	0.38	Cytoskeletal protein
6	P24572	Myosin light chain alkali, smooth-muscle isoform	1	1.00	0.48 ± 0.03	0.63	Select regulatory molecule
7	P52907	F-actin capping protein alpha-1 subunit	2	1.00	0.54 ± 0.05	0.86	Cytoskeletal protein
8	P07737	Profilin I	3	1.00	0.63 ± 0.09	0.10	Cytoskeletal protein
9	P47756	F-actin capping protein beta subunit	2	1.00	0.63 ± 0.09	0.86	Cytoskeletal protein
10	Q8NAG3	Hypothetical protein FLJ35393	1	1.00	0.63 ± 0.29	NA[d]	Cytoskeletal protein
11	Q9Y3F5	A6 related protein	1	1.00	0.68 ± 0.13	NA[d]	Cytoskeletal protein
12	O75083	WD-repeat protein 1	2	1.00	0.69 ± 0.12	0.58	Cytoskeletal protein
13	O43707	Alpha-actinin 4	1	1.00	1.37 ± 0.07	1.59	Cytoskeletal protein
14	P21333	Filamin A	11	1.00	1.44 ± 0.07	1.87	Cell adhesion molecule
15	P15924	Desmoplakin	3	1.00	1.57 ± 0.12	2.07	Cytoskeletal protein
16	P02545	Lamin A/C	1	0.99	2.11 ± 0.72	0.90	Cytoskeletal protein
17	P27816	Microtubule-associated protein 4	1	0.95	2.29 ± 0.37	0.66	Cytoskeletal protein

119

Table I (Continued)

	UniProt	protein name	peptide number	prob.[a]	cICAT[b]	Affymetrix[c]	molecular function
			Cell Structure and Motility				
18	Q9NQW6	Actin binding protein anillin	1	1.00	2.58 ± 0.45	NA[d]	Cytoskeletal protein
19	P13647	Cytoskeletal 5	1	1.00	3.43 ± 1.10	NA[d]	Cytoskeletal protein
20	P08670	Vimentin	1	0.99	25.67 ± 5.81	NA[d]	Cytoskeletal protein
			Developmental Processes				
1	P21291	Cysteine-rich protein 1	1	1.00	0.3 ± 0.04	0.59	Ion binding
2	Q14192	Skeletal muscle LIM-protein 3	1	0.93	0.54 ± 0.09	0.92	Transcription factor
3	Q09666	Neuroblast differentiation associated protein AHNAK	2	1.00	0.67 ± 0.13	0.44	Molecular function unclassified
4	Q15668	Epididymal secretory protein E1 precursor	1	1.00	0.63 ± 0.04	0.23	Signaling molecule
5	Q9HDC9	Adipocyte plasma membrane-associated protein	1	1.00	1.36 ± 0.42	0.82	Molecular function unclassified
6	Q16658	Fascin	4	1.00	2.98 ± 0.39	1.07	Cytoskeletal protein
			Electron Transport				
1	P23634	Plasma membrane calcium-transporting ATPase 4	1	0.99	0.00 ± 0.00	0.06	Hydrolase
2	P08574	Cytochrome c1, heme protein, mitochondrial precursor	1	1.00	0.68 ± 0.04	0.82	Oxidoreductase
3	Q9NQ11	Hypothetical protein	1	0.99	1.41 ± 0.11	NA[d]	Hydrolase
4	P22695	Ubiquinol-cytochrome C reductase complex core protein 2	2	1.00	1.56 ± 0.24	0.72	Reductase
5	P51970	NADH-ubiquinone oxidoreductase 19 kDa subunit	2	1.00	1.90 ± 0.36	1.34	Oxidoreductase
6	O96000	NADH-ubiquinone oxidoreductase PDSW subunit	1	0.92	2.17 ± 0.47	NA[d]	Oxidoreductase
			Immunity Defenses				
1	O14879	Interferon-induced protein with tetratricopeptide repeats 4	3	1.00	0.08 ± 0.05	NA[d]	Defense/immunity protein
2	P09914	Interferon-induced protein with tetratricopeptide repeats 1	2	1.00	0.29 ± 0.14	NA[d]	Molecular function unclassified
3	Q03405	Urokinase plasminogen activator surface receptor precursor	2	1.00	0.42 ± 0.12	0.16	Receptor
4	P30041	Peroxiredoxin 6	2	1.00	0.55 ± 0.07	0.67	Oxidoreductase
5	P01892	HLA class I histocompatibility antigen, A-10 alpha chain (Fragment)	1	1.00	0.64 ± 0.16	NA[d]	Defense/immunity protein
6	P13987	CD59 glycoprotein precursor	1	0.98	0.67 ± 0.56	0.39	Signaling molecule
7	P30044	Peroxiredoxin 5, mitochondrial precursor	1	1.00	1.84 ± 0.89	NA[d]	Oxidoreductase
8	P09382	Galectin-1	4	1.00	2.33 ± 0.72	0.90	Signaling molecule
			Protein Traffic				
1	Q96C19	Swiprosin 1	2	1.00	0.34 ± 0.04	0.28	Nucleic acid binding
2	O60664	Cargo selection protein TIP47	1	1.00	0.55 ± 0.13	0.40	Receptor
3	Q9NR31	GTP-binding protein SAR1a	2	1.00	0.59 ± 0.18	0.78	Select regulatory molecule
4	O60684	Importin alpha 7 subunit	1	0.94	0.67 ± 0.09	0.75	Membrane traffic protein
5	P05218	Tubulin beta-5 chain	13	1.00	1.33 ± 0.22	0.50	Cytoskeletal protein
6	Q9BS26	Thioredoxin domain containing protein 4 precursor	5	1.00	1.33 ± 0.21	0.86	Isomerase
7	P55072	Transitional endoplasmic reticulum ATPase	8	1.00	1.35 ± 0.12	0.95	Hydrolase
8	Q14204	Dynein heavy chain, cytosolic	3	1.00	1.44 ± 0.17	1.03	Cytoskeletal protein
9	O00159	Myosin Ic	2	1.00	1.45 ± 0.64	0.57	Cytoskeletal protein
10	P10809	Heat shock protein 60	9	1.00	1.56 ± 0.09	1.13	Chaperon
11	Q13509	Tubulin beta-4 chain	1	0.98	1.77 ± 0.33	0.77	Cytoskeletal protein
12	O43765	Small glutamine-rich tetratricopeptide repeat-containing protein	2	1.00	1.88 ± 0.40	NA[d]	Chaperon
13	P30740	Leukocyte elastase inhibitor	1	0.91	2.41 ± 0.44	3.76	Select regulatory molecule
			Lipid, Fatty Acid, and Steroid Metabolism				
1	Q99541	Adipophilin	1	0.99	0.01 ± 0.00	N. A.	Molecular function unclassified
2	Q01581	Hydroxymethylglutaryl-CoA synthase	2	1.00	0.13 ± 0.03	0.18	Synthase and synthetase
3	Q9Y6L9	Titin	1	0.99	0.16 ± 0.01	NA[d]	Cytoskeletal protein
4	Q9UBJ2	Peroxisomal farnesylated protein	2	1.00	0.43 ± 0.08	0.21	Miscellaneous function
5	P37802	Transgelin 2	2	1.00	0.56 ± 0.01	0.79	Cytoskeletal protein-
6	P67936	Tropomyosin alpha 4 chain	2	1.00	0.61 ± 0.16	0.83	Cytoskeletal protein-
7	Q5T0M7	Fatty acid synthase	2	1.00	0.65 ± 0.17	NA[d]	Synthase
8	P49327	Fatty acid synthase	2	1.00	0.65 ± 0.17	0.48	Synthase and synthetase
9	O00151	PDZ and LIM domain protein 1	1	0.99	0.67 ± 0.78	0.17	Cytoskeletal protein-
10	Q16850	Cytochrome P450 51A1	1	0.92	0.67 ± 0.08	1.24	Oxidoreductase
11	P04083	Annexin 1	4	1.00	0.68 ± 0.07	1.02	Select calcium binding protein
12	P21964	Catechol O-methyltransferase	2	1.00	1.35 ± 0.55	0.81	Transferase
13	Q08257	Quinone oxidoreductase	1	1.00	1.40 ± 0.28	10.73	Oxidoreductase
14	P36969	Phospholipid hydroperoxide glutathione peroxidase	1	0.99	1.56 ± 0.55	1.14	Oxidoreductase
15	Q9H845	Acyl-CoA dehydrogenase family member 9	1	1.00	1.58 ± 0.77	NA[d]	Oxidoreductase
16	Q15738	NAD(P)-dependent steroid dehydrogenase	2	1.00	1.92 ± 0.24	NA[d]	Oxidoreductase
17	Q01469	Fatty acid-binding protein	2	1.00	2.45 ± 0.21	1.67	Transfer/carrier protein
18	Q99714	3-hydroxyacyl-CoA dehydrogenase type II	2	1.00	2.51 ± 0.80	1.90	Oxidoreductase
			Nucleic Acid Metabolism				
1	Q7Z2W4	Zinc-finger CCCH type antiviral protein 1	3	1.00	0.27 ± 0.05	2.51	Molecular function unclassified
2	Q13951	Core-binding factor, beta subunit	1	1.00	0.31 ± 0.05	0.40	Transcription factor
3	P48512	Transcription initiation factor IIB	1	1.00	0.39 ± 0.11	1.25	Transcription factor
4	P53384	Nucleotide-binding protein 1	2	1.00	0.44 ± 0.05	0.40	Nucleic acid binding
5	Q8TEK0	FLJ00195 protein (Fragment)	1	0.98	0.46 ± 0.07	0.31	Transcription factor
6	P18583	SON protein	1	0.98	0.47 ± 0.11	0.86	Nucleic acid binding
7	Q8N1F7	Hypothetical protein KIAA0095	1	1.00	0.52 ± 0.16	NA[d]	Nucleic acid binding
8	P78527	DNA-dependent protein kinase catalytic subunit	7	1.00	0.55 ± 0.16	0.41	Kinase

120

Table I (Continued)

	UniProt	protein name	peptide number	prob.[a]	cICAT[b]	Affymetrix[c]	molecular function
			Nucleic Acid Metabolism				
9	Q12769	Nuclear pore complex protein Nup160	1	0.94	0.55 ± 0.11	1.02	transporter
10	O75534	UNR protein	2	1.00	0.56 ± 0.16	0.98	Nucleic acid binding
11	P33991	MCM4 minichromosome maintenance deficient 4	2	1.00	0.56 ± 0.07	0.18	Nucleic acid binding
12	P33992	DNA replication licensing factor MCM5	3	1.00	0.58 ± 0.25	0.15	Nucleic acid binding
13	Q96EI0	Similar to KIAA0801 gene product	1	0.99	0.58 ± 0.28	NA[d]	Nucleic acid binding
14	Q16576	Histone acetyltransferase type B subunit 2	1	1.00	0.58 ± 0.11	0.54	Miscellaneous function
15	Q86VP6	TIP120 protein	3	1.00	0.58 ± 0.04	NA[d]	Transcription factor
16	Q92878	RAD50	1	0.96	0.58 ± 0.18	NA[d]	Nucleic acid binding
17	P17812	CTP synthase	4	1.00	0.59 ± 0.03	0.81	Synthase and synthetase
18	O75766	TRIP protein	3	1.00	0.59 ± 0.14	0.92	Transcription factor
19	Q96KR1	Putative zinc finger protein	2	1.00	0.59 ± 0.09	1.04	Nucleic acid binding
20	Q9P0L0	Vesicle-associated membrane protein-associated protein A	2	1.00	0.59 ± 0.17	0.83	Synthase and synthetase
21	Q00839	Heterogeneous nuclear ribonucleoprotein U	6	1.00	0.60 ± 0.20	1.13	Nucleic acid binding
22	Q15097	Polyadenylate-binding protein 2	3	1.00	0.64 ± 0.09	1.33	Nucleic acid binding
23	P11518	60S ribosomal protein L7a	3	1.00	0.67 ± 0.09	1.26	Nucleic acid binding
24	P82979	Nuclear protein Hcc-1	1	0.96	0.67 ± 0.05	NA[d]	Nucleic acid binding
25	Q08945	Structure-specific recognition protein 1	4	1.00	0.68 ± 0.14	1.19	Transcription factor
26	Q9NXD9	Hypothetical protein FLJ20303	2	1.00	0.68 ± 0.29	NA[d]	Nucleic acid binding
27	O43172	U4/U6 small nuclear ribonucleoprotein Prp4	2	1.00	0.69 ± 0.29	0.55	Nucleic acid binding
28	P26358	DNA (cytosine-5)-methyltransferase 1	1	0.99	0.69 ± 0.04	0.70	Nucleic acid binding
29	P26368	Splicing factor U2AF 65 kDa subunit	2	1.00	0.69 ± 0.06	1.26	Nucleic acid binding
30	Q09161	80 kDa nuclear cap binding protein	3	1.00	1.32 ± 0.52	1.73	Nucleic acid binding
31	P14866	Heterogeneous nuclear ribonucleoprotein L	2	1.00	1.33 ± 0.29	1.15	Nucleic acid binding
32	P48634	Hypothetical protein (Fragment)	2	1.00	1.33 ± 0.13	1.19	Nucleic acid binding
33	Q13242	Splicing factor, arginine/serine-rich 9	2	1.00	1.33 ± 0.22	0.75	Nucleic acid binding
34	Q9NQT4	Exosome complex exonuclease RRP46	1	0.97	1.36 ± 0.13	NA[d]	Nucleic acid binding
35	Q9GZT3	DC50 (DC23)	2	1.00	1.41 ± 0.26	NA[d]	Nucleic acid binding
36	P31949	Calgizzarin	2	1.00	1.44 ± 0.19	2.06	Select calcium binding protein
37	P33240	Cleavage stimulation factor, 64 kDa subunit	1	0.90	1.44 ± 0.25	0.73	Nucleic acid binding
38	Q9UKK9	ADP-sugar pyrophosphatase YSA1H	1	1.00	1.44 ± 0.21	NA[d]	Hydrolase
39	P13489	Placental ribonuclease inhibitor	6	1.00	1.45 ± 0.24	1.02	Select regulatory molecule
40	P49321	Nuclear autoantigenic sperm protein	2	1.00	1.50 ± 0.34	0.77	transporter
41	Q96B26	U6 snRNA-associated Sm-like protein LSm7	1	0.99	1.52 ± 0.20	3.41	Nucleic acid binding
42	P33316	Deoxyuridine 5′-triphosphate nucleotidohydrolase	3	1.00	1.54 ± 0.21	1.14	Phosphatase
43	P12956	ATP-dependent DNA helicase II, 70 kDa subunit	2	1.00	1.61 ± 0.20	0.81	Nucleic acid binding
44	Q96P11	NOL1R	1	1.00	1.61 ± 0.32	NA[d]	Nucleic acid binding
45	P55795	Heterogeneous nuclear ribonucleoprotein H′	1	0.99	1.62 ± 0.41	1.12	Nucleic acid binding
46	Q01081	Splicing factor U2AF 35 kDa subuni	1	0.99	1.63 ± 0.24	1.29	Nucleic acid binding
47	P49915	GMP synthase [glutamine-hydrolyzing]	2	0.98	1.71 ± 0.34	1.23	Synthase
48	P05455	Lupus La protein	1	1.00	1.82 ± 0.10	1.51	Nucleic acid binding
49	Q9BV68	Hypothetical protein	2	0.93	1.82 ± 0.28	1.35	Nucleic acid binding
50	Q9Y3A5	Shwachman-Bodian-Diamond syndrome protein	1	1.00	1.83 ± 0.30	NA[d]	Molecular function unclassified
51	P55769	NHP2-like protein 1	2	1.00	1.86 ± 0.69	2.01	Nucleic acid binding
52	P09429	High mobility group protein 1	5	1.00	1.92 ± 0.24	1.25	Transcription factor
53	P18754	Regulator of chromosome condensation	1	0.99	1.92 ± 0.25	0.87	Nucleic acid binding
54	P31939	Bifunctional purine biosynthesis protein PURH	4	1.00	2.07 ± 0.64	2.21	Hydrolase
55	Q9Y265	RuvB-like 1	1	0.99	2.03 ± 0.38	0.70	Nucleic acid binding
56	Q16531	DNA damage binding protein 1	1	0.93	2.26 ± 0.13	1.25	Nucleic acid binding
57	Q15365	Poly(rC)-binding protein 1	5	1.00	2.29 ± 0.34	1.38	Nucleic acid binding
58	P00492	Hypoxanthine-guanine phosphoribosyltransferase	4	1.00	2.67 ± 0.19	1.25	Transferase
59	Q9HCU5	Prolactin regulatory element-binding protein	1	0.98	3.24 ± 0.29	5.10	Nucleic acid binding
60	P36959	GMP reductase 1	1	0.99	33.64 ± 6.76	1.57	Oxidoreductase
			Oncogenesis				
1	P08729	Keratin, type II cytoskeletal 7	1	1.00	0.00 ± 0.00	0.02	Select regulatory molecule
2	Q9BYX2	TBC1 domain family member 2	1	0.96	0.13 ± 0.03	NA[d]	Select regulatory molecule
3	Q06136	Follicular variant translocation protein 1 precursor	1	1.00	0.31 ± 0.05	0.43	Oxidoreductase
4	P57764	DFN5-like protein FLJ12150	1	1.00	0.33 ± 0.24	NA[d]	Molecular function unclassified
5	P13797	T-plastin	4	1.00	0.34 ± 0.21	0.33	Cytoskeletal protein
6	P46013	Antigen KI-67	3	1.00	0.52 ± 0.05	0.49	Miscellaneous function
7	P18206	Vinculin	4	1.00	0.54 ± 0.27	0.40	Cytoskeletal protein
8	Q92688	Acidic leucine-rich nuclear phosphoprotein 32 family member B	2	1.00	1.66 ± 0.16	1.01	Select regulatory molecule
9	P39687	Acidic leucine-rich nuclear phosphoprotein 32 family member A	2	0.99	1.67 ± 0.41	1.40	Select regulatory molecule
			Other Metabolism				
1	Q16881	Thioredoxin reductase, cytoplasmic precursor	1	0.93	0.6 ± 0.20	0.56	Oxidoreductase
2	Q04760	Lactoylglutathione lyase	2	1.00	1.31 ± 0.20	1.11	Lyase
3	P49189	Aldehyde dehydrogenase, E3 isozyme	1	0.99	1.44 ± 0.86	0.65	Oxidoreductase
4	P10599	Thioredoxin	3	1.00	1.63 ± 0.10	2.11	Oxidoreductase
5	Q8UBL6	Uroporphyrinogen decarboxylase	1	1.00	1.99 ± 0.27	0.98	Lyase
6	Q9BW04	Hypothetical protein FLJ36507	1	1.00	6.72 ± 0.92	NA[d]	Select regulatory molecule

121

Table I (Continued)

	UniProt	protein name	peptide number	prob.[a]	cICAT[b]	Affymetrix[c]	molecular function
		Protein Metabolism and Modification					
1	P21980	Protein-glutamine gamma-glutamyltransferase	1	0.97	0.00 ± 0.00	NA[d]	Transferase
2	Q9UK22	F-box only protein 2	2	1.00	0.14 ± 0.04	1.26	Miscellaneous function
3	Q86YM9	Calpastatin (Fragment)	1	1.00	0.25 ± 0.22	0.78	Select regulatory molecule
4	P48594	Squamous cell carcinoma antigen 2	1	1.00	0.27 ± 0.03	NA[d]	Select regulatory molecule
5	P63208	S-phase kinase-associated protein 1A	1	0.97	0.35 ± 0.05	0.90	Nucleic acid binding
6	Q15418	Ribosomal protein S6 kinase alpha 1	2	1.00	0.39 ± 0.09	0.27	Kinase
7	P15170	G1 to S phase transition protein 1 homologue	2	1.00	0.41 ± 0.27	0.60	Nucleic acid binding
8	O43776	Asparaginyl-tRNA synthetase, cytoplasmic	2	1.00	0.48 ± 0.13	0.96	Nucleic acid binding
9	P18282	Destrin	5	0.91	0.50 ± 0.13	0.93	Cytoskeletal protein
10	Q13564	Amyloid protein-binding protein 1	2	1.00	0.50 ± 0.05	0.43	Ligase
11	P36578	60S ribosomal protein L4	2	1.00	0.51 ± 0.05	1.86	Nucleic acid binding
12	Q16763	Ubiquitin-conjugating enzyme E2−24 kDa	1	0.98	0.54 ± 0.07	1.17	ligase
13	P13862	Casein kinase II beta chain	2	1.00	0.55 ± 0.09	1.84	Kinase
14	P04643	40S ribosomal protein S11	3	1.00	0.59 ± 0.05	1.57	Nucleic acid binding
15	P04645	60S ribosomal protein L30	2	1.00	0.60 ± 0.03	1.34	Nucleic acid binding
16	Q12765	Y193_HUMAN Hypothetical protein KIAA0193	1	1.00	0.60 ± 0.26	1.13	Select regulatory molecule
17	P02433	60S ribosomal protein L32	2	1.00	0.63 ± 0.18	1.11	Nucleic acid binding
18	P50914	60S ribosomal protein L14	4	1.00	0.64 ± 0.08	2.35	Nucleic acid binding
19	P28838	Cytosol aminopeptidase	3	1.00	0.64 ± 0.25	0.95	Protease
20	Q92524	26S protease regulatory subunit S10B	2	1.00	0.65 ± 0.11	1.91	Hydrolase
21	P31689	DnaJ homologue subfamily A member 1	3	1.00	0.67 ± 0.52	0.56	Chaperone
22	Q15070	Cytochrome oxidase biogenesis protein OXA1, mitochondrial precursor	2	1.00	0.67 ± 0.09	0.88	Transporter
23	Q93009	Ubiquitin carboxyl-terminal hydrolase 7	1	1.00	0.67 ± 0.13	0.82	Protease
24	Q9Y5M8	Signal recognition particle receptor beta subunit	2	1.00	0.67 ± 0.05	0.96	signaling molecule
25	P08238	Heat shock protein 90 beta	4	1.00	0.68 ± 0.21	0.89	Chaperone
26	P49721	Proteasome subunit beta type 2	3	1.00	0.68 ± 0.11	1.08	Protease
27	Q96AE4	FUSE binding protein	1	1.00	0.69 ± 0.12	0.79	Nucleic acid binding
28	Q8N425	Likely ortholog of mouse ubiquitin-conjugating enzyme E2−230K	2	1.00	0.69 ± 0.07	NA[d]	ligase
29	Q99543	Zuotin related factor-1	1	0.96	1.39 ± 0.29	3.39	Chaperone
30	P30405	Peptidyl-prolyl cis−trans isomerase, mitochondrial precursor	1	1.00	1.40 ± 0.23	1.62	Isomerase
31	Q02790	FK506-binding protein 4	2	1.00	1.46 ± 0.15	1.17	Isomerase
32	Q9NR50	Translation initiation factor eIF-2B gamma subunit	1	0.99	1.48 ± 0.35	0.90	Nucleic acid binding
33	P49591	Seryl-tRNA synthetase	1	0.99	1.49 ± 0.41	2.87	Nucleic acid binding
34	P36776	Lon protease homolog, mitochondrial precursor	1	1.00	1.57 ± 0.41	1.25	protease
35	Q92598	Heat-shock protein 105 kDa	7	1.00	1.60 ± 0.17	1.33	Chaperone
36	P07858	Cathepsin B	3	1.00	1.61 ± 0.14	2.16	Protease
37	P53634	Cathepsin C	1	1.00	1.62 ± 0.36	0.28	Protease
38	P34932	Heat shock 70 kDa protein 4	3	1.00	1.67 ± 0.26	2.24	Chaperone
39	P35998	26S protease regulatory subunit 7	2	1.00	1.69 ± 0.51	2.37	Hydrolase
40	P14868	Aspartyl-tRNA synthetase	1	0.96	1.73 ± 1.30	2.36	Nucleic acid binding
41	P62276	40S ribosomal protein S29	1	1.00	1.74 ± 0.32	1.59	Nucleic acid binding
42	Q13404	DNA-binding protein	1	0.94	1.74 ± 0.06	NA[d]	Ligase
43	Q99538	Legumain precursor	1	0.97	1.77 ± 0.30	NA[d]	Protease
44	Q9UBT2	ANTHRACYCLINE-associated resistance ARX	3	1.00	1.86 ± 0.23	2.19	Ligase
45	Q15765	Prefoldin subunit 3	2	1.00	1.87 ± 0.43	3.08	transporter
46	P27924	Ubiquitin-conjugating enzyme E2−25 kDa	1	0.96	1.95 ± 0.23	1.60	Ligase
47	Q92507	ES1 protein homologue, mitochondrial precursor	1	1.00	2.28 ± 0.24	110.10	Miscellaneous function
48	P25685	DnaJ homologue subfamily B member 1	2	1.00	2.46 ± 0.41	1.58	Chaperone
49	P29144	Tripeptidyl-peptidase II	4	1.00	3.01 ± 1.10	2.92	Hydrolase
50	P41250	Glycyl-tRNA synthetase	1	1.00	6.8 ± 2.66	2.79	Synthase and synthetase
		Signal Transduction and Regulation					
1	Q86ST5	Similar to centaurin, gamma 3	1	0.99	0.00 ± 0.00	NA[d]	GTP binding
2	Q9UBI6	Guanine nucleotide-binding protein G(I)/G(S)/G(O) gamma-12 subunit	2	1.00	0.20 ± 0.04	0.58	Select regulatory molecule
3	P35613	Basigin precursor	2	1.00	0.30 ± 0.03	0.56	Signaling molecule
4	P06749	Transforming protein RhoA	4	1.00	0.35 ± 0.22	1.13	Select regulatory molecule
5	P05362	Intercellular adhesion molecule-1 precursor	2	1.00	0.38 ± 0.05	NA[d]	Cell adhesion molecule
6	Q13578	DNA repair protein	1	1.00	0.41 ± 0.07	NA[d]	Phosphatase
7	P30086	Phosphatidylethanolamine-binding protein	1	0.98	0.48 ± 0.09	0.62	Select regulatory molecule
8	P08134	Transforming protein RhoC	2	0.99	0.54 ± 0.13	0.58	Select regulatory molecule
9	P84097	Rho-related GTP-binding protein RhoG	1	1.00	0.55 ± 0.13	0.83	Select regulatory molecule
10	Q9Y572	Receptor-interacting serine/threonine protein kinase 3	1	0.91	0.58 ± 0.05	NA[d]	Kinase
11	P43490	Pre-B cell enhancing factor precursor	2	1.00	0.65 ± 0.09	1.46	Signaling molecule
12	P60953	Cell division control protein 42 homologue	3	1.00	0.67 ± 0.20	0.88	Select regulatory molecule
13	P04901	Guanine nucleotide-binding protein G(I)/G(S)/G(T) beta subunit 1	1	1.00	0.68 ± 0.05	0.70	Select regulatory molecule
14	P04899	Guanine nucleotide-binding protein G(i), alpha-2 subunit	1	1.00	1.32 ± 0.24	0.44	Select regulatory molecule
15	Q9HCY8	S100 calcium-binding protein A14	2	1.00	1.41 ± 0.19	0.36	Select calcium binding protein
16	P29312	14-3-3 protein zeta/delta	3	1.00	1.48 ± 0.12	1.40	Select regulatory molecule

Table I (Continued)

	UniProt	protein name	peptide number	prob.[a]	cICAT[b]	Affymetrix[c]	molecular function
		Signal Transduction and Regulation					
17	Q12797	Aspartyl/asparaginyl beta-hydroxylase	1	0.91	1.69 ± 0.34	1.09	Oxidoreductase
18	O60716	Catenin, 120ctn	1	1.00	1.78 ± 0.34	1.16	Cell junction protein
19	P16144	Integrin beta-4	2	1.00	1.96 ± 0.96	1.91	Cell adhesion molecule
20	P01116	Transforming protein p21A	1	0.98	2.07 ± 0.49	2.78	Select regulatory molecule
21	P16422	Tumor-associated calcium signal transducer 1 precursor	1	0.99	2.12 ± 0.43	1.49	Signaling molecule
22	Q86VB7	Similar to CD163 antigen	1	0.95	2.18 ± 0.46	NA[d]	Receptor
23	P31947	14−3−3 protein sigma	4	1.00	2.45 ± 0.17	1.79	Select regulatory molecule
24	P27348	14−3−3 protein tau	3	1.00	2.51 ± 0.24	1.56	Select regulatory molecule
25	P23229	Integrin alpha-6	1	0.99	3.34 ± 1.06	1.81	Cell adhesion molecule
26	P35222	Catenin, beta	4	1.00	5.89 ± 1.3	1.91	Signaling molecule
27	O95996	APCL protein	1	0.99	8.37 ± 0.35	NA[d]	Cytoskeletal protein
28	Q8IXW0	Hypothetical protein	1	0.94	9999 ± 0.00	NA[d]	Signaling molecule
		Transport					
1	P16615	Sarcoplasmic/endoplasmic reticulum calcium ATPase 2	2	1.00	0.64 ± 0.16	0.50	Transporter
2	P35658	Nuclear pore complex protein Nup214	2	1.00	0.69 ± 0.08	NA[d]	Transporter
3	P45880	Voltage-dependent anion-selective channel protein 2	1	1.00	0.69 ± 0.13	1.34	Ion channel
4	O00299	Chloride intracellular channel protein 1	4	1.00	2.38 ± 0.63	1.99	Ion channel
		Biological Process Unclassified					
1	Q9H690	Hypothetical protein FLJ22484	2	1.00	0.00 ± 0.00	NA[d]	Molecular function unclassified
2	Q9BSE0	Hypothetical protein	1	0.94	0.13 ± 0.01	NA[d]	Molecular function unclassified
3	Q8N8W6	Hypothetical protein FLJ38753	2	1.00	0.24 ± 0.08	NA[d]	Molecular function unclassified
4	Q96G34	DC12 protein	1	0.91	0.37 ± 0.09	NA[d]	Molecular function unclassified
5	Q9BTE3	Hypothetical protein FLJ13081	2	1.00	0.50 ± 0.05	NA[d]	Molecular function unclassified
6	Q96FT1	Hypothetical protein (Fragment)	1	0.98	0.50 ± 0.08	NA[d]	Nucleic acid binding
7	Q86U38	Similar to RIKEN cDNA 2610027L16 gene	1	1.00	0.56 ± 0.07	NA[d]	Molecular function unclassified
8	Q9BQ69	Protein LRP16	2	1.00	0.56 ± 0.22	NA[d]	transporter
9	Q9Y2L0	KIAA1007 protein (Fragment)	2	1.00	0.59 ± 0.08	NA[d]	Molecular function unclassified
10	Q9Y4W6	AFG3-like protein 2	4	1.00	0.63 ± 0.12	0.81	protease
11	Q14166	Hypothetical protein KIAA0153	2	0.98	0.65 ± 0.04	1.30	Molecular function unclassified
12	Q13826	Autoantigen	2	1.00	0.69 ± 0.14	NA[d]	protein binding
13	P42704	130 kDa leucine-rich protein	2	1.00	1.54 ± 0.17	1.32	Nucleic acid binding
14	Q8N3B3	Hypothetical protein (Fragment)	2	1.00	1.57 ± 0.25	NA[d]	Molecular function unclassified
15	Q9H3K6	My016 protein	1	0.95	1.91 ± 0.41	3.44	Molecular function unclassified
16	O75223	Hypothetical protein	2	1.00	2.2 ± 0.23	2.60	Molecular function unclassified
17	Q9H4L5	Oxysterol binding protein-related protein 3	1	1.00	3.06 ± 5.19	3.73	Protein binding
18	Q810P0	similar to testis expressed sequence 13A	1	1.00	7.51 ± 9.10	NA[d]	Molecular function unclassified
19	Q9H6W2	Hypothetical protein FLJ21810	1	0.98	11.04 ± 2.88	NA[d]	Molecular function unclassified

[a] ProteinProphet score. [b] The fold change in the protein ratio of TMC-1/SC-M1 cells. [c] The fold change in the mRNA ratio of TMC-1/SC-M1 cells. [d] ND, not available.

of microarray and proteomic results were performed by their corresponding gene names. Among the 240 differentially expressed proteins, 226 of the proteins found by cICAT analysis could be matched to their corresponding mRNA expression levels. In the correlation scattergram shown in Figure 4, proteins for which mRNA fold changes have a positive correlation with protein level changes appear on or near the 45° diagonal. The majority of differentially expressed mRNAs and cognate proteins correlated positively with a statistically significant correlation coefficient of 0.29. In TMC-1 cells, 29 of the 226 proteins with elevated mRNA levels were found to be at least overexpressed by 1.3-fold at the protein level. Likewise, 38 TMC-1 cell proteins showed a correlation between reduced protein levels and reduced mRNA levels. However, the result also revealed that some proteins are not transcriptionally regulated or show opposite regulation patterns. As shown in Figure 4, seven proteins showed a negative correlation between protein and mRNA expression levels. This is in accordance with the conclusion that noncell-structure-related proteins show poor correlation between mRNA and protein levels.[30]

Validation of Candidate Genes That Are Differentially Expressed in SC-M1 and TMC-1 Cells. To further evaluate the results obtained from the global comparative expression studies, we examined the expression status of several candidate

genes identified by comparative proteomics in the SC-M1 and TMC-1 cells. β-Catenin, galectin 1, IQ motif-containing GTPase activating protein (IQGAP1), vimentin, integrin α6, and integrin β4 were chosen because they have been previously shown to be involved in the pathogenic development of tumor formation and progression, and in particular, some are implicated in the process of acquiring metastatic capability in various cancers (Table 3). Semiquantitative RT-PCR analysis was performed to examine the transcript levels of these genes. In agreement with the proteomic and genomic findings, higher levels of β-catenin, galectin 1, vimentin, integrin α6, and integrin β4 transcripts were observed in the metastatic TMC-1 cells, whereas IQGAP1 was expressed at a lower level in TMC-1 cells (Figure 5A). Integrins are the major cell surface receptors involved in cell−cell attachment and cell migration. The flow cytometry analysis showed significantly higher levels of integrin α6 and β4 were localized at the cell surface of metastatic TMC-1 cells than SC-M1 cells (Figure 5B). β-Catenin plays dual roles in adhesion and transducer/transcriptional regulaton.[31] When the Wnt signal is activated, β-catenin is not phosphorylated and accumulates in the cytoplasm, leading to the subsequent nuclear translocation.[32] Therefore, we examined the expression status of β-catenin by immunocytostaining. As shown in Figure 5C, β-catenin was abundantly expressed and accumulated in the

123
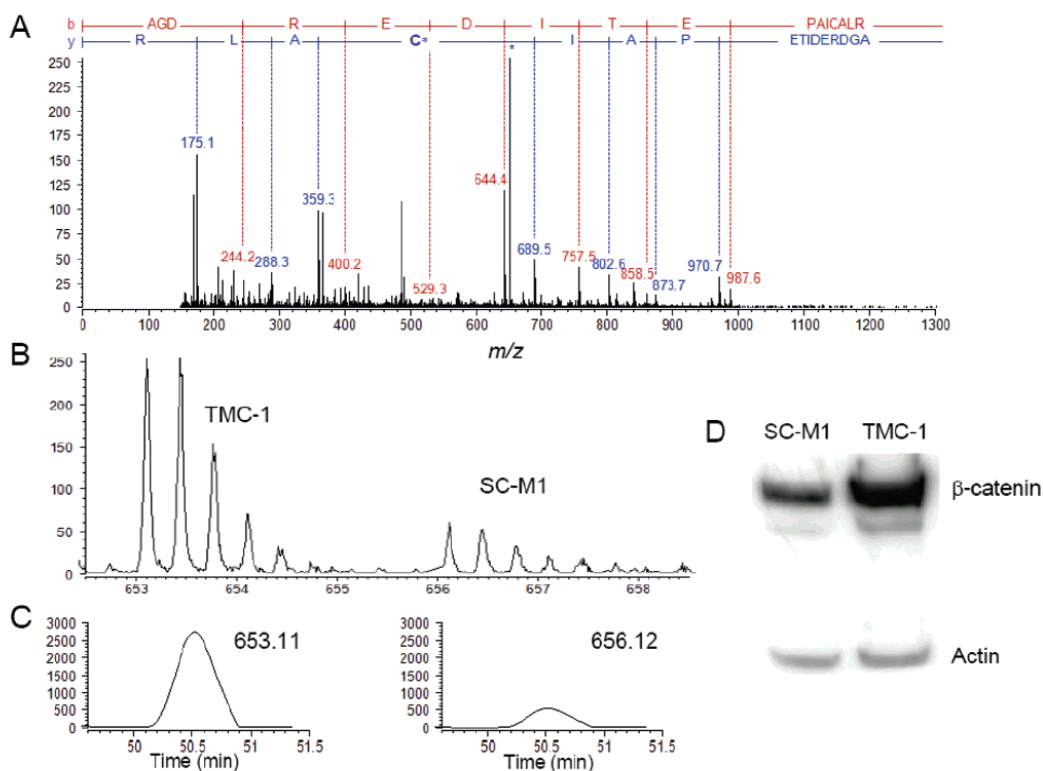
Figure 3. Quantitation and confirmation of differential expression of β-catenin in SC-M1 and TMC-1 cells. The MS/MS spectrum (A) and MS spectrum (B) of the light (TMC-1) and heavy (SC-M1) cICAT isotope-labeled peptide AGDREDITEPAICALR. (C) The corresponding extracted ion chromatogram revealed a 5.9-fold overexpression of β-catenin in TMC-1 cells. (D) Western blotting analysis confirmed that β-catenin was overexpressed in TMC-1 cells.

Table 2. Pathways Containing Genes Differentially Expressed between TMC-1 and SC-M1 Cells from Microarray Gene Expression Measurements

pathway	N^a	T^b	% differentially expressed genes
Proepithelin Conversion to Epithelin and Wound Repair Control	6	6	100
Inhibition of Matrix Metalloproteinases	8	10	80
IL-18 Signaling Pathway	7	9	78
OX40 Signaling Pathway	5	7	71
Multidrug Resistance Factors	5	7	71
Neuroregulin Receptor Degradation Protein-1 Controls ErbB3 Receptor Recycling	9	13	69
Antigen-dependent B Cell Activation	11	16	69
GATA3 Activation of the Th2 Cytokine Genes Expression	10	15	67
CDK Regulation of DNA Replication	6	9	67
Nitric Oxide Signaling Pathway	6	9	67
Bystander B Cell Activation	7	11	64
Platelet Amyloid Precursor Protein Pathway	7	11	64
Sonic Hedgehog (Shh) Pathway	7	11	64
TSP-1-Induced Apoptosis in Microvascular Endothelial Cells	5	8	63
Vit-C in Brain	5	8	63
METS Effect on Macrophage Differentiation	12	20	60
FOSB Gene Expression and Drug Abuse	3	5	60

^{a} N = number of differentially expressed genes in the pathway. ^{b} T = the total number of probed genes in the pathway.

cytoplasm of TMC-1 cells, whereas it had a more restricted distribution in SC-M1 cells, mostly localized to the plasma membranes.

Because apoptosis dysfunction in metastases has been suggested to participate in their poor response to conventional anticancer treatments[33] and because of our finding of dif-

124
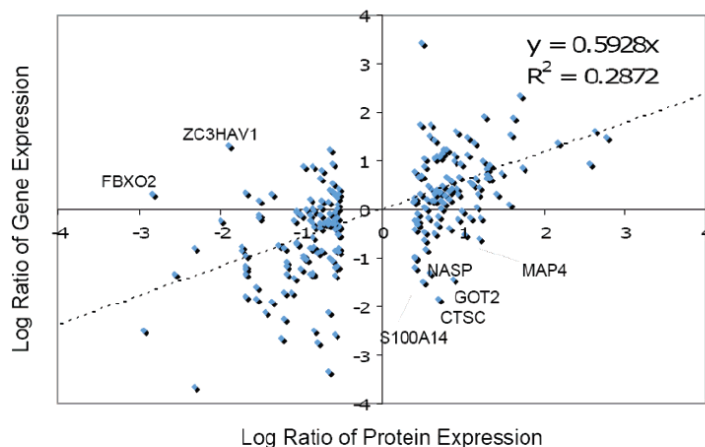
Figure 4. Scatter plot showing the protein ratios obtained by the cICAT analysis, and 2D-LC−MS/MS and mRNA ratios obtained from the Affymetrix DNA microarray for SC-M1 and TMC-1 cells. The labeled proteins showed a significant negative correlation between protein and mRNA expression levels. Both expression ratios are plotted in logarithmic scale.

ferential expression of proteins in the TSP-1-induced apoptosis pathway, we also examined whether SC-M1 and TMC-1 cells displayed different degrees of resistance toward chemotherapeutic drug-induced apoptosis. Cell viabilityies were measured after treatment with increasing concentrations of 5-fluorouracil. As shown in Figure 6, 5-fluorouracil increased cell death in a time- and dose-dependent manner in SC-M1 cells. By comparison, TMC-1 cells were more resistant to 5-fluorouracil-induced cell death.

Discussion

Comparison of Genomic and Proteomic Profiling. In this study, we compared the global protein and mRNA patterns of nonmetastatic SC-M1 and metastatic TMC-1 gastric cancer cells to elucidate the molecular changes associated with carcinogenesis and metastasis. As shown in Tables 1 and 2, the functional classification of the differentially expressed proteins and mRNAs indicates that the DNA microarray and cICAT technique have different functional category detection preferences. The limited correlation ($r^2 = 0.2872$, Figure 4) between the steady-state levels of mRNA and protein abundance is not surprising, because they are individually controlled by their own rates of synthesis and turnover, determined by, for example, gene-specific chromatin structure, sequence content, and binding of accessory proteins.[34] Alternatively, some observed examples of negative correlation may suggest unexpected biological uncoupling between the expression levels of mRNA and the corresponding proteins.

DNA microarrays are generally considered to have better sensitivity and to provide more comprehensive identification and quantification of transcriptional changes. However, about 67 proteins (30% of the differentially expressed proteins) that were reproducibly identified and quantified by cICAT were not detected by DNA microarray analysis. Many of these orphan proteins were identified with multiple peptide hits; therefore, we are confident of their identification. Most prominent among these proteins are transcription initiation factor IIB (in the nucleic acid metabolism category), microtubule-associated

protein RP/EB family member 1, cytochrome P450 51A1, lnnexin 1, and GMP reductase 1 (Table 1). These observations highlight the advantage of the addition of the cICAT strategy to a genomics analysis to reveal subtle changes in the proteome not observed in the transcriptome.

Proteins Differentially Expressed between SC-M1 and TMC-1 Cells. Although the changes in protein and mRNA levels did not show a strong linear correlation, the proteome and transcriptome analysis identified gene products from functionally similar categories. Of particular interest, a significant number of gene products that were up-regulated in TMC-1 cells are involved in cancer metastasis, such as cell−cell adhesion signaling (catenin-120nt, α-catenin, β-catenin, integrin α6, integrin β4, RhoG, and IQGAP1), cell metastasis and motility (cytokeratin, myosin, S100 calcium binding protein (S100) family, and vimentin), cell cycle and proliferation (cdc42 and cell division protein kinase 6), tumor immunity and defense (galectin 1 and high mobility group protein 1), and protein degradation (cathepsin B, C). The protein expression levels and a comparison of the results of this study with previous reports are shown in Table 3. The different expression levels of these proteins may reflect biological differences leading to the distinct phenotype of the metastatic TMC-1 cell line.

Identification of accurate prognostic factors helps in therapeutic decision-making, in particular in patients with advanced stage cancer. To explore the possibility that the identified proteins may also serve as markers of metastasis for other types of human cancers, we examined the expression of a subset of proteins, β-catenin, galectin 1, vimentin, integrin α6, and integrin β4 by semiquantitative RT-PCR analysis in various cancer cells with differing invasion potential as assessed by the Boyden chamber assay. Our results showed that higher levels of vimentin and galectin 1 were readily detected in all of the cell lines with demonstrated invasive capability, whereas much lower or insignificant levels of expression were observed in cell lines with low invasiveness (unpublished data, Supplemental Figure 1, Supporting Information). Galectins are a family of structurally related carbohydrate-binding proteins and con-

Table 3. Summary of Differentially Expressed Proteins Related to Metastasis

gene name	UniProt ID	protein name	prob.[a]	molecular function	this study cICAT[b]	this study Affymetrix[c]	reproted expression change[d]	cancer type[f]
Cell to Cell Adhesion Signaling								
CTNND1	O60716	Catenin, 120ctn	1.00	Interacts with cadherin to regulate cell-adhesion properties	1.78	1.21	Up	Fibroblasts and Epithelial Cells (1)
CTNNA1	P35221	Catenin, alpha-1	1.00	Actin cross linking at adherens junctions	0.97	0.90	Down	Lung Carcinomas (2), Prostate Cancer (3)
CTNNB1	P35222	Catenin, beta	1.00	Modulates of cytoskeletal dynamics and cell proliferation	5.89	1.91	Down	Breast Cancer (4), Colorectal Cancer (5)(6)
ITGA6	P23229	Integrin alpha 6	0.99	Cell−matrix adhesion,cell-substrate junction assembly, cell adhesion	3.34	1.81	Up	Breast Carcinoma Cells (7)
ITGB4	P16144	Integrin beta 4	1.00	Cell−matrix adhesion, cell adhesion	1.96	1.80	Up	Breast Carcinoma Cells (7)
PRDX5	P30044	Peroxiredoxin 5	1.00	Contains high antioxidant efficiency to effect cell differentiation and apoptosis	1.84	NA[e]	Up	Gastric Cancer (8)
PBP	P30086	Raf kinase inhibitor protein	0.98	Suppresses metastasis through decreasing angiogenesis and vascular invasion	0.48	0.62	Down	Osteosarcoma (9)
RHOG	P84097	Rho-related GTP-binding protein RhoG	1.00	Small GTPase-mediated signal transduction, positive regulation of cell proliferation, actin cytoskeleton organization	0.55	0.83	Up	Breast Cancer (10)
IQGAP1	P46940	Ras GTPase-activating-like protein IQGAP1	1.00	Involves in actin cytoskeleton assembly and E-cadherin-mediated cell adhesion	0.35	0.19	Up	Gatric Cancer (11)
VCL	P18206	Vinculin	1.00	Mediates the interactions between integrins and the actin cytoskeleton	0.54	0.40	Down	Basal and Squamous Cell Tumors (12)
Cell Metastasis and Migration								
ACTN4	O43707	Alpha-actinin 4	1.00	Anchors actin to a variety of intracellular structures	1.37	1.59	Up	Colorectal Cancer (13)
ANXA1	P04083	Annexin I	1.00	Regulates of cell proliferation, promotes membrane fusion	0.68	1.02	Up/down	Hepatocellular Carcinoma (14), Lung Cancer (15), Head/Neck Cancer (16), Breast Carcinoma (17)
KRT17	Q04695	Cytoskeletal 17	1.00	Marker of basal cell differentiation in complex epithelia	0.03	NA[e]	Up	Breast Cancer (18)
KRT5	P13647	Cytoskeletal 5	1.00	Epidermis development, cytoskeleton organization and biogenesis, cellular morphogenesis	3.43	NA[e]	Up	Breast Cancer (18)
TPM3	Q8NAG3	Tropomyosin 3	1.00	Stabilizes of actin filaments	0.48	NA[e]	Down	Prostate Cancer (19), Breast Cancer (20)
TPM4	P67936	Tropomyosin 4	1.00	Binds to actin filaments in muscle and nonmuscle cells	0.61	0.82	Up/down	Lung Cancer (21)
VIM	P08670	Vimentin	0.99	Intermediate filament-based process in mesenchymal cells related to migration	25.67	NA[e]	Up	Breast Carcinoma (17), Hepatocellular Carcinoma (22), Propstate Cancer (23)
S100A11	P31949	S100 calcium-binding protein A11	1.00	Actin filament bundle formation and cell motility	1.34	NA[e]	Up	Hepatocellular Carcinoma (14)
COMT	P21964	Catechol O-methyltransferase	1.00	Involved in cancer progression and lymph node metastasis	1.35	0.81	Up	Breast Cancer (24)
Cell Cycle and Cell Proliferation Regulation								
SKP1A	P63208	S-phase kinase-associated protein 1A	0.97	Mediates the ubiquitination of proteins involved in cell cycle progression, signal transduction and transcription	0.35	0.80	Up	Colorectal Carcinoma (25), Hepatocellular Carcinoma (26)
CDC42	P60953	Cell division control protein 42 homologue	1.00	Regulates cadherin-mediated cell−cell adhesion	0.67	0.88	Up	Breast Cancer (27)
CDK6	Q00534	Cell division kinase 6	1.00	Related to cell proliferation, tumor heterogeneity, invasion and metastasis	1.72	NA[e]	Up	Retinoblastoma (28)Immunity and Defense
Immunity and Defense								
HMGB1	P09429	High mobility group protein 1	1.00	Interacts with transcription factors and regulates of transcription related to tumor growth and invasion	1.92	1.24	Up	Gastrointestinal Stromal Tumors (29)
CD44	Q16208	CD44	0.96	Mediates cell−cell and cell−matrix interactions through high affinity for hyaluronic acid	1.01	0.58	Up	Melanoma (30), Gastric Carcinoma (31)
LGALS1	P09382	Galectin-1	1.00	Promotes cancer cell invasion and metastasis	2.33	0.90	Up	Breast Carcinoma (32), Astrocytoma, Melanoma, Prostate, Colon, Bladder, Ovary (33)
HSPD1	P10809	Heat shock protein 60	1.00	Facilitates the correct folding of imported proteins	1.5	1.12	Down	Lung Cancer (15)
HSPCB	P08238	Heat shock protein 90 beta	1.00	Promotes the maturation of MMP2 involved in invasive cancer	0.68	0.87	Up	Murine Fibrosarcoma (34)
HLAA	P10892	MHC class I antigen	1.00	Inhibits evasion of the immune system and enhances tumor growth	0.64	NA[e]	Up	Gastric Cancer (35)

126

Table 3. (Continued)

gene name	UniProt ID	protein name	prob.[a]	molecular function	this study cICAT[b]	this study Affymetrix[c]	reproted expression change[d]	cancer type[f]
				Protein Degradation				
CTSB	P07858	Cathepsin B	1.00	Protein targeting, proteolysis and peptidolysis	1.61	2.16	Up	Melanoma (30), Breast Cancer (4), Lung cancer (31)
CTSC	P53634	Cathepsin C	1.00	Intracellular protein degradation and turnover	1.62	0.28	Up	Nonsmall Cell Lung Cancer (36)
CCT2	P78371	T-complex protein beta subunit	1.00	Related to p53 and activates DNA damage checkpoints	1.23	NA[e]	Down	Breast Carcinoma (17)

[a] ProteinProphet Score. [b] The fold change in the protein ratio of TMC-1/SC-M1 cells. [c] The fold change in the mRNA ratio of TMC-1/SC-M1 cells. [d] Literature report(s) of change in protein level in metastatic specimens. [e] NA, not avaiable. [f] References were provided as Supporting Information.
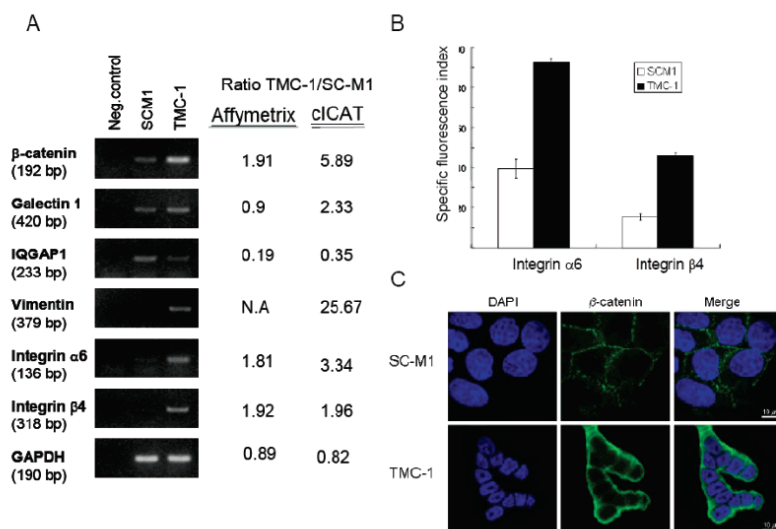
Figure 5. Expression of candidate genes in SC-M1 and TMC-1 cell lines. (A) RT-PCR analysis of *β-catenin, galectin 1, vimentin, integrin α6,* and *integrin β4* transcripts. The TMC-1/SC-M1 cell expression ratios obtained by Affymetrix DNA microarray and cICAT analysis are also shown for comparison. (B) Cell surface expression of integrins 6 and 4 as measured by flow cytometry. The specific fluorescence index was calculated as the ratio of the mean fluorescence values obtained with the specific Ab and the isotype control Ab. (C) The immunocytostaining images of *β-catenin* in SC-M1 and TMC-1 cells obtained by confocal laser microscopy.

tribute to tumor transformation, cell cycle regulation, apoptosis, cell adhesion, migration, and inflammation.[9,10] Their expression correlates with tumor aggressiveness and acquisition of a metastatic phenotype in different tumor types.[35] Vimentin is a cytoskeletal protein that is often expressed when epithelial cells are stimulated to proliferate by growth factors.[36] In cancer, vimentin expression is associated with a dedifferentiated malignant phenotype, increased motility and invasiveness, and poor clinical prognosis.[36] The significant overexpression of galectin 1 and vimentin we observed in TMC-1 cells is consistent with the reported correlation between cellular adhesion and tumor aggregation[37] and may be possible markers for metastasis.[38]

Although expression level changes in all of the proteins listed in Table 3 have been shown to be closely related to cancer metastasis, to the best of our knowledge, most have not been linked to gastric cancer. Previous studies have shown that the members of S100 family, S100A4, S100A6, and S100A11, are involved in cell motility, proliferation, differentiation, and cancer cell progression in breast cancer, colorectal cancer,[39]

gall bladder cancer, and hepatocellular carcinomas.[40] We also found overexpression of the S100A11 protein in TMC-1 cells. Annexin I is reportedly up-regulated in highly metastatic lung carcinoma cell lines[41] and down-regulated in a nonmetastatic type of breast cancer.[42] Increased expression of S100A11 may be correlated with observed down-regulation of Annexin I, the binding target of S100A11.

In addition, cathepsin B and cathepsin C were up-regulated in metastatic TMC-1 cells compared to the nonmetastatic SC-M1 cells. Elevated expression of these lysosomal proteases, cathepsins B, L, and D, and diminished levels of their inhibitors have been observed in breast and prostate cancer, especially in aggressive cancer cells.[43] Evidence suggests that capthepsin B has an important function in matrix degradation and invasion, facilitating the growth capability of invasive carcinomas through loss of calcium-dependent cell−cell adhesion and proteolysis of E-cadherin, which is a tumor suppressor and effector of adherens junction function.[44] Our results suggest that cathepsin C may also be involved in the metastasis of gastric cancer cells.
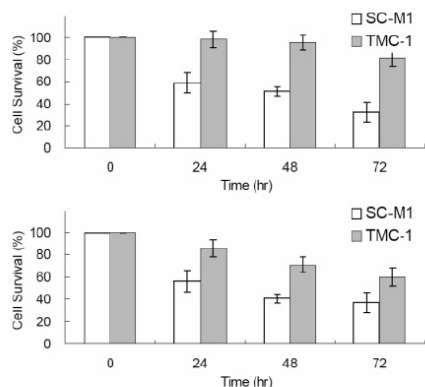
Figure 6. Inhibition of cell viability of the SCM-1 and TMC-1 cell lines by 5-fluorouracil. The cell lines were incubated with (A) 10 μM or (B) 50 μM 5-fluorouracil for 24, 48, and 72 h. Cells were then assayed by Alamar Blue dye uptake.

Metastasis-Perturbed Pathway. Furthermore, the differentially expressed proteins identified in the current comparative approach enabled us to study their correlations in multiple cellular pathways. Using the pathway analysis tools available at the BioCarta, KEGG, PANTHER, and PathwayAssist, we found differences in expression of proteins in the pathways related to cytoskeleton rearrangement, cell−cell adhesion, and cell−ECM attachment between the metastatic TMC-1 and nonmetastatic SC-M1 cells. Figure 7 depicts a summary of these proteins and pathways, including the integrin signaling pathway, the

Rho cell motility signaling pathway, and pathways associated with cell−cell adhesion and adherens junctions.

Recently, increasing evidence suggests that epithelial−mesenchymal transitions (EMT) play a specific role in the migration of cells from primary tumors into the circulation.[45] The defining event for the epithelial−mesenchymal transition is disruption of E-cadherin-mediated cell−cell adhesion, which results in loss of epithelial morphology and acquisition of a motile, mesenchymal phenotype.[46] Cancer cells that undergo the EMT, therefore, lose their ability to adhere to their neighboring cells, resulting in weakened cell−cell adhesion and subsequent tumor cell migration. Much evidence indicates that loss or reduction of E-cadherin-mediated adhesion, thus, allowing cell migration, is required for the metastatic conversion of carcinomas. Cadherins are calcium-dependent adhesion molecules responsible for the establishment of tight cell−cell contact. Anchorage to the actin cytoskeleton occurs through the binding of the cytoplasmic domain of cadherins to β-catenin or γ-catenin, which concurrently binds to α-catenin.[47,48] β-Catenin plays a central role in linking the membrane-bound E-cadherin to the cytoskeleton, and the interaction of β-catenin and IQGAP1 negatively regulates E-cadherin-mediated cell−cell adhesion.[49] Fukata et al. have proposed that β-catenin exists in a dynamic equilibrium between the E-cadherin−β-catenin−α-catenin complex and the E-cadherin−β-catenin−IQGAP1 complex at sites of cell−cell contact. Weakening cell−cell adhesion shifts the balance of β-catenin from the cadherin-bound pool to the cytoplasmic pool. In this study, immunocytostaining showed more cytoplasmic localization of β-catenin in the metastatic TMC-1 cells (Figure 5). A newly discovered β-catenin interaction partner, 14-3-3 ζ,[50] enhances the transcription of β-catenin target promoters, leading to elevated
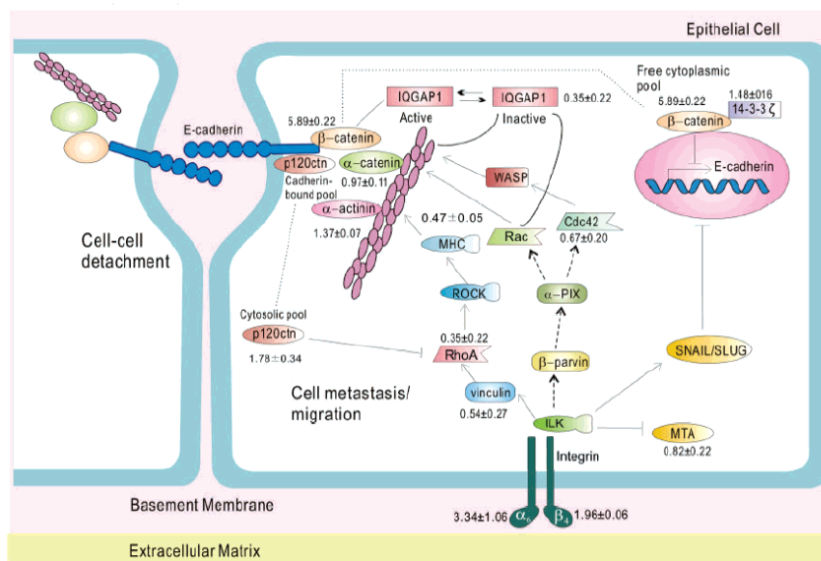
Figure 7. Summary of differentially expressed proteins in multiple pathways involved in cell−cell adhesion and cell−ECM interactions. The fold changes and standard deviation of the cICAT TMC-1/SC-M1 cell expression ratios are indicated. The solid lines indicate pathways derived from the BioCarta, KEGG, and PANTHER databases, and dashed lines indicate those found in the literature (using PathwayAssist).

steady-state levels of β-catenin in the cytoplasm. The accumulation of free cytosolic β-catenin has been reported to lead to translocation of β-catenin to the nucleus, which results in sustained transcriptional activation of oncogenes and causes tumor growth.[51] Although we did not observe β-catenin in the nucleus, up-regulation of both 14-3-3 ζ and β-catenin in TMC-1 cells was observed, which suggests activation of the Wnt signaling pathway.[50]

In addition, anchoring junction dynamics can be regulated by intricate interactions of the cadherin−catenin complex with Cdc42, a member of the Rho GTPase subfamily known for its role in regulating cell division.[52] Rac1 and Cdc42 might also regulate the cleavage and endocytosis of E-cadherin, thereby modifying E-cadherin-mediated cell−cell adhesion. Meanwhile, Cdc42 and Rac1 also regulate cell−cell adhesion through IQGAP1 by the interaction of IQGAP1 with β-catenin, leading to stabilization of the E-cadherin−catenin complex.[53,54] The decreased levels of IQGAP1 and Cdc42 we observed seem to imply that the Rac1−Cdc42−IQGAP1 complex is involved in the weak intercellular adhesion of TMC-1 cells.

The dysregulation of ECM adhesion, which is mediated mainly by integrins through GTPases, is another crucial determinant for tumor progression.[55] E-cadherin-mediated adhesion may also be regulated by integrin $\alpha_6\beta_4$ signaling through phosphatidylinositol 3 kinase to Rac, or alternatively, the transcription of E-cadherin can be suppressed through integrin-linked kinase (ILK) by up-regulating the transcriptional suppression of E-cadherin by repressors SNAL/SLUG.[55] In addition, the p120ctn in the cytosol and in the cadherin-based complex provides one mechanism for communication between cadherin-mediated cell−cell junctions and the motile machinery of cells.[56] The observed up-regulation of p120ctn and down-regulation of RhoA suggest that p120ctn may negatively modulate RhoA to affect other downstream effectors. Active RhoA increases the stability of actin-based focal adhesions. Therefore, the decreased level of RhoA and its downstream effectors, vinculin and myosin heavy/light chain (MHC), that we observed in the cICAT analysis of TMC-1 cells also implies a weakened capability to adhere to the ECM.

In general, advanced gastric cancer is refractory to chemotherapy, leading to poor prognosis. To search for novel targets for screening and therapeutic intervention, it is increasingly important to recognize that discovery of disease-perturbed pathways is more fruitful than identification of individual gene products.[57] In summary, our results that both the cell−cell adhesion and the cell−ECM attachment pathways are disrupted provide identification of several differentially expressed pathways. Their associated proteins may be potential biomarkers of metastatic gastric tumor cells and of invasiveness. The regulation of cell−cell adhesion or dissociation is extremely complicated, and the plasticity the cells exhibit likely requires real-time control by transcriptional networks. Further investigation on the temporal profiling of these complex signaling cascades will provide insight into the invasive behavior and the metastatic potential of cancer cells.

Abbreviations: cICAT, cleavable isotope-coded affinity tag; TCEP, Tris-(2-carboxyethyl)phosphine; SCX, strong cation exchange; DAPI, 4′,6-diamidino-2-phenylindole-dihydrochloride; ECM, extracellular matrix.

Supporting Information Available: Figure showing the semiquantitative analysis of *galectin 1, vimentin, IQGAP1,* and *β-catenin* transcripts in different cancer cell lines, including breast, colon, ovary, bladder, and lung cancer; tables showing the protein identification summaries of TMC-1 and SC-M1 cells and of the cICAT analysis. This material is available free of charge via the Internet at http://pubs.acs.org.

References

(1) Parkin, D. M.; Pisani, P.; Ferlay, J. Estimates of the worldwide incidence of 25 major cancers in 1990. *Int. J. Cancer* **1999**, *80*, 827−41.

(2) Stadtlander, C. T.; Waterbor, J. W. Molecular epidemiology, pathogenesis and prevention of gastric cancer. *Carcinogenesis* **1999**, *20*, 2195−208.

(3) Peddanna, N.; Holt, S.; Verma, R. S. Genetics of gastric cancer. *Anticancer Res.* **1995**, *15*, 2055−64.

(4) Hippo, Y.; Taniguchi, H.; Tsutsumi, S.; et al. Global gene expression analysis of gastric cancer by oligonucleotide microarrays. *Cancer Res.* **2002**, *62*, 233−40.

(5) Cai, Z.; Chiu, J. F.; He, Q. Y. Application of proteomics in the study of tumor metastasis. *Genomics, Proteomics Bioinf.* **2004**, *2*, 152−66.

(6) Wang, W.; Goswami, S.; Sahai, E.; Wyckoff, J. B.; Segall, J. E.; Condeelis, J. S. Tumor cells caught in the act of invading,, their strategy for enhanced cell motility. *Trends Cell Biol.* **2005**, *15*, 138−45.

(7) Lin, B.; White, J. T.; Lu, W.; et al. Evidence for the presence of disease-perturbed networks in prostate cancer cells by genomic and proteomic analyses: a systems approach to disease. *Cancer Res.* **2005**, *65*, 3081−91.

(8) Sinha, P.; Poland, J.; Schnolzer, M.; Celis, J. E.; Lage, H. Characterization of the differential protein expression associated with thermoresistance in human gastric carcinoma cell lines. *Electrophoresis* **2001**, *22*, 2990−3000.

(9) Choi, Y. R.; Kim, H.; Kang, H. J.; et al. Overexpression of high mobility group box 1 in gastrointestinal stromal tumors with KIT mutation. *Cancer Res.* **2003**, *63*, 2188−93.

(10) Chen, J.; Kahne, T.; Rocken, C.; et al. Proteome analysis of gastric cancer metastasis by two-dimensional gel electrophoresis and matrix assisted laser desorption/ionization-mass spectrometry for identification of metastasis-related proteins. *J. Proteome Res.* **2004**, *3*, 1009−16.

(11) He, Q. Y.; Cheung, Y. H.; Leung, S. Y.; Yuen, S. T.; Chu, K. M.; Chiu, J. F. Diverse proteomic alterations in gastric adenocarcinoma. *Proteomics* **2004**, *4*, 3276−87.

(12) Das, S.; Sierra, J. C.; Soman, K. V.; et al. Differential protein expression profiles of gastric epithelial cells following *Helicobacter pylori* infection using ProteinChips. *J. Proteome Res.* **2005**, *4*, 920−30.

(13) Juan, H. F.; Chen, J. H.; Hsu, W. T.; et al. Identification of tumor-associated plasma biomarkers using proteomic techniques: from mouse to human. *Proteomics* **2004**, *4*, 2766−75.

(14) Washburn, M. P.; Wolters, D.; Yates, J. R., III. Large-scale analysis of the yeast proteome by multidimensional protein identification technology. *Nat. Biotechnol.* **2001**, *19*, 242−7.

(15) Washburn, M. P.; Ulaszek, R.; Deciu, C.; Schieltz, D. M.; Yates, J. R., III. Analysis of quantitative proteomic data generated via multidimensional protein identification technology. *Anal. Chem.* **2002**, *74*, 1650−7.

(16) Aebersold, R.; Mann, M. Mass spectrometry-based proteomics. *Nature* **2003**, *422*, 198−207.

(17) Gygi, S. P.; Rist, B.; Gerber, S. A.; Turecek, F.; Gelb, M. H.; Aebersold, R. Quantitative analysis of complex protein mixtures using isotope-coded affinity tags. *Nat. Biotechnol.* **1999**, *17*, 994−9.

(18) Li, J.; Steen, H.; Gygi, S. P. Protein profiling with cleavable isotope-coded affinity tag (cICAT) reagents: the yeast salinity stress response. *Mol. Cell. Proteomics* **2003**, *2*, 1198−204.

(19) Li, C.; Hong, Y.; Tan, Y. X.; et al. Accurate qualitative and quantitative proteomic analysis of clinical hepatocellular carcinoma using laser capture microdissection coupled with isotope-coded affinity tag and two-dimensional liquid chromatography mass spectrometry. *Mol. Cell. Proteomics* **2004**, *3*, 399−409.

(20) Tzeng, C. C.; Meng, C. L.; Jin, L.; Hsieh, H. F. Cytogenetic studies of gastric adenocarcinoma. *Cancer Genet. Cytogenet.* **1991**, *55*, 67−71.

(21) Shyu, R. Y.; Jiang, S. Y.; Jong, Y. J.; et al. Establishment and characterization of a human gastric carcinoma cell line TMC-1. *Cells Tissues Organs* **2004**, *177*, 37−46.

(22) Keller, A.; Nesvizhskii, AI.; Kolker, E.; Aebersold, R. Empirical statistical model to estimate the accuracy of peptide identifications made by MS/MS and database search. *Anal. Chem.* **2002**, *74*, 5383−92.

(23) Nesvizhskii, A. I.; Keller, A.; Kolker, E.; Aebersold, R. A statistical model for identifying proteins by tandem mass spectrometry. *Anal. Chem.* **2003**, *75*, 4646−58.

(24) Li, X. J.; Zhang, H.; Ranish, J. A.; Aebersold, R. Automated statistical analysis of protein abundance ratios from data generated by stable-isotope dilution and tandem mass spectrometry. *Anal. Chem.* **2003**, *75*, 6648−57.

(25) Kim, J. M.; Sohn, H. Y.; Yoon, S. Y.; et al. Identification of gastric cancer-related genes using a cDNA microarray containing novel expressed sequence tags expressed in gastric cancer cells. *Clin. Cancer Res.* **2005**, *11*, 473−82.

(26) Wechsler-Reya, R. J.; Elliott, K. J.; Prendergast, G. C. A role for the putative tumor suppressor Bin1 in muscle cell differentiation. *Mol. Cell. Biol.* **1998**, *18*, 566−75.

(27) Su, M. W.; Dorocicz, I.; Dragowska, W. H.; et al. Aberrant expression of T-plastin in Sezary cells. *Cancer Res.* **2003**, *63*, 7122−7.

(28) Gerk, P. M.; Vore, M. Regulation of expression of the multidrug resistance-associated protein 2 (MRP2) and its role in drug disposition. *J. Pharmacol. Exp. Ther.* **2002**, *302*, 407−15.

(29) Reiher, F. K.; Volpert, O. V.; Jimenez, B.; et al. Inhibition of tumor growth by systemic treatment with thrombospondin-1 peptide mimetics. *Int. J. Cancer* **2002**, *98*, 682−9.

(30) Nishizuka, S.; Charboneau, L.; Young, L.; et al. Proteomic profiling of the NCI-60 cancer cell lines using new high-density reverse-phase lysate microarrays. *Proc. Natl. Acad. Sci. U.S.A.* **2003**, *100*, 14229−34.

(31) Mulholland, D. J.; Dedhar, S.; Coetzee, G. A.; Nelson, C. C. Interaction of nuclear receptors with the Wnt/beta-catenin/Tcf signaling axis: Wnt you like to know? *Endocr. Rev.* **2005**, *26*, 898−915.

(32) Feng, Y.; Lee, N.; Fearon, E. R. TIP49 regulates beta-catenin-mediated neoplastic transformation and T-cell factor target gene induction via effects on chromatin remodeling. *Cancer Res.* **2003**, *63*, 8726−34.

(33) Oliver, L.; Cordel, S.; Barbieux, I.; et al. Resistance to apoptosis is increased during metastatic dissemination of colon cancer. *Clin. Exp. Metastasis* **2002**, *19*, 175−80.

(34) Dechering, K. J. The transcriptome's drugable frequenters. *Drug Discovery Today* **2005**, *10*, 857−64.

(35) Rabinovich, G, A. Galectin-1 as a potential cancer target. *Br. J. Cancer* **2005**, *92*, 1188−92.

(36) Yoon, W. H.; Song, I. S.; Lee, B. H.; et al. Differential regulation of vimentin mRNA by 12-O-tetradecanoylphorbol 13-acetate and all-trans-retinoic acid correlates with motility of Hep 3B human hepatocellular carcinoma cells. *Cancer Lett.* **2004**, *203*, 99−105.

(37) Kasamatsu, A.; Uzawa, K.; Nakashima, D.; et al. Galectin-9 as a regulator of cellular adhesion in human oral squamous cell carcinoma cell lines. *Int. J. Mol. Med.* **2005**, *16*, 269−73.

(38) Irie, A.; Yamauchi, A.; Kontani, K.; et al. Galectin-9 as a prognostic factor with antimetastatic potential in breast cancer. *Clin. Cancer Res.* **2005**, *11*, 2962−8.

(39) Komatsu, K.; Kobune-Fujiwara, Y.; Andoh, A.; et al. Increased expression of S100A6 at the invading fronts of the primary lesion and liver metastasis in patients with colorectal adenocarcinoma. *Br. J. Cancer* **2000**, *83*, 769−74.

(40) Cui, J. F.; Liu, Y. K.; Pan, B. S.; et al. Differential proteomic analysis of human hepatocellular carcinoma cell line metastasis-associated proteins. *J. Cancer Res. Clin. Oncol.* **2004**, *130*, 615−22.

(41) Jiang, D.; Ying, W.; Lu, Y.; et al. Identification of metastasis-associated proteins by proteomic analysis and functional exploration of interleukin-18 in metastasis. *Proteomics* **2003**, *3*, 724−37.

(42) Kreunin, P.; Urquidi, V.; Lubman, D. M.; Goodison, S. Identification of metastasis-associated proteins in a human tumor metastasis model using the mass-mapping technique. *Proteomics* **2004**, *4*, 2754−65.

(43) Nomura, T.; Katunuma, N. Involvement of cathepsins in the invasion, metastasis and proliferation of cancer cells. *J. Med. Invest.* **2005**, *52*, 1−9.

(44) Jawhari, A. U.; Noda, M.; Farthing, M. J.; Pignatelli, M. Abnormal expression and function of the E-cadherin-catenin complex in gastric carcinoma cell lines. *Br. J. Cancer* **1999**, *80*, 322−30.

(45) Huber, M. A.; Kraut, N.; Beug, H. Molecular requirements for epithelial-mesenchymal transition during tumor progression. *Curr. Opin. Cell Biol.* **2005**, *17*, 548−58.

(46) Rosivatz, E.; Becker, I.; Specht, K.; et al. Differential expression of the epithelial-mesenchymal transition regulators snail, SIP1, and twist in gastric cancer. *Am. J. Pathol.* **2002**, *161*, 1881−91.

(47) Beavon, I. R. The E-cadherin-catenin complex in tumour metastasis: structure, function and regulation. *Eur. J. Cancer* **2000**, *36*, 1607−20.

(48) Fukata, M.; Nakagawa, M.; Itoh, N.; et al. Involvement of IQGAP1, an effector of Rac1 and Cdc42 GTPases, in cell−cell dissociation during cell scattering. *Mol. Cell. Biol.* **2001**, *21*, 2165−83.

(49) Fukata, M.; Kaibuchi, K. Rho-family GTPases in cadherin-mediated cell−cell adhesion. *Nat. Rev. Mol. Cell Biol.* **2001**, *2*, 887−97.

(50) Tian, Q.; Feetham, M. C.; Tao, W. A.; et al. Proteomic analysis identifies that 14−3−3zeta interacts with beta-catenin and facilitates its activation by Akt. *Proc. Natl. Acad. Sci. U.S.A.* **2004**, *101*, 15370−5.

(51) Sparks, A. B.; Morin, P. J.; Vogelstein, B.; Kinzler, K. W. Mutational analysis of the APC/beta-catenin/Tcf pathway in colorectal cancer. *Cancer Res.* **1998**, *58*, 1130−4.

(52) Lui, W. Y.; Mruk, D. D.; Cheng, C. Y. Interactions among IQGAP1, Cdc42, and the cadherin/catenin protein complex regulate Sertoli-germ cell adherens junction dynamics in the testis. *J. Cell. Physiol.* **2005**, *202*, 49−66.

(53) Kuroda, S.; Fukata, M.; Nakagawa, M.; et al. Role of IQGAP1, a target of the small GTPases Cdc42 and Rac1, in regulation of E-cadherin-mediated cell−cell adhesion. *Science* **1998**, *281*, 832−5.

(54) Fukata, M.; Kuroda, S.; Nakagawa, M.; et al. Cdc42 and Rac1 regulate the interaction of IQGAP1 with beta-catenin. *J. Biol. Chem.* **1999**, *274*, 26044−50.

(55) Guo, W.; Giancotti, F. G. Integrin signalling during tumour progression. *Nat. Rev. Mol. Cell Biol.* **2004**, *5*, 816−26.

(56) Noren, N. K.; Liu, B. P.; Burridge, K.; Kreft, B. p120 catenin regulates the actin cytoskeleton via Rho family GTPases. *J. Cell. Biol.* **2000**, *150*, 567−80.

(57) Kramer, R.; Cohen, D. Functional genomics to new drug targets. *Nat. Rev. Drug Discovery* **2004**, *3*, 965−72.

PR060212G

130

Conference Proceedings

MicroRNA-148a Suppresses Cell Metastasis through Targeting 14-3-3β in Gastric Cancer

Chien-Wei Tseng[1], Chen-Ching Lin[2], Kai-Neng Chuang[1], Chiung-Nien Chen[3,4,*], Hsuan-Cheng Huang[5,*], and Hsueh-Fen Juan[1,2,*]

[1]Institute of Molecular and Cellular Biology and Department of Life Science, National Taiwan University, Taipei, Taiwan

[2]Institute of Biomedical Electronics and Bioinformatics, National Taiwan University, Taipei, Taiwan

[3]Angiogenesis Research Center, National Taiwan University, Taipei, Taiwan

[4]Department of Surgery, National Taiwan University Hospital and College of Medicine, Taipei, Taiwan

[5]Institute of Biomedical Informatics and Center for Systems and Synthetic Biology, National Yang-Ming University, Taipei, Taiwan

Correspondence e-mail address:

CNC: ccchen@ntu.edu.tw; HCH: hsuancheng@ym.edu.tw; HFJ: yukijuan@ntu.edu.tw

Abstract

Gastric cancer is the second leading cause of cancer deaths worldwide (WHO 2009 report). Patients diagnosed with advanced stages have a survival rate of less than 35% beyond 5 years. The poor prognosis is mainly related to tumor metastasis. In addition, some microRNAs (miRNAs) are reported as oncomirs which function as either oncogenes or tumor suppressors and involved in tumorigenesis and cancer progression. Here, we studied the mechanisms of gastric cancer metastasis and identified an antimetastatic miRNA, miR-148a, that was down-regulated in tumor tissues. Kaplan–Meier survival method revealed that patients with higher miR-148a expression levels had higher 5-year overall survival rates (71.4%) compared with patients with low miR-148a levels (32.1%, $P = 0.03$). Clinical data indicated that elevated miR-148a levels highly correlated with distant metastasis ($P = 0.043$), organ ($P = 0.013$) and peritoneal invasion ($P = 0.04$). Over-expression of miR-148a could decrease invasiveness, migration and growth of tumor cells. Furthermore, we verified that miR-148a could directly regulate 14-3-3β expression using luciferase assay. 14-3-3β levels were elevated in tumor tissues ($N = 40$, $P < 0.01$), and serum 14-3-3β levels in cancer patients ($N = 145$) were also significantly higher than healthy controls ($N = 63$) ($P < 0.0001$). Patients with higher serum 14-3-3β levels had worse overall survival ($P = 0.038$). Over-expression of 14-3-3β enhanced the growth, invasiveness and migration of tumor cells. Finally, integration of proteomics and network analysis was performed to reveal that the downstream regulation of 14-3-3β was involved in anti-apoptosis and tumor progression. In conclusion, miR-148a may function as a tumor suppressor and suppresses cell metastasis through targeting 14-3-3β, a potential detective and prognostic marker in gastric cancer.

(MiR-148a paper is in revision by BMC Systems Biology & 14-3-3β paper is accepted by Proteomics, 2011)

Key words: miR-148a; 14-3-3β; gastric cancer; metastasis

TPS
Taiwan Proteomics Society

2011 Translational Medicine Conference and Taiwan Proteomics Society Annual Symposium
April 27 – 28, 2011, Taipei, Taiwan

Poster Award

This Poster Award Certificate has been presented to

Chien-Wei Tseng
National Taiwan University

The abstract presented for this award was entitled

"MicroRNA-148a Suppresses Cell Metastasis through Targeting 14-3-3β in Gastric Cancer"

President of TPS

MicroRNA-148a Suppresses Cell Metastasis through Targeting 14-3-3β in Gastric Cancer

Chien-Wei Tseng[1], Chen-Ching Lin[2], Chiung-Nien Chen[3,4,*], Hsuan-Cheng Huang[5,*], and Hsueh-Fen Juan[1,2,*]

[1]Institute of Molecular and Cellular Biology and Department of Life Science, National Taiwan University, Taipei, Taiwan
[2]Institute of Biomedical Electronics and Bioinformatics, National Taiwan University, Taipei, Taiwan
[3]Angiogenesis Research Center, National Taiwan University, Taipei, Taiwan
[4]Department of Surgery, National Taiwan University Hospital and College of Medicine, Taipei, Taiwan
[5]Institute of Biomedical Informatics and Center for Systems and Synthetic Biology, National Yang-Ming University, Taipei, Taiwan

CNC: ccchen@ntu.edu.tw; HCH: hsuancheng@ym.edu.tw; HFJ: yukijuan@ntu.edu.tw

Background

Gastric cancer is the second leading cause of cancer deaths worldwide (WHO 2009 report). Patients diagnosed with advanced stages have a survival rate of less Here, we studied the mechanisms of gastric cancer metastasis and identified an antimetastatic miRNA, miR-148a, that was down-regulated in tumor tissues. Kaplan–Meier survival method revealed that patients with higher miR-148a expression levels had better overall survival ($P = 0.03$). Over-expression of miR-148a could decrease invasiveness, migration, adhesion and growth of tumor cells. Furthermore, we verified that miR-148a could directly regulate 14-3-3β expression using luciferase assay. 14-3-3β levels were elevated in tumor tissues ($N = 40$, $P < 0.01$), and serum 14-3-3β levels in cancer patients ($N = 145$) were also significantly higher than healthy controls ($N = 63$) ($P < 0.0001$). Patients with higher serum 14-3-3β levels had worse overall survival ($P = 0.038$). Over-expression of 14-3-3β enhanced the growth, invasiveness and migration of tumor cells. Finally, integration of proteomics and network analysis was performed to reveal that the downstream regulation of 14-3-3β was involved in anti-apoptosis and tumor progression. In conclusion, miR-148a may function as a tumor suppressor and suppresses cell metastasis through targeting 14-3-3β, a potential detective and prognostic marker in gastric cancer. 14-3-3β paper is accepted (Proteomics, 2011) ; miR-148a paper is in revision (BMC Systems Biology, 2011)

Experimental Design
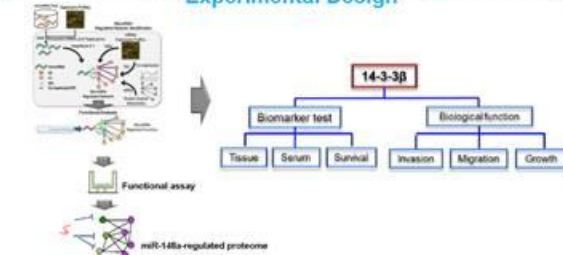
miR-148a regulates metastasis-related network
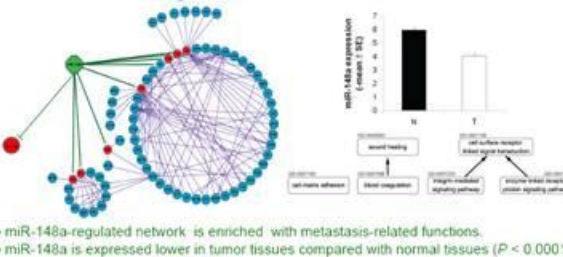
- miR-148a-regulated network is enriched with metastasis-related functions.
- miR-148a is expressed lower in tumor tissues compared with normal tissues ($P < 0.0001$).

miR-148a suppresses gastric cancer metastasis
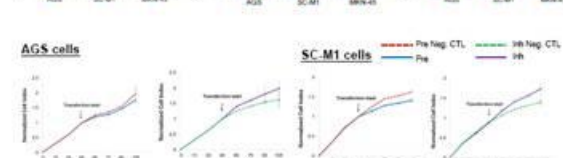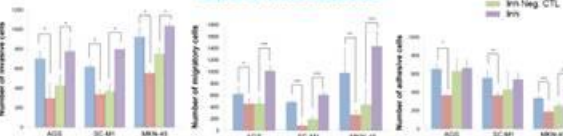
- miR-148a suppresses invasion, migration, adhesion and growth of tumor cells.

miR-148a inhibits metastasis through its regulated network
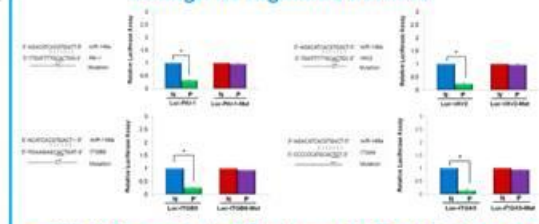
miR-148a-regulated Proteome in Gastric Cancer
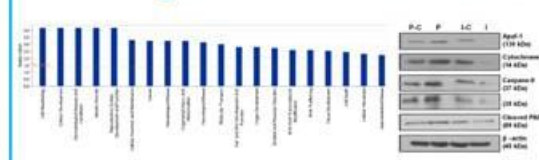
- Associated functions of miR-148a-regulated proteome were identified using IPA.
- miR-148a could induce gastric cancer cell apoptosis.

miR-148a Is a Potential Detective and Prognosis Marker
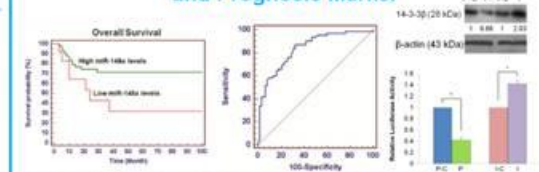
- miR-148a is a detective and prognostic marker in gastric cancer and directly regulates 14-3-3β expression.

14-3-3β Is an Oncogene and Potential Detective and Prognostic Biomarker

- Serum 14-3-3β is a detective and prognostic marker in gastric cancer.
- 14-3-3β promotes invasion, migration and growth of tumor cells.

Conclusion

國立台灣大學
分子與細胞生物學研究所

壁報競賽獎狀

學生 曾建偉 參加 99 學年度本所
學生壁報競賽，成績優異，經評審為博
士班傑出獎，殊堪嘉許，特頒此狀以資
獎勵。

所長 周子賓

中華民國 100 年 6 月

14-3-3β Is A Novel Biomarker for Early Detection and Prognosis in Gastric Cancer

Chien-Wei Tseng[1], Chiung-Nien Chen[2,3,4*], Hsueh-Fen Juan[1,5,6,7*]

[1]Institute of Molecular and Cellular Biology, National Taiwan University; [2]Angiogenesis Research Center, National Taiwan University; [3]Department of Surgery, National Taiwan University Hospital and College of Medicine
[4]Division of Mechanics, Research Center for Applied Sciences, Academia Sinica; [5]Department of Life Science, National Taiwan University; [6]Institute of Biomedical Electronics and Bioinformatics, National Taiwan University, Taipei, 106 Taiwan
[7]Center for Systems Biology and Bioinformatics, National Taiwan University, Taipei, 106 Taiwan

Abstract

The 14-3-3 proteins form a highly conserved family of dimeric proteins and regulate signal transduction, cell cycle, apoptosis and tumorigenesis. Since 14-3-3β protein is involved in tumorigenesis and cell spreading and migration, it is of great interest to study the role of 14-3-3β protein on gastric cancer. To investigate whether 14-3-3β is a gastric cancer-associated protein, we probed into the expression of 14-3-3β in 40 paired normal and tumor tissues. Our results showed that 14-3-3β was significantly over-expressed in tumor tissues compared with normal tissues ($p = 0.003$). Immunohistochemical staining studies further confirmed the observation of elevated 14-3-3β levels in tumor tissues. Furthermore, we analyzed preoperative serum 14-3-3β levels in 63 normal and 145 tumor subjects using ELISA. The results indicated the expression levels of 14-3-3β in gastric cancer patients were significantly higher than those in normal controls ($p < 0.0001$), where patients with stage I tumors had 14-3-3β levels 1.7 times higher than normal controls. Serum 14-3-3β levels were increased with increasing tumor stage (stage I v II v III v IV, $r = 0.273$, $p = 0.0009$). Clinical analyses revealed that preoperative serum 14-3-3β levels were associated with clinical factors, including age ($r = 0.239$, $p = 0.0004$), number of lymph node metastasis ($r = 0.166$, $p = 0.045$) and tumor size ($r = 0.452$, $p < 0.001$). ROC curves for 14-3-3β and CEA were compared. The approximate area under the curve for 14-3-3β was 0.83, and 0.51 for CEA, indicating 14-3-3β was a better diagnostic marker for gastric cancer compared to CEA ($p < 0.05$). Furthermore, patients with higher 14-3-3β levels had worse overall ($p = 0.038$) and recurrence-free survival ($p = 0.037$). These results suggest that 14-3-3β may represent a novel marker for early detection and prognosis in gastric cancer.

Introduction

Gastric adenocarcinoma is a health problem of great concern, as it is one of the most common malignancies and leading causes of death worldwide[1,2]. Moreover, patients with an overall 5 years survival rate are less than 10%. Thus, early detection of gastric cancer is essential for improved survival. The tests of serological markers for the detection of early stage cancers in asymptomatic patients are easily and economically and therefore considered as publicly acceptable screening methods. Unlike breast or prostate cancers, there is no effective marker to detect early stage gastric cancer. Thus, the identification of new diagnostic markers of gastric cancer for screening purposes is important.

Currently, carcinoembryonic antigen (CEA) is a tumor marker available for screening gastric cancer. It was first described as a tumor-associated antigen in colon cancer tissue extract[3] and a cell adhesion-associated glycoprotein[4]. Although CEA levels in many cancers were elevated, including gastric (GC) and colorectal cancers (CC)[5]; however, it lacked good sensitivity as well as specificity (49% sensitivity for GC, 43% sensitivity for CC). Therefore, there is a need for a new and better diagnostic marker of gastric cancer.

The 14-3-3 proteins refer to a family of acidic dimeric proteins that are expressed in all eukaryotic cells, and they play important roles in regulating multiple cellular processes including apoptosis, signal transduction, cell cycle checkpoint, DNA repair, cell differentiation and cell adhesion and mobility[6,7]. Seven 14-3-3 isoforms (β, γ, ε, ζ, η, σ, θ) have been identified in mammalian cells, and each of them has distinct tissues localization and isoform-specific functions[8]. Reports indicated that 14-3-3β was involved in tumorigenesis. Reduced 14-3-3β protein was associated with decreased vascular endothelial growth factor (VEGF) production, inhibition of angiogenesis, increase in apoptosis and much decrease in tumor size[9]. Moreover, 14-3-3β promoted metastasis of tumors[9] and interacted with integrin β1 to promote the spreading and mobility of cells[10].

In this study, we identified 20 differential expressed proteins in gastric cancer SC-M1 cells after 5-FU treatment from proteomic profiling. Among them, 14-3-3β was significantly down-regulated in 5-FU-treated SC-M1 cells. Furthermore, we further studied the 14-3-3β expression in normal and tumor tissues to confirm that 14-3-3β is a gastric cancer-associated protein. On the other hand, we analyzed serum 14-3-3β levels in gastric cancer patients to determine if 14-3-3β was elevated in early-stage tumors. The purpose of this study was to determine if 14-3-3β represents a possible marker for early-stage gastric cancer and might be useful for early detection and prognosis in gastric cancer.

Results

Fig 1. 2-DE profiling of 5-FU-treated and SC-M1 cells control.
(a) Protein spots from 5-FU-treated (right) and SC-M1 cells control (left) were compared. Differential expressed proteins were selected and identified by MS/MS. Enlarged images (b) and 3-D profiles (c) of 14-3-3β on the gels were showed. 14-3-3β was expressed higher in SC-M1 cells control (d).

Fig 2. 14-3-3β was overexpressed in tumor tissues.
(a) 14-3-3β expression in 40 tumor and paired normal tissues was analyzed by western blotting. β-actin serves as a loading control. The results showed that 14-3-3β was significantly expressed higher in tumor tissues when compared to that in normal tissues (**$p < 0.01$). 14-3-3β expression in normal (b) and intestinal type (c) and diffuse type (d) tumor tissues was analyzed. The results further confirmed 14-3-3β was expressed higher in tumor tissues (×200 original magnification).

Fig 3. Serum 14-3-3β levels in gastric cancer patients were elevated.
Serum 14-3-3β levels in patients were significant higher relative to normal and non-disease controls ($p < 0.001$); moreover, 14-3-3β levels were positive correlative with increasing stage of the tumor (stage I v II v III v IV, $r = 0.273$, $p = 0.0009$).

Fig 4. The relationship between serum 14-3-3β and clinical factors.
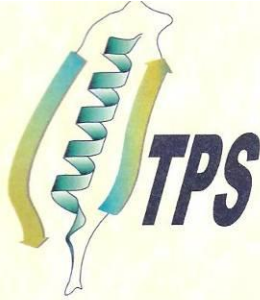The correlation of preoperative serum 14-3-3β levels in gastric cancer patients relative to (a) age (n = 145); (b) lymph node metastasis (n = 145); (c) tumor size (n = 139) and (d) 14-3-3β expression in tumor tissues (n = 31).

Fig 5. Receiver operating characteristic curves of 14-3-3β and CEA.
(a) Serum 14-3-3β and CEA in stage I tumor ($p = 0.0004$ and 0.364, respectively); (b) Stage II tumor ($p < .0001$ and 0.434); (c) Stage III tumor ($p < .0001$ and 0.803); (d) Stage IV tumor ($p < 0.0001$ and 0.548) were compared.

Fig 6. The correlation between serum 14-3-3β levels and survival rate. Blue line: higher serum 14-3-3β levels; Red line: lower serum 14-3-3β levels. The results indicated patients with higher serum 14-3-3β levels had poor overall (a, $p = 0.038$) and recurrence-free survival (b, $p = 0.037$). (c) Postoperative 14-3-3β levels were reduced ($p < 0.0001$).

Conclusion

14-3-3β may represent a novel marker for early detection and prognosis in gastric cancer. Moreover, 14-3-3β levels are associated with metastasis of tumor cells. These results enhance our understanding of the roles and provide useful insights of 14-3-3β in human gastric cancer.

References

[References illegible]

TPS

2008 Taiwan-Japan Proteomics Symposium

This Certificate is Awarded to

Chien-Wei Tseng

In Recognition of Excellence in Poster Presentation

Shui-Tein Chen, Ph. D.
President, Taiwan Proteomics Society
Institute of Biological Chemistry
Academia Sinica